Comparative Study of the Corrosion Behaviour of Conventional Carbon Steel and Corrosion Resistant Reinforcing Bars

A Thesis
Submitted to the College of Graduate Studies and Research
In Partial Fulfillment of the Requirements
for the
Degree of Master of Science
in the
Department of Civil Engineering
University of Saskatchewan
Saskatoon

by
Nedal Mohamed

PERMISSION TO USE

The author has agreed that the library, University of Saskatchewan, may make this thesis freely available for inspection. Moreover, the author has agreed that permission for extensive copying of this thesis for scholarly purposes may be granted by the professors who supervised the thesis work recorded herein or, in their absence, by the head of the Department or the Dean of the College in which the thesis work was done. It is understood that due recognition will be given to the author of this thesis and to the University of Saskatchewan in any use of the material in this thesis. Copying, publication, or any other use of the thesis for financial gain without approval by the University of Saskatchewan and the author's written permission is prohibited.

Requests for permission to copy or to make any other use of material in this thesis in whole or part should be addressed to:

Head of Department of Civil Engineering
University of Saskatchewan
Engineering Building
57 Campus Drive
Saskatoon, Saskatchewan
Canada, S7N 5A9

ABSTRACT

Reinforcing bars (rebars) are used to reinforce concrete structures and are usually made from carbon steel. Due to the relatively poor corrosion resistance of carbon steel, alternative metals with better corrosion resistance have been suggested as alternatives. Type 316LN stainless steel and micro-composite steel (MMFX-2) are among these metals. However, the high cost of these alternative rebar materials and the lack of reliable information regarding the corrosion behaviour of these alloys in concrete have made it difficult to justify their use. The main objective of this research is to provide a quantitative evaluation of the corrosion behaviour of these alloys in synthetic concrete pore solutions. Another objective is to investigate the effect of the presence of chloride ions on Time Domain Reflectometry (TDR) measurements for moisture content inside mortar.

Synthetic concrete pore solutions that emulate solutions in both fresh non-carbonated and carbonated concrete under chloride ion attack were used in this study. Direct current (DC) corrosion evaluation techniques, including open circuit potential measuring, linear polarization and potentiodynamic scans, were used to characterize the corrosion behaviour (in terms of the chloride threshold level and the corrosion currents) of metals under investigation in solutions contaminated with fixed concentrations of chloride ions (from 0.001M to 2M). The total exposure period was seven days. Electrochemical Impedance Spectroscopy (EIS), which is an alternating current technique, was used to study passive film formation on the metal surface in solutions subjected to incremental chloride ion increases from chloride free to 2 M.

The results showed that 316LN stainless has much higher corrosion resistance in these solutions compared to both carbon and micro-composite steels. In both solutions, the chloride threshold of 316LN stainless steel was not reached until a chloride concentration of 2M. In both solutions, the measured corrosion currents ranged between

0.01 and 0.05 μA/cm^2 (corresponding corrosion rates ranged between 0.1 and 0.5 μm/year) after seven days of exposure.

However, micro-composite steel (MMFX-2) performed better than carbon steel. In the fresh concrete pore solution, it was found that the critical chloride threshold of MMFX-2 falls between chloride concentrations of 0.1M and 0.5M. The corrosion current density at 0.1M and 0.5M (Cl^-/OH^- = 0.63 and 3.16) was 0.07 and 0.41 μA/cm^2, respectively. From a durability point of view, the maximum acceptable corrosion current for rebars embedded in concrete is 0.1 μA/cm^2. In the carbonated concrete pore solution, micro-composite steel was able to remain passive at chloride ion concentrations up to 0.1 M, after which the corrosion current increased to 2 μA/cm^2 at 0.5M and 25 μA/cm^2 at 2M.

The findings related to the corrosion behaviour of carbon steel are in good agreement with the published literature. In the fresh concrete pore solution, it was found that the chloride threshold level of carbon steel is 0.05M (Cl^-/OH^- = 0.32). In the carbonated concrete pore solution, carbon steel exhibited very high corrosion currents (i_{corr} = 10-30 μA/cm^2) regardless the amount of chloride in the solution.

Finally, it was found that the presence of the chloride ions with a concentration of 5% of cement weight would cause an overestimation of the measured dielectric constant and consequently the volumetric moisture content, compared to the chloride free samples. The overestimation in the calculated water content was 30% after 3 days of casting, decreasing to 11% after 60 days.

DEDICATION

I would like to dedicate this thesis to my parents for their persistent support of my education through many years of hardship

ACKNOWLEDGEMENTS

I wish to express my deepest gratitude to my supervisors, Dr. Mohamed Boulfiza and Dr. Richard Evitts for their encouragement and endless support throughout the research steps. This research would not have been successfully completed in this form without their advice and support. They always kept a cheerful and welcoming attitude.

Special thanks goes to Mr. Henry Berg and Cam Tarasoff, Engineering shops, Mr. Doug Fisher, Environmental Engineering Laboratory, and Mr. Brennan Pokoyoway, Structural Engineering Laboratory for their help in the experimental work in this thesis.

I also would like to show my gratitude to my family and all of my friends in Canada and Egypt for their infinite emotional support and patience through my hard times until this work came to completion.

Finally, thanks and appreciations are expressed to the University of Saskatchewan and ISIS Research Network for financial support.

TABLE OF CONTENTS

LIST OF TABLES

LIST OF FIGURES

CHAPTER 1
INTRODUCTION

1.1 Background

The durability of concrete structures and their long-term performance have emerged over the last few decades as a primary concern for structural engineers, infrastructure owners, and consumers. Most reinforced concrete structures are expected to last at least 75 years (Pfeifer, 2000). However, problems may start to occur within only a few years, not because of a structural problem, but because of a durability issue. The deterioration of a concrete structure may occur due to many processes, which act individually or synergistically. Some examples of processes that cause material deterioration include alkali aggregate reactivity, sulphate attack, freezing and thawing, and corrosion of reinforcement inside the concrete.

Corrosion of reinforcing bars (rebars) inside concrete is one of the most important phenomenons that reduce the service life of a concrete structure, and it causes a huge load on the maintenance budget of the affected structure. Once initiated, corrosion products, which have higher volume than the parent metal, will accumulate in the space between the rebar and concrete, and since there is insufficient space to accommodate these products, cracking and spalling of the concrete cover will occur. If the rebar cross sectional loss is severe, structural problems may start to occur. Figure 1.1 shows an example of concrete cover spalling due to the corrosion of the reinforcing bars of a beam that supports a bridge superstructure. This sight, although may not be structurally dangerous, is a source of concern to the public. Thus, a repairing process is required.

Figure 1.1 Corrosion of a cross girder that supports the main bridge deck (Thompson and Yunovich, 2003)

In a study funded by the Federal Highway Administration on the cost of the corrosion in the USA, it was found that the annual direct cost of corrosion for highway bridges is approximately $8.3 billion. This cost includes money to replace structurally deficient bridges, for maintenance of the main bridge deck or substructures, and for maintenance and painting of steel bridges (Koch et al., 2001).

In order to avoid such high repair costs, new types of rebars have been developed that are more corrosion resistant than conventional reinforcements. These include rebar made from stainless steels (for example 316LN, 304), micro-composite steel (MMFX-2), epoxy-coated steel, zinc-coated steel and stainless steel clad over carbon steel. However, there are difficulties using some of these materials. For example, when using epoxy-coated steel and stainless steel clad over carbon steel, extra care must be taken when handling and placing the rebars to avoid making holes or defects in the coating or cladding. If defects are caused, the carbon steel may corrode at very high rates. For stainless steel and micro-composite steel, the high initial cost and the lack of information on the corrosion behaviour of these metals in concrete environments (especially Micro-composite steel) may make the use of these materials unattractive.

As will be discussed later, there are two main causes for steel corrosion in concrete: carbonation or chloride ion attack. The first one occurs when the atmospheric carbon dioxide reacts with concrete alkalis, causing a drop in the pH of the concrete pore solution, which reduces its ability to protect steel from corrosion (Broomfield, 1997). The second one occurs when chloride ions diffuse through the concrete cover and attackss the reinforcement directly, inducing very high corrosion rates (Broomfield, 1997). The use of de-icing salts, chloride-contaminated aggregates and the exposure to seawater are the main sources for chloride ions in concrete (Liu, 1996).

1.2 Objectives

A detailed literature review shows that the corrosion behaviour of carbon steel, 316LN stainless steel, and micro-composite steel in concrete pore solution (carbonated and non-carbonated) under chloride ion attack has not been thoroughly investigated. Thus, the objectives of this research are to

- Determine the critical chloride ion concentration in concrete pore solution (carbonated and non-carbonated) that is sufficient to initiate corrosion (chloride threshold level) for carbon steel, micro-composite steel (MMFX-2) and 316LN stainless steel;
- Quantify the effect of gradually increasing the concentration of the chloride ions in the solution on the electrochemical properties of the passive layer formed on the surface of the metals under investigation when immersed in carbonated and non-carbonated concrete pore solution;
- Determine the effect of the change of water content and the degree of pore saturation on the corrosion current of carbon steel in mortar; and
- Determine the effect of the presence of chloride ions on Time Domain Reflectometry (TDR) measurements for moisture content inside mortar.

1.2 Scope and Methodology

This study aimed to investigate experimentally the corrosion behaviour of 316LN stainless steel and micro-composite steel rebars in comparison with conventional carbon steel using a number of different electrochemical techniques. There are two ways to

investigate the corrosion behaviour of rebars in a concrete environment: either rebars are embedded in cast mortar, or concrete or rebar samples are immersed in emulated concrete pore solutions. However, the latter is more preferable due to the elimination of many variables associated with the concrete mix (Hurely and Scully 2002). Based on that, in this research, synthetic solutions were made to emulate both fresh and carbonated concrete environments under chloride ion attack to study the corrosion behaviour of the metals under investigation. The concentrations of chloride ions ranged from 0.001 M to 2 M.

Three different electrochemical techniques were used to determine the critical chloride concentration for corrosion initiation for the metals under investigation as well as their corrosion rates in these solutions. These techniques were Open Circuit Potential measurement $E_{OC,}$ linear polarization LPR test, and potentiodynamic scan. In this experiment, the desired amount of chloride ions was dissolved in the solution before immersing the sample. Corrosion measurements were taken after 1 hour, 24 hours, and 7 days of immersion.

Electrochemical Impedance Spectroscopy (EIS) was used to examine the electrochemical properties of the passive film formed on the surface of the rebar when immersed in the solution. In this experiment, the sample was immersed in the chloride free solution first and then a certain chloride ion dose was added every 24 hours until a maximum limit of 2 M was reached. The EIS test was applied every 24 hours and before adding the next chloride dose.

Since it was not found in the published literature, cyclic polarization scan was applied only on micro-composite steel samples immersed in both solutions with chloride contamination up to 2 M after 24 hours of exposure. In all cases, chloride ions were added in the form of NaCl.

In addition, six carbon steel rebar samples were embedded in mortar and were subjected to a chloride contamination of 5% of cement weight added to the mix in the

form of NaCl. Potentiodynamic scan was applied after 3 days, 7 days, 14 days, 28 days, and 60 days of casting to measure the corrosion current. The change in the water content inside mortar in the same period (60 days) was monitored using the TDR technique. TDR measurements were applied on samples that had the same mix proportions. The degree of pore saturation PS was calculated after measuring the porosity .

Finally, two sets of cement mortar samples, one contaminated with chloride ions by 5% of cement weight and the other was chloride free, were used to examine the effect of the presence of chloride ion on TDR measurements of volumetric moisture content in mortar.

1.4 Thesis Outline

This thesis consists of five chapters, plus references and appendices. Chapter 1 presents an introduction, objectives, scope and methodology of the thesis.

Chapter 2 provides a literature review on the process of steel corrosion inside concrete and its causes, the electrochemical techniques that are used in this study to characterize the corrosion of samples, and an overview on the research done by others regarding the corrosion behaviour of carbon steel, 316LN stainless steel, and micro-composite steel in concrete and solutions emulating concrete. Finally, a brief introduction to the Time Domain Reflectometry (TDR) technique and its use to determine the volumetric water content in porous media (i.e., soil and concrete) will be introduced.

Chapter 3 describes the composition of the solutions and materials used, sample size and shape, sample preparation and testing procedure.

Chapter 4 presents the test results and a detailed discussion of these results, including a comparison between corrosion rates of metals under investigation and their

chloride threshold levels. In addition, results obtained from TDR measurements are presented.

Chapter 5 presents the conclusions of the study.

CHAPTER 2
LITERATURE REVIEW

2.1 Overview of the Problem of Rebar Corrosion inside Concrete

The process of steel corrosion inside concrete is defined as the removal of iron atoms (Fe) from steel and their dissolution in the surrounding water solution, appearing as ferrous ions (Fe^{+2}) (Bentur et al., 1997). Because of this dissolution, steel loses mass, and its cross section becomes smaller. Rust is a result of the corrosion process. For this process to occur, moisture and oxygen must be present, and both of them are available in concrete. However, due to the high alkalinity inside concrete (pH > 13), steel will be able to form a very thin film (~ 10 nm (0.01 μm)) called the passivation layer (Bentur et al., 1997), which acts as a protective coating that prevents the metal from taking part in the corrosion process. Unfortunately, this layer can be disrupted due to either carbonation or chloride ion attack. The chemical reactions are similar for both of them.

The corrosion process actually involves two separate, but coupled, electrochemical reactions that take place simultaneously at two different sites on the steel surface (Broomfield, 1997). These two chemical reactions are known as the anodic and cathodic reactions. The areas on which they occur in the steel are called anodic and cathodic areas or simply anode and cathode. The two reactions are as follows:

Anodic reaction

$$\underset{\text{metallic atoms at the steel surface}}{Fe} \rightarrow \underset{\text{ions dissolved in the solution}}{Fe^{+2}} + 2e^- \qquad [2.1]$$

Cathodic reaction

$$\underset{\text{Dissolved oxygen molecules}}{\tfrac{1}{2} O_2} + \underset{\text{Dissolved ions in the solution}}{H_2O} + 2e^- \rightarrow 2(OH)^- \qquad [2.2]$$

The anodic and cathodic reactions (Eq. 2.1 and 2.2) are only the first step in the process of creating rust. Several more stages must occur for rust to form:

$$Fe^{+2} + 2OH^{-} \rightarrow \underset{\text{Ferrous hydroxide}}{Fe(OH)_2} \quad [2.3]$$

$$4Fe(OH)_2 + O_2 + 2H_2O \rightarrow \underset{\text{Ferric hydroxide}}{4Fe(OH)_3} \quad [2.4]$$

$$2Fe(OH)_3 \rightarrow \underset{\text{Hydrated ferric oxide (rust)}}{Fe_2O_3.H_2O} + 2H_2O \quad [2.5]$$

The hydrated ferric oxide has a volume of three to six times that of the original volume of steel (Broomfield, 1997) and since there is not enough space at the concrete/steel interface, these products will accumulate and cause tension stresses on the concrete cover. Eventually, these stresses will exceed the concrete tensile strength causing cracking and spalling of the concrete cover. Figure 2.1 shows a schematic diagram for the process of steel corrosion inside concrete.

2.1.1 Carbonation

In the case of carbonation, atmospheric carbon dioxide (CO_2) diffuses through concrete and reacts with pore water alkalis according to the following reactions;

$$\underset{\text{Gas}}{CO_2} + H_2O \rightarrow \underset{\text{Carbonic acid}}{H_2CO_3} \quad [2.6]$$

$$\underset{\text{Pore solution}}{Ca(OH)_2} + H_2CO_3 \rightarrow CaCO_3 + 2H_2O \quad [2.7]$$

This consumes reserve alkalinity and reduces the pH of the pore water to the range of 8 to 9, where carbon steel is no longer passive (i.e., the passivation layer will vanish), and

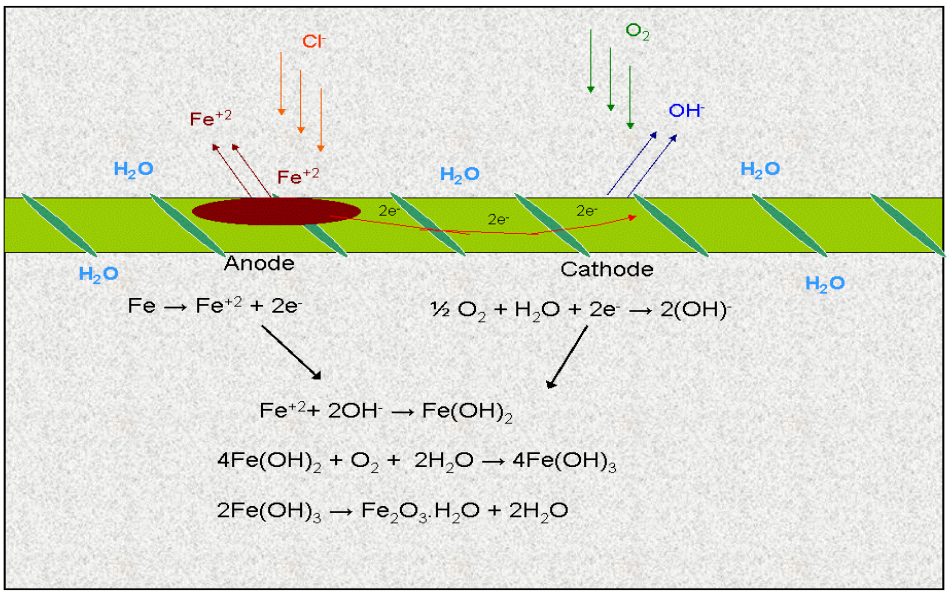

Figure 2.1 Schematic diagram for the process of steel corrosion in concrete (after Brown, 2002)

then it will start to corrode. In other words, carbonation causes deterioration of the passive layer by reducing the concentration of the OH^- ions in the concrete pore water. Thin concrete cover and poor concrete quality increases the risk of carbonation (Gaal, 2004).

Measuring the carbonation depth is done by exposing a fresh (i.e., not exposed to the atmospheric air) concrete surface to an indicator solution (Phenolphthalein in 50:50 alcohol water solution). The solution is colorless, will remain colorless on carbonated areas, and will turn pink on the alkaline sites. A fresh concrete surface can be obtained by coring concrete samples, then cutting or splitting core samples in the laboratory (Broomfield, 1997).

2.1.2 Chloride induced corrosion

Beside carbonation, the steel passive layer in concrete can be disrupted due to the presence of chloride ions that accumulate on the rebar surface until they reach a certain concentration; afterwards, the passivation layer is disrupted. The source of chloride ions could be either external (by using de-icing salts or from seawater in marine environments) or internal (by using contaminated aggregate or using concrete admixtures

that contain chloride). This kind of depassivation is local and is accompanied by a type of corrosion called pitting corrosion. On the contrary, the depassivation by carbonation is general and uniform corrosion will occur on the entire rebar surface. The concentration of chloride ions required to initiate rebar corrosion is called the chloride threshold level (CTL). Chloride threshold level can be expressed either as a percentage of total or free chloride content per cement weight or as a ratio between the concentrations of chloride ion and hydroxyl ion dissolved in the concrete pore water (Cl^-/OH^-).

Some of the chloride content in concrete may be bound either physically or chemically in the concrete matrix. Physical binding happens by chloride adsorption on the surface of silicate hydrate or within the C-S-H gel (Arya and Newman, 1990). Chemical binding happens by the reaction of tri calcium aluminates C_3A with chloride ions to form $3CaO.Al_2O_3.CaCl_2.10H_2O$ (Friedel's salt) (Ann and Song, 2007).

Both total and free chloride content in concrete can be measured through lab testing. Firstly, core samples are taken from different depths and then ground. To determine the free chloride content (water-soluble chlorides), concrete dust is boiled in water and then the chloride concentration can be determined using a chloride sensitive electrode. This process is described in ASTM standard C1218. To determine the total chloride content (acid-soluble chlorides); a chemical analysis (titration) has to be applied on concrete dust. The process is described in ASTM standard C1152. Then the total or free chloride content is expressed as a percentage of cement weight.

There is a disagreement among researchers regarding the role of bound chloride in the process of rebar corrosion inside concrete. Some insist that bound chloride ions are not movable and will not reach the rebar surface and thus bound chlorides should not be accounted for when calculating the chloride threshold level (Hope et al. 1985 and Castellote et al., 2000). Others argue that there is a risk of freeing bound chloride after the pH of concrete drops due to depassivation or carbonation (Glass et al., 2000). Thus, it has been suggested that the use of Cl^-/OH^- ratio is more appropriate as it represents the competitive action of both ions and it is not affected by the cement type (Castellote et al.,

2000). The most common method used for determination of the Cl^-/OH^- ratio is by titration of extracted concrete pore solution. Concrete pore solution can be squeezed out of concrete or mortar samples by applying high pressure (up to 375MPa) on samples confined in a cylindrical pressure vessel (Barneyback and Diamond, 1981 and Page and Vennesland, 1983). This method was used by Page and Vennesland (1983); Huessian et al. (1995); Alonso et al. (2000); Izquierdo et al. (2004) and many other researchers. However, this method for measuring Cl^-/OH^- has been criticized, as it is expensive and difficult to conduct. Recently, new methods that are based on chemical leaching have been used to extract the free chloride content in the liquid phase. While Chaussadent and Arliguie (1999) suggested the use of demineralised water at 20^o C as a solvent, Castellote et al. (2000) used an alkaline solution of 0.3 M NaOH (pH of 13.5).

2.1.3 Prediction of the service life of an RC structure subjected to corrosion of reinforcement

The total service life of a reinforced concrete member subjected to corrosion of reinforcement is considered to be the sum of two phases: the initiation phase and the propagation phase, as shown in Figure 2.2. This model was first introduced by Tuutti (1982). The initiation phase is the time required by chloride ions to penetrate the concrete cover and accumulate on the rebar surface until the critical limit is reached, or the time needed for the carbonation front to reach the rebar level, after this time, corrosion of the embedded rebar will start. The time elapsed in this phase is dependant on the chloride threshold level of the reinforcement material and its ability to remain passive when the pH of the surrounding environment drops due to carbonation. In addition, the initiation phase is dependant on the rate of transportation of the aggressive species through the concrete cover. The propagation phase is the time needed by corroding rebars to cause cracking and spalling of the concrete cover. Thus, the propagation phase is dependant on the corrosion rate of the metal, and the thickness and properties of the concrete cover.

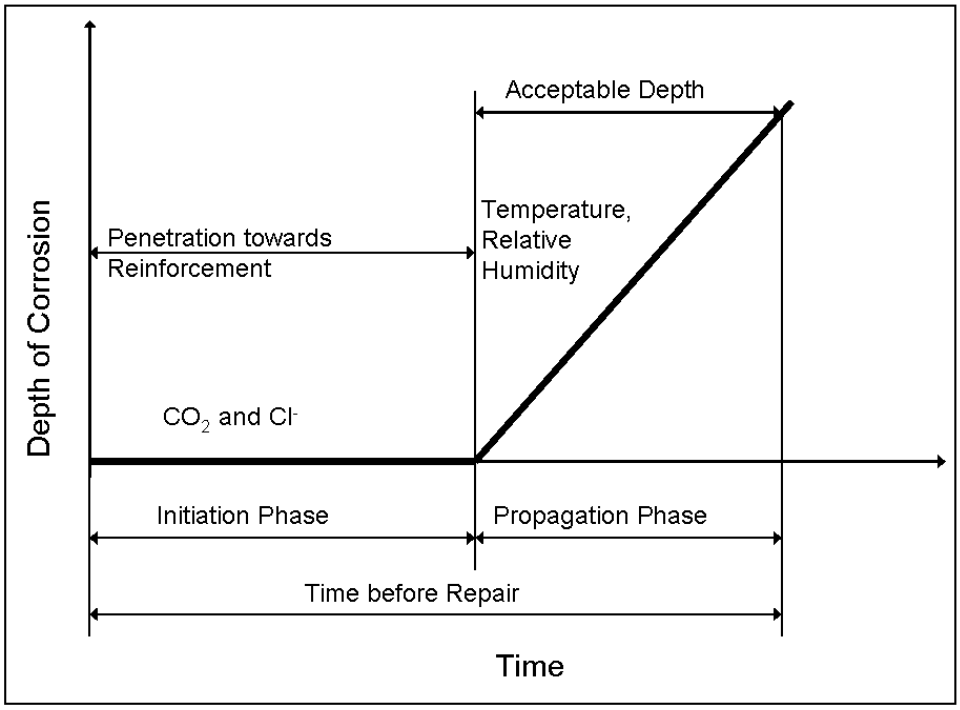

Figure 2.2 Schematic of Tuutti's (1982) model of the consequent phases of steel corrosion inside concrete (redrawn after Liu, 1996)

2.2 Kinetics of Corrosion

When a metal M is immersed in a solution that contains its own ions M^{+n}, two processes occur simultaneously; the oxidation of the metal atoms and the reduction of the ions in the solution:

$$M^{+n} + ne^{-} \underset{oxidation}{\overset{reduction}{\rightleftharpoons}} M \qquad [2.8]$$

At equilibrium, the rate of reduction i_{red} equals the rate of oxidation i_{ox}, so that all the free electrons are consumed. The exchange current density i_o is the rate of oxidation or reduction at equilibrium. The reaction in Equation [2.8] is referred to as the half-cell reaction and it has a certain potential that is called the half-cell potential $e_{M^{+2}/M}$. Equation [2.9] is the general equation for the half-cell reaction:

$$aA + mH^+ + ne^- = bB + dH_2O \qquad [2.9]$$

where A and B are the corrosion product and the metal respectively.

H^+ is the hydrogen ion

n is the number of electrons exchanged

a, b, m, n are the stoichiometric coefficients

The half-cell potential of that reduction/oxidation reaction $e_{M^{+2}/M}$ can be calculated using the Nernst equation:

$$e = e^0 - \frac{RT}{nF} \ln \frac{(B)^b (H_2O)^d}{(A)^a (H^+)^m} \qquad [2.10]$$

where e^0 is the potential of the half cell reaction at the standard state (i.e. 1 molar solution at 1 atmospheric pressure)

R is the gas constant

T is the absolute temperature

F is Faraday constant

(A) is the concentration of A in the solution, and it is called the activity

Both the exchange current density i_o and the standard half-cell potential e^0 are metal parameters, and can be measured experimentally.

When a metal is corroding (immersed in a corrosive solution, e.g. an acid solution) the reaction in Equation [2.8] goes in the reverse direction (oxidation) and is called the anodic reaction. Since the whole system has to be in equilibrium, the liberated electrons are consumed up by another reduction reaction referred to as the cathodic reaction. An example of the cathodic reaction is the oxygen reduction (see Equation 2.2). The cathodic reaction has a half-cell potential and an exchange current density of its own. Since the two potentials of the two half-cells cannot exist on the same surface, each one of them must change potential (polarize) to an intermediate potential named the corrosion

potential E_{corr} or the open circuit potential E_{OC} (Jones, 1996). At E_{corr}, the rate of oxidation i_{ox} and reduction i_{red} is the same and is equal to the corrosion current $i_{corr.}$ ($i_{corr} = i_{ox} = i_{red}$). Figure 2.3 shows the corrosion potential E_{corr} and the corrosion current i_{corr} of iron Fe in acid solution. Both half-cell potentials will change according to Equations 2.11 and 2.12 until they equal E_{corr}:

$$\eta_a = \beta_a x \log \frac{i_a}{i_o} \qquad [2.11]$$

$$\eta_c = \beta_c x \log \frac{i_c}{i_o} \qquad [2.12]$$

where η_a and η_c is the extent of anodic or cathodic polarization ($E - E_{corr}$)

β_a and β_c are constants known as the anodic and cathodic Tafel slopes, respectively

i_a and i_c are anodic and cathodic current density, respectively

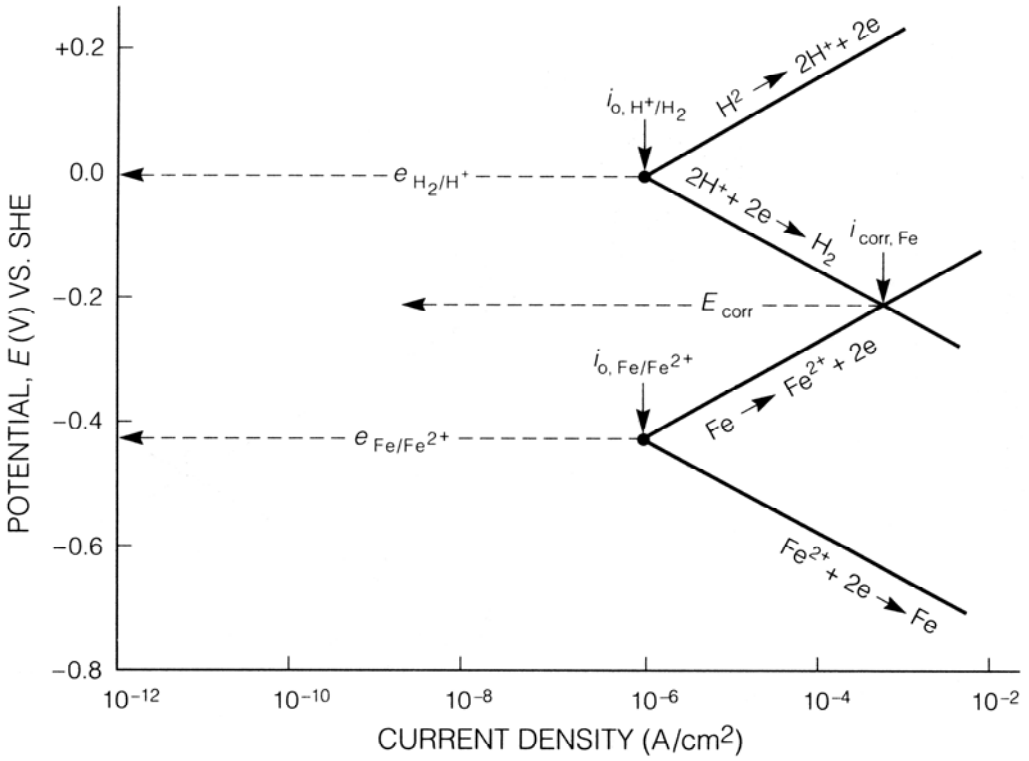

Figure 2.3 The mixed potential E_{corr} and the corrosion current i_{corr} of iron Fe in acid solution (Jones, 1996)

2.3 Corrosion Detection Techniques

Since corrosion is an electrochemical process that involves charge (electrons) transfer through an electrolyte (concrete pore solution), different electrochemical techniques can be employed to evaluate the state of a specimen from a corrosion point of view. These techniques were developed and have been used for lab measurements; however, civil engineers managed to adapt a number of them to be used in field applications. The following section provides an explanation of electrochemical techniques that were used in this study.

2.3.1 Open circuit potential (half cell measurements) E_{OC}

The open circuit potential of a metal is a measure of its tendency to corrode. It is measured in Volts against an electrode that has a predetermined potential. This electrode is referred to as the Reference Electrode. The most common Reference Electrode that is used in corrosion studies in the laboratory is the Saturated Calomel Electrode (SCE), which has a potential of +242 mV vs. the Standard Hydrogen Electrode (SHE) (assumed potential of 0.0 V) at room temperature. The more negative the potential, the higher the metal tendency to corrode. The electrochemical potential of a metal in a certain solution is dependant on the type of the metal, the composition of the solution and its pH, oxygen content, and temperature (Prukner, 2001).

This technique can be used in the field to investigate the state of rebars embedded in concrete. Guidance for interpretation of results is given in ASTM standard C876-91 and is summarized in Table 2.1. Figure 2.4 shows the use of a copper/copper sulphate half-cell as the Reference Electrode in measuring the free corrosion potential of reinforcement inside concrete (Liu, 1996).

Hausmann (1967) and Li and Sagues (2001) used a sudden drop in the open circuit potential E_{OC} of samples immersed in concrete pore solutions as a sign of corrosion initiation and that the chloride threshold level was reached.

Table 2.1 ASTM criteria for corrosion of steel in concrete using different standard half-cells (Broomfield, 1997)

Copper/Copper Sulphate	Silver/Silver Chloride	Standard Hydrogen Electrode	Calomel	Corrosion condition
> -200 mV	> -106 mV	> +116 mV	> -126 mV	Low (10 % risk of Corrosion)
-200 to -350 mV	-106 to -256 mV	+116 to -34 mV	-126 to -276 mV	Intermediate corrosion risk
< -350 mV	< -256 mV	< -34 mV	< -276 mV	High (< 90% risk of corrosion)
< -500 mV	< -406 mV	< -184 mV	< -426 mV	Severe corrosion

2.3.2 Potentiodynamic scan and cyclic polarization

The potentiodynamic scan is used to examine the overall corrosion behaviour of a system and to predict the corrosion current density i_{corr} of a metal in a certain environment. In a typical potentiodynamic scan, the potential E is swept over a pre-

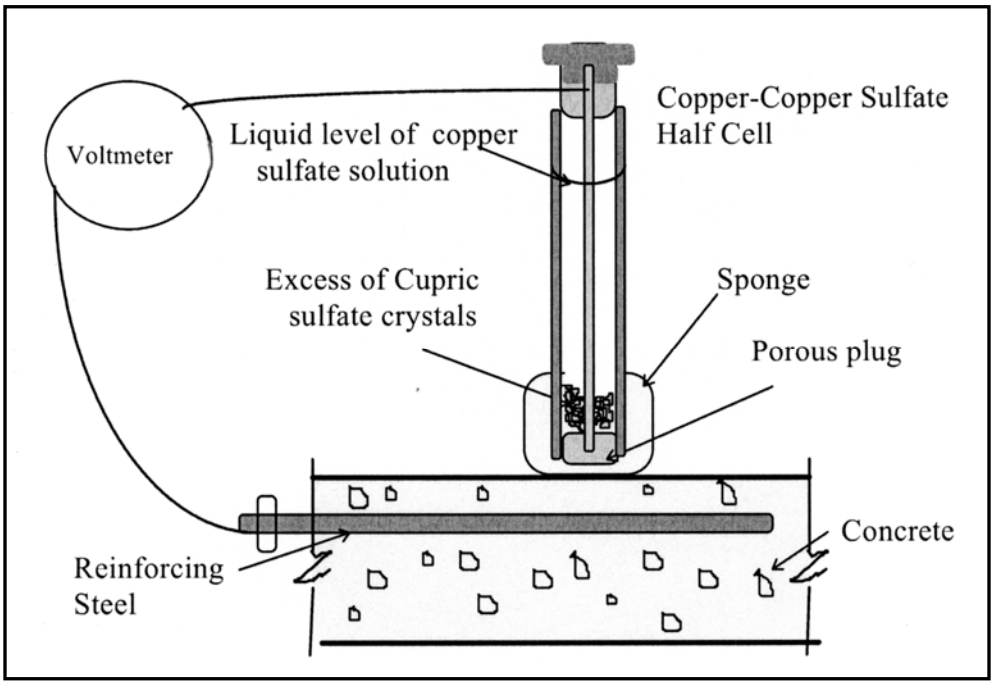

Figure 2.4 The use of a Copper/Copper Sulphate electrode in measuring E_{OC} in the field (Liu, 1996)

determined range and the induced current is recorded. The graphical output of a potentiodynamic scan is referred to as Evans diagram, which is a plot of the potential (E) versus the logarithm of the current density (log i). To allow several tests to be performed on one sample (i.e., non-destructive test) the scan range has to be within the Tafel region (i.e., scan range between 150 mV ± E_{OC}). Applying too much anodic potential will force the sample to corrode (i.e. destructive testing). The expected corrosion current density for the tested metal in this particular solution i_{corr} can be estimated from the intersection of the open circuit potential E_{OC} and the extrapolation of the Tafel region (see Figure 2.5).

Knowing the corrosion current density i_{corr}, the corrosion rate, CR, or the rate of thinning can be calculated using Eq. [2.13]:

$$CR = \frac{i_{corr}.EW}{F.\rho} \qquad [2.13]$$

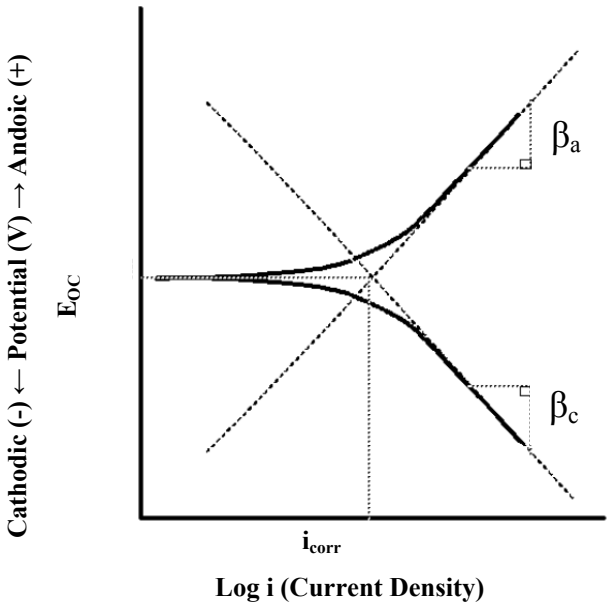

Figure 2.5 Typical potentiodynamic scan (Enos and Scribner, 1997)

where EW is the theoretical mass of metal that will be lost from the sample after one Faraday of anodic charge has been passed (EW = atomic weight/valence)

F is the Faraday constant = 96485 coulomb/mole

ρ is the metal density [g/cm^3]

Goni and Andrade (1990), Glass and Buenfeld (1997), Alonso et al. (2002), Dehwah et al. (2002) and Mohammed and Hamada (2006) used a limit of 0.1- 0.2 $\mu A/cm^2$ for corrosion current density to identify the initiation of active corrosion and hence the chloride threshold. This criterion has the advantage of providing quantitative information about the actual loss of the rebar cross section. The limit of i_{corr} = 0.1- 0.2 $\mu A/cm^2$ or corrosion rate of 1.16-2.32 μm/year (for carbon steel) is not considered too small or too conservative to be used as a separating limit between passive and active state for steel inside concrete for a couple of reasons. Firstly, this corrosion current is measured only at the surface of the metal and it was found that the penetration rate at the bottom of the corrosion pit is 10 times higher than the top (Gonzalez et al., 1995 and Alonso et al., 2000). Secondly, from a durability point of view, the accumulation of corrosion products is the main concern not the loss in the rebar cross section. Gonzalez et al. (1995) reported that the amount of iron oxide generated during the corrosion of 10-50 μm of metal (depending on rebar diameter) is enough to crack a concrete cover of 2-3 cm. This means that many concrete covers will be cracked after 1-3 years because of corrosion rates of only 10-30 μm/year (Gonzalez et al., 1995). Similarly, Pfeifer (2000) reported that the concrete cover would crack when 25 μm of the steel surface corrodes. Thus, at corrosion rate of only 1 μm/year, cracking and spalling of the concrete cover will occur after 25 years, which is considered a relatively short service life for a reinforced concrete structure.

The difference between the potentiodynamic scan and the cyclic polarization test is that in the latter, the applied anodic overpotential has to be high enough to ensure initiation of pitting corrosion, as the test is used mainly to investigate the metal's tendency to pitting corrosion in a certain environment. Once the predetermined anodic potential limit E_{rev} is reached, the direction of the scan is reversed towards the cathodic

direction until the final predetermined potential is reached. The pitting potential E_{pit} is the potential at which the induced current sharply increases. The potential where the loop closes on the reverse scan is called the protection potential E_{prot}, below which no pitting corrosion is expected to occur. If the protection potential E_{prot} is more positive than the pitting potential $E_{pit,}$ there will be no tendency to pit. If E_{prot} is more negative than E_{pit}, pitting could occur. Generally, the size of the hysteresis loop is an indication of the metal's tendency to pit, the larger the loop, the greater the tendency to pit. Figure 2.6 shows a graphical output of a cyclic polarization scan.

In order to apply the potentiodynamic scan or the cyclic polarization scan, three electrodes are immersed in the testing solution and connected to a potentiostat (a machine that is used to apply overpotential and record the induced current or visa versa). These electrodes are the working electrode, which is the tested sample itself, the counter electrode, which is used to deliver the current to the working electrode and to close the electrical circuit, and finally the reference electrode, which is used to measure the potential difference.

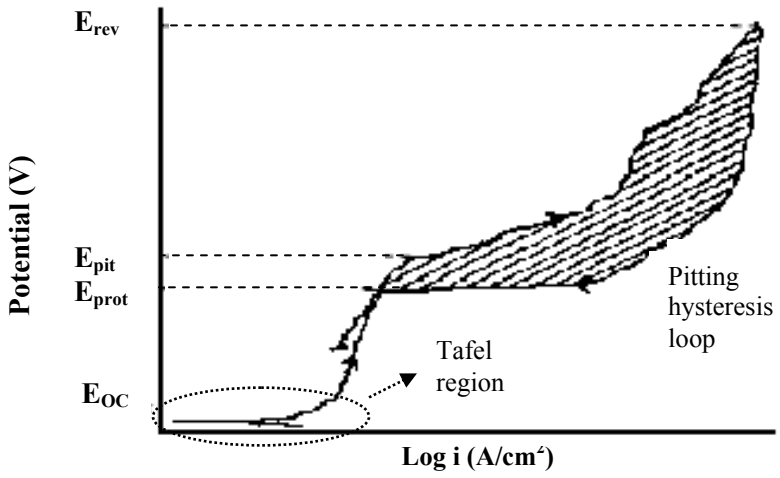

Figure 2.6 Cyclic polarization test (Esmaeilpoursaee 2007)

The experiment is computer controlled and the data acquisition and analysis is done using software that is provided by the manufacturer. Potentiodynamic scan and cyclic polarization are used exclusively in lab measurements.

2.3.3 Linear polarization resistance

The linear polarization resistance measurement is a non-destructive technique that can be used in both lab and field measurements. It was first introduced by Stern and Geary (1957). In this method, overpotential in the range of 25 mV about E_{OC} (the open circuit potential of the sample) is applied and the induced current is recorded. Since the applied voltage is small, the current response will be linear (see Figure 2.7). The corrosion current density is given by the following Stern-Geary equation (Stern and Geary, 1957):

$$i_{corr} = \frac{B}{R_P} \qquad [2.14]$$

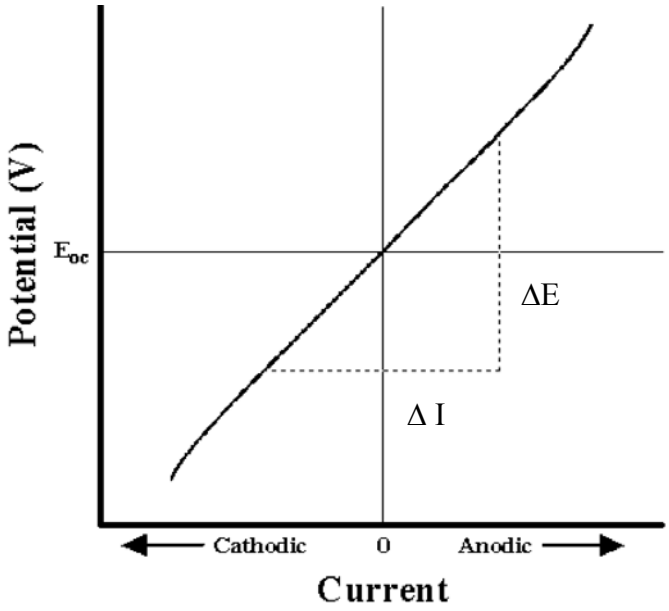

Figure 2.7 Linear polarization resistance LPR (Enos and Scribner, 1997)

where i_{corr} is the corrosion current density, [$\mu A/cm^2$]

R_P is the polarization resistance (The slope of the linear portion of the

curve $R_P = \frac{\triangle E}{\triangle I}$), [KΩ.cm^2]

B is Stern-Geary constant ($B = \frac{\beta_a.\beta_c}{2.303(\beta_a + \beta_c)}$ where β_a, β_c are the anodic and cathodic Tafel slopes)

Similar to the potentiodynamic scan and cyclic polarization, in order to conduct the linear polarization resistance test, three electrodes have to be attached to a potentiostat. These are the working electrode, the counter (auxiliary) electrode and the reference electrode. Figure 2.8 shows a schematic for the linear polarization resistance test for a steel sample embedded in concrete.

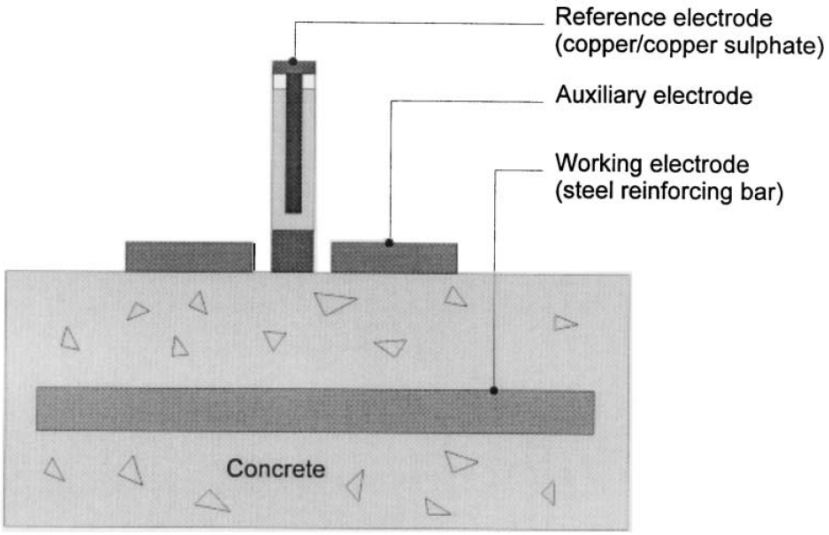

Figure 2.8 Schematic for the three electrodes linear polarization resistance (LPR) measurements [Millard et al., 2001]

Trejo and Pillai (2003) and (2004) and Qian et al. (2008) used the sudden increase in the inverse of polarization resistance ($1/R_P$) as an indication that the sample was corroding actively and the chloride threshold level had been reached.

2.3.4 Electrochemical impedance spectroscopy EIS

In this technique, an AC (Alternated Current that changes its magnitude and direction with time according to a certain function; i.e. sinusoidal function) overpotential with varying frequencies is applied to the sample and the induced current response is measured. The impedance (the opposition that faces the AC current) is then automatically

calculated from this data. The AC voltage excitation should be small (a few mV rms) to keep in the linear region and not to destroy the sample. In the linear region, the induced AC current will have the same frequency as the original AC voltage excitation, but with a phase shift and different amplitude. Impedance is a complex quantity that contains real and imaginary parts and has the same units as Resistance (Ohms). The following equation is used to calculate the impedance, Z:

$$Z = \frac{E(t)}{I(t)} = \frac{E_o * cos(\omega t)}{I_o * \cos(\omega t - \varphi)} = Z_o \frac{cos(\omega t)}{\cos(\omega t - \varphi)} \qquad [2.15]$$

where E (t) is the potential at time t,

E_o is the amplitude of the potential signal

ω is the radial frequency

I (t) is the current at time t,

I_o is the amplitude of the current signal

φ is the phase shift between potential and current

From the above, impedance, Z, can be expressed as a complex number:

$$Z = Z_o.\exp(j.\varphi) = Z_o(\cos\varphi + j.\sin\varphi) \qquad [2.16]$$

where j is the square root of (-1).

A plot of the real part of the Impedance on the X-axis and negative the imaginary part on the Y-axis is referred to as a Nyquist plot. The impedance is represented as a vector of length |Z| and the angle between the vector and X-axis, which is the phase φ. Each point represents the Impedance at a particular frequency; however, the value of that frequency cannot be extracted from the plot. In a Nyquist plot, low frequency data are on the right side of the plot and higher frequencies are on the left. This is true for EIS data where impedance usually falls as frequency rises (GAMRY Instruments user's manual, 2005).

The curve has to be modelled and fitted with an equivalent circuit model that is representative of the ongoing electrochemical processes at the interface. Afterwards, various parameters can be determined using the modelled data (i.e. solution resistance, double layer capacitance and charge transfer resistance). Figures 2.9 and 2.10 show an example of a Nyquist plot and Randles circuit, which is used for modelling the curve, respectively.

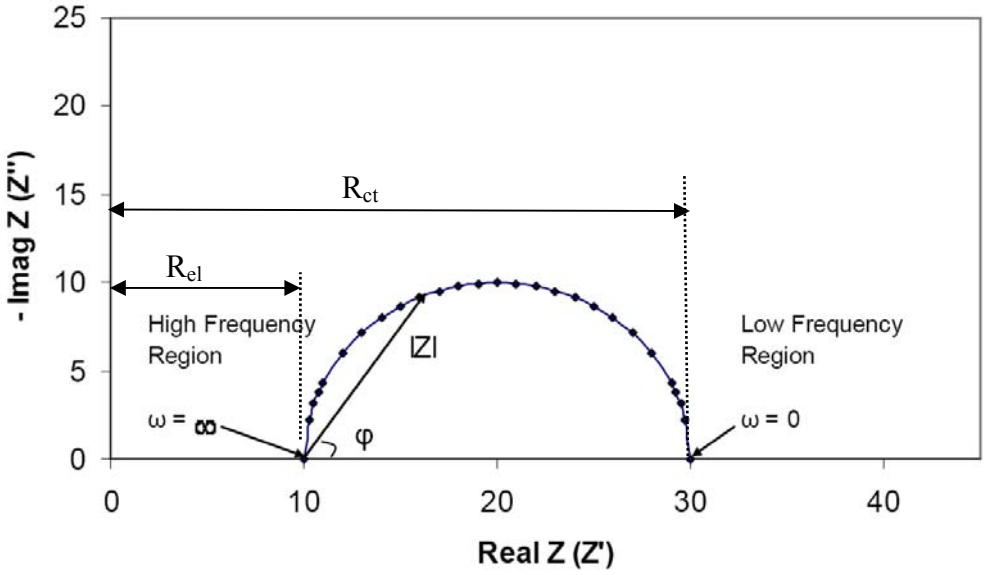

Figure 2.9 Nyquist plot (Parakala, 2005)

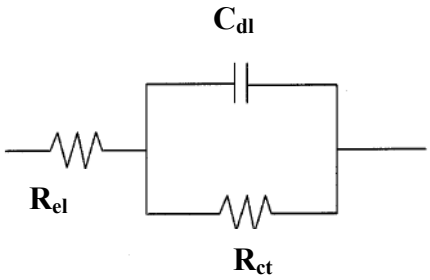

Figure 2.10 Randles Circuit

The modelling circuit consists of an ohmic resistance R_{el} connected in series to a loop that consists of a capacitor C_{dl} and another resistance R_{ct} connected in parallel. The resistance R_{el} illustrates to the solution/electrolyte resistance. The capacitance C_{dl} and the

second resistance R_{ct} illustrate to the double layer capacitance and the charge transfer resistance, respectively. To clarify when a metal is immersed in an aqueous solution, two electrochemical phenomena are expected to occur. The first one is the charge transfer resistance, which controls the speed of metal dissolution into the electrolyte. The second phenomenon is referred to as the double layer. The term double layer refers to the formation of two layers of water molecules on the metal/electrolyte interface that prevents the close approach of dissolved ions from the bulk solution (Jones, 1996). The first layer is water molecules that are attracted to the negatively charged (free electrons) metal surface. The second layer is water molecules that are attracted to the charged ions (cations) in the solution (see Figure 2.11). This structure behaves experimentally as a charged capacitor (Jones, 1996).

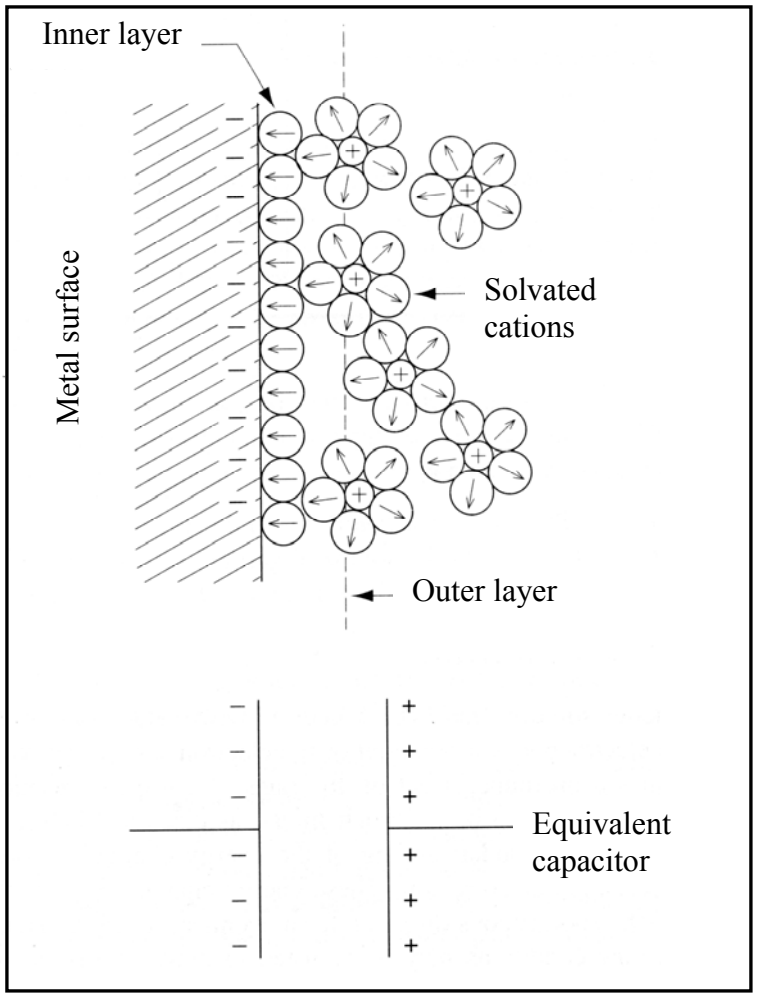

Figure 2.11 Schematic of the double layer phenomenon and its electrical equivalent (Jones, 1996)

2.4 Review of Previous Research Conducted on Metals under Investigation

2.4.1 Carbon steel

As mentioned earlier, the chloride threshold level CTL is defined as the concentration of chloride ions on the rebar surface required to initiate rebar corrosion (Broomfield, 1997). While most researchers agree on that definition, a unique accepted value for it has not yet been established (Hurley, 2007). The fact that concrete itself is not a homogenous material and its properties can vary very widely with the change in its components and their proportions in the mix (such as type and amount of cement, water/cement ratio, method and period of curing and addition of cementious materials) precludes the existence of a unique value, particularly when expressing this value as a percentage of cement weight. Thus, many researchers are inclined to use well-controlled synthetic solutions to emulate concrete environment and prefer to use the Cl^-/OH^- parameter as an indication of chloride threshold level. Less scattered results and more repeatable data are obtained when using this parameter (Hurley, 2007).

Hausmann (1967) was the first to use the fully saturated $Ca(OH)_2$ solution (pH 12.6) to emulate a concrete environment in studying the corrosion behaviour of steel in concrete. Since then, many researchers have used the same solution in their work (Ishikawa et. al., 1968; Gouda and Halaka, 1970; Andrade and Gonzalez, 1977; Vrable and Wilde, 1980 and Lopez, 1993). However, the analysis of the extracted concrete pore solution shows that it has an extremely low content of calcium hydroxide (Page and Vennesland, 1983 and Corbo and Farazam, 1989) and it consists mainly of potassium and sodium hydroxides. Corbo and Farazam (1989) stated clearly, *"Concentration of calcium ions decreased drastically with time and became nil after 14 days of curing"*. The same conclusion has been reached by Marchand et al. (2001). Therefore, the use of a solution that is a mix of potassium and sodium hydroxides is considered more representative of the concrete pore solution than the fully saturated calcium hydroxide solution. Table 2.2 shows the results of the concrete pore solution analysis conducted by Marchand et al. (2001) for a cement paste that had a water/cement ratio of 0.4.

Table 2.2 Pore solution composition for a concrete mix of water/cement ratio of 0.4 [Marchand et al. 2001]

Ion	W/C=0.40 (m Mole)
Hydroxyl, OH^-	700
Sodium, Na^+	192
Potassium, K^+	592
Sulphate, SO_4^{-2}	44
Calcium, Ca^{+2}	2

Studying the corrosion behaviour of carbon steel in synthetic concrete pore solutions started as early as 1967 (Hausmann, 1967 and 1968) and is still in progress until now (Hausmann, 2007; Qian et al. 2008 and Freire et al. 2009). Most of the existing research generally agrees that the Cl^-/OH^- threshold ratio for carbon steel is < 1 (Alonso et al., 2000 and Hurley, 2007). However, much higher chloride threshold values have also been reported. The primary reason is the lack of agreement on a unique technique to be used and polarization potential to hold the sample at (potentials ranged from +1050 mV to -600 mV vs. SCE) (Alonso et al., 2002). Recently, Veleva et al. (2002 and 2005) found that the passive layer that formed naturally under open circuit potential is more protective than those formed under anodic polarization; besides it has the additional advantage of being more natural (Veleva et al., 2002 and 2005). Table 2.3 shows a summary of available literature on chloride threshold level (CTL) of carbon steel in artificial concrete pore solutions (adapted after Alonso et al. 2002) and indicates the change of the obtained CTL with the change of the technique and polarization potential used.

In addition, the effect of mill scale removal on the corrosion resistance of carbon steel in concrete and synthetic concrete pore solutions has been studied (Mammoliti et al., 1996; Hou et al., 1997; Alonso et al., 2000; Li and Sagues, 2001; Pillai and Trejo, 2005; Poursaee and Hansson, 2007 and Hurley, 2007). While some contradictions can be spotted in their findings, they all agreed that the effect of mill scale removal is not

significant. Hou et al. (1997) found that sand blasting slightly decreased the corrosion current density for rebars embedded in concrete samples (from 1.4 $\mu A/cm^2$ to 1.0 $\mu A/cm^2$ after five weeks). Alonso et al. (2000) found no significant difference in corrosion current density between ribbed (as received) and mechanically smoothed- mill scaled rebars. On the contrary, Mammoliti et al. (1996) reported that the ribbed rebars have lower corrosion rates than mechanically smoothed-mill scaled rebars. Li and Sagues (2001) reported a slightly higher Cl^-/OH^- threshold ratio for sand blasted rebars ($Cl^-/OH^- = 0.6$) than as received rebars ($Cl^-/OH^- = 0.3$). Pillai and Trejo (2005) found that mill scale removal and polishing is beneficial for ASTM A706 carbon steel (chloride threshold level increased from 0.2 to 0.3 kg/m^3) and harmful for ASTM A615 (chloride threshold level decreased from 0.5 to 0.3 kg/m^3). Poursaee and Hansson (2007) stated that although the as- received rebars showed higher corrosion rates than the sand blasted ones; *"the difference was neither significant nor persistent"*. This conclusion was also supported by Hurely (2007). Moreover, Hurely (2007) found that the corrosion products in both cases were nearly identical.

The performance of carbon steel in solutions emulating carbonated concrete has been investigated also. According to Anstice et al. (2005), the pore solution of carbonated concrete consists of sodium, potassium and calcium carbonates and bicarbonates in low concentrations. Alonso and Andrade (1989) found that carbon steel will be passive in high concentrated solutions of Na_2CO_3 and $NaHCO_3$ and these solutions will act as corrosion inhibitors if their concentrations are high enough. They suggested a concentration of 0.1M and 0.01M for $NaHCO_3$ and Na_2CO_3, respectively, to be the limit between activity and passivity of steel immersed in them (Alonso and Andrade, 1989). They found that the corrosion current of carbon steel immersed in solutions that had low concentrations of $NaHCO_3$ and Na_2CO_3 was about $10\mu A/cm^2$. Moreno et al. (2004) reported the same i_{corr} value and they found that the addition of Cl^- ions to the solution (up to 0.1 %) had no effect on the corrosion current density.

Table 2.3 Summary of available literature on testing carbon steel in synthetic concrete solutions (adapted after Alonso et al. 2002)

Reference	Emulated concrete pore solution	Electrochemical technique	Polarization potential mV vs. SCE	Threshold Cl^- M/L	Threshold Cl^-/OH^-
Hausmann, (1967)	$Ca(OH)_2$ (pH12.5), NaCl, NaOH (pH 13.2)	Measurement of E_{corr}	-50 to -230, -185	< 0.1	0.5- 1.08, 0.83
Hausmann (1968)	$Ca(OH)_2$ (pH12.5), NaCl	Potentiostatic	-125, -325, -375, -400, -425	0.02, 0.08, 0.15, 0.35, 0.65	0.5, 2, 3.75, 8.75, 16.25
Ishikawa et al. (1968)	$Ca(OH)_2$ (pH 12.5) KCl	Potentiostatic	-400 to -500	0.08-0.6	2 - 15
Gouda and Halaka (1970)	NaOH (pH 11.9), $Ca(OH)_2$ (pH12.1), NaOH (12.6), NaCl	Galvanostatic	-200, -300 to -450, -100, -500, -600	0.02, 0.05- 0.1, 0.1, 0.15, 0.2	4, 4.1- 8.33, 2.5, 3.8, 5
Pourbaix (1972)	NaOH +NaCl (pH 12) (pH13) (pH 14)	Potentiodynamic	+1050, +125, -140, +230, -80, +400, +0	0.01, 0.1, 1, 0.1, 1, 0.1, 1	1, 10, 100, 1, 10, 0.1, 1
Andrade and Gonzalez (1977)	$Ca(OH)_2$+ NaCl (pH 12.5)	Potentiodynamic Galvanostatic Potentiostatic	+600 to +60, -210 to +250, +600 to +290, -140, +20 to +40	0.01, 0.1	1, 10
Vrable and Wilde (1980)	$Ca(OH)_2$+NaCl (pH 12.5)	Potentiodynamic	-175, -275, -350, -600	0.5, 1, 3, 6	16.66, 30, 100, 200
Alvarez and Galvele (1984)	NaOH + NaCl (pH 12- 10)	Potentiostatic	-80, -100, -120, -60, -22	1, 0.1, 0.01	100, 10^3, 10^4, 10^3, 100

Reference	Emulated concrete pore solution	Electrochemical technique	Polarization potential mV vs. SCE	Threshold Cl^- M/L	Threshold Cl^-/OH^-
Goni and Andrade (1990)	$Ca(OH)_2$ + KOH (pH 12 to 13.2) NaCl, $CaCl_2$	Potentiodynamic	+500, +100, +150, 0, -100, -200 to -300	0.75, 0.5, 0.75, 0.5, 0.5, 0.75, 0.75 to 0.5	1.8, 1.2, 4.5, 2.9, 8, 12.3, 13.5, 19.2, 12.6
Lopez (1992)	$Ca(OH)_2$ (pH 12.5), NaCl	Potentiodynamic, Potentiostatic, Galvanostatic	-300 to -400, -200 to -400, -100 to -375, +0 to -275, +100 to -200, +300 to -150	1, 0.25, 0.1, 0.025,0.01, 0.001	33, 8.3, 3.3, 0.83, 0.33, 33, 8.3, 3.3, 0.033
Guilbaud et al. (1994)	NaOH, KOH, (pH 13.1) $CaCl_2$	Potentiostatic	-450	_	2
Gutierrez (1995)	$Ca(OH)_2$ (pH 12 to 12.6) NaCl	Potentiostatic	0, -100, -150, -200, -250, -300	0.023,0.072, 0.016, 0.016, 0.023, 0.220, 0.01, 0.03, 0.4, 0.5, 0.013, 0.142, 0.097	0.03, 0.23, 0.02, 0.06, 0.23, 1.37, 0.12, 0.4, 1.6, 2, 0.05, 0.42, 0.54
Bertolini et al. (1996)	$Ca(OH)_2$, NaCl	Potentiodynamic	+350, +100, -100	0.4, 1, 2 % in sol.	_
Mammoliti et al. (1996)	$Ca(OH)_2$ (pH 12.5), NaCl	Potentiodynamic	+450 to -250, +500 to -100	1- 5% in sol., 3- 7% in sol.	_
Li and Sagues, (2001)	$Ca(OH)_2$ (pH 12.6), NaOH + KOH (pH 13.3)(pH 13.6), NaCl	Measurement of E_{corr}	-100 to -500 -100 to -500 -150 to -350	0.01 0.2 1	0.25 1 2.5

Reference	Emulated concrete pore solution	Electrochemical technique	Polarization potential mV vs. SCE	Threshold Cl^- M/L	Threshold Cl^-/OH^-
Saremi and Mahallati (2002)	$Ca(OH)_2$ (pH 12.3), NaCl	Potentiodynamic	up to +700	-	0.6
Hurley (2007)	$Ca(OH)_2$ (pH 12.6), NaCl	Potentiodynamic Potentiostatic	+200 +200	0.01 0.01 – 0.015	0.25 0.25-0.34

2.4.2 316LN stainless steel

316LN is a type of stainless steel that belongs to the Austenitic family that has high chromium (Cr ~ 18%) and nickel (Ni ~ 10%) contents with low carbon content (C < 0.15 %). The letter "L" means low carbon content (C =0.03%), while the letter "N" means nitrogen addition (Beddoes, 1999).

Research on the behaviour of stainless steel rebars immersed in synthetic solutions emulating concrete under chloride ion attack or carbonated concrete started in the mid 1990s (Pernice et al., 1994 and Bertolini et al., 1996) and is still going on until now (Bautista et al., 2009). The main conclusion of all the studies is that 316LN stainless steel has a much higher corrosion resistance than carbon steel and breaking its passivity will require very high Cl^-/OH^- that is not practically expected in concrete structures. Table 2.4 shows a summary of the available literature on testing stainless steel in synthetic concrete solutions.

The effect of mill scale removal on the corrosion resistance of 316LN stainless steel has been studied recently (Pillai and Trejo, 2005 and Hurely, 2007); however, they reported opposing results. While Pillai and Trejo (2005) found that mill scale removal and polishing will significantly decrease the chloride threshold level of 316LN stainless steel (from 10.8 Kg/m^3 to 6.9 Kg/m^3), Hurley 2007 reported a Cl^-/OH^- threshold ratio of 0.49 for 316LN stainless steel with the mill scale intact and 24.9 for acid washed (to rem-

Table 2.4 Summary of available literature on testing Stainless Steel in synthetic concrete solutions

Reference	Specimens	Testing Environment	Used techniques	Results
Pernice et al. (1994)	CS, 304 and 316 SS bar	Saturated $Ca(OH)_2$ solutions with up to 125 mg/l Cl^- added	E_{OC} measurements, Potentiodynamic Scans and Critical Pitting Potential tests	No corrosion occurred on both 304 and 316 SS
Bertolini et al. (1996)	Type 304, 304L, 410, duplex 23Cr4Ni SS and CS- bar surface polished	Saturated $Ca(OH)_2$ (pH 12.5), 0.9M NaOH (pH 13.9), emulated carbonated concrete solution (pH 9), tab water (pH 7.6) with Cl^- added up to 10 %- room temperature and 40 C^o	Potentiostatic holdings at +200mV vs. SCE and Potentiodynamic scan	Increased corrosion resistance with pH and decreased with temperature- Austenitic SS and higher grades showed high corrosion resistance
Seibert (1998)	Type 316 and duplex M33 SS and CS- polished surface	Saturated $Ca(OH)_2$ (pH 12.5), 0.26M KOH +0.45 NaOH (pH 13.5) with $CaCl_2$ added up to 20 %	Linear Polarization, EIS and E_{OC} measurements	SS were free of corrosion in high pH solutions with up to 20 % Cl^-
Hurley and Scully (2002)	Clad 316L and Solid 316LN SS and CS- different rebar surface conditions	Saturated $Ca(OH)_2$ (pH 12.5) with various amounts of added NaCl	Potentiostatic holdings at -200 mV, 0.0 mV and + 200 mV vs. SCE- E_{OC} measurements	At -200mV and 0.0 Cl^-/OH^- threshold was greater than 100 while at +200mV was nearly 24- In all cases 316LN showed chloride threshold much higher than CS
Escudero et al. (2002)	Type 304-316 SS and CS	Saturated $Ca(OH)_2$ (pH 12.5) with 0.1 % and 3.5 % of NaCl added	E_{OC} measurements- Polarization Resistance- Potentiodynamic Scans	Only 304 and 316 SS were able to repassivate after pits formation even in the 3.5 % NaCl solution

Reference	Specimens	Testing Environment	Used techniques	Results
Matsushima (2002)	Type 304 SS and CS flat plates	Saturated $Ca(OH)_2$ with varied amounts of $CaCO_3$ added to reduce solution's pH (pH 12.4-10.5) and various amounts of NaCl	Visual Inspection	In pH 12.5 no corrosion up to 15 % NaCl- Corrosion occurred in pH 11.5, 7 at 15 % and 3 % NaCl respectively
Bautista et al. (2006)	Type 204Cu, 304, 304L, 316, 316L and 316Ti SS cold worked corrugated bars	Saturated $Ca(OH)_2$ and saturated $Ca(OH)_2$ with CO_2 bubbling to emulate carbonated concrete media- NaCl added up to 5 %	Cyclic Polarization	204Cu has similar behaviour as 304 and 316 SS except in highly aggressive solutions. No sign of corrosion occurred on 304 and 316 in both media
Blanco et al. (2006)	Type 304, 316L 2205 duplex and 204cCu low Ni SS corrugated bars	Saturated $Ca(OH)_2$ and saturated $Ca(OH)_2$ with CO_2 bubbling to emulate carbonated concrete media- NaCl added up to 5 %	Cyclic Polarization and EIS	Charge transfer resistance R_t is increased with the time immersion and decreased with the addition of Cl^- 304 and 316 are subjected to pitting only at very high potentials
Tae and Ujiro (2007)	Rebar samples contain Cr from 0% (CS) to 16% (304 SS)	Saturated $Ca(OH)_2$ with 0.27%, 1.07% and 21.4% of NaCl added- pH from 12.5 to 9 adjusted using HCl	Pitting Potential and EIS	Increased corrosion resistance with %Cr- More negative pitting potentials with increasing % NaCl and decreasing pH- no sign of corrosion on 304SS in solution with pH 10 and 21.4% NaCl

-ove the scale) samples. This suggests that the effect of mill scale removal on the corrosion resistance of 316LN stainless steel should be a subject for a future research.

2.4.3 Micro-composite steel (MMFX-2)

A new steel alloy containing 9% chromium was introduced to the market by MMFX Steel Corporation in 1998. It has a brand name of MMFX-2. The manufacturer claims that this type of steel has corrosion resistance that approaches that of stainless steel with much lower cost due to the use of a new production technology that minimizes the formation of the so-called micro-galvanic cells in the steel structure (MMFX Technologies corp. web page). Since its production, a number of studies have been conducted to study the corrosion resistance of this new type of reinforcement (Trejo and Pillai, 2004; Gong et al., 2004; Nachiappan and Cho, 2005; Jing, 2006 and Kahl, 2007).

Trejo and Pillai (2004) found that MMFX-2 has a chloride threshold of about 9 times that of ASTM A615 carbon steel using a sudden increase in the inverse of polarization resistance R_P values as an indication of corrosion initiation. Gong et al. (2004) found that MMFX-2 exhibited macrocell corrosion rates between one-third and two-thirds that of carbon steel. Nachiappan and Cho (2005) reported a similar ratio of 0.4 between corrosion currents of MMFX-2 and carbon steel for metal samples embedded in concrete and subjected to NaCl solutions of 1.7% and 3% concentration after 132 days of exposure. However, Gong et al. (2004) concluded that using MMFX-2 is not cost effective compared to the use of epoxy-coated steel; this conclusion was supported by Jing (2006). Kahl (2007), on the other hand, concluded contradictory results in his work. He estimated that using MMFX-2 is more cost effective than epoxy-coated steel and that it can extend the structure's life by 12 years more than epoxy-coated steel.

All the previous studies were performed on samples embedded in concrete or mortar; only Hurley (2007) studied the corrosion behaviour of micro-composite steel in saturated $Ca(OH)_2$ solution. He found that it has a chloride threshold value Cl^-/OH^- ranging from 0.1 to 4.9, depending on the technique used as well as the test setup and surface condition.

2.5 Moisture and Corrosion

The availability of moisture is vital for the process of steel corrosion inside concrete in both the corrosion initiation and propagation stages. High moisture content in concrete will delay carbon dioxide diffusion, although a certain moisture content has to be present for the reaction between carbon dioxide and the portlandite $Ca(OH)_2$ (Pruckner 2001). In the case of chloride ion attack, moisture availability facilitates ion penetration through the concrete cover. In the propagation stage, an intermediate level of moisture has to be maintained at all times inside concrete in order to keep the corrosion process active. Very dry conditions will induce very low corrosion rates, as electrolytic concrete resistivity will increase. Also, low corrosion rates are obtained in very wet concrete (i.e. concrete under water surface) due to the obstruction of the oxygen supply. Fastest oxygen diffusivity occurs when the concrete pores are partially filled with water, which explains why corrosion rates in structures located in the tidal and splash zone are higher than those below the tidal zone (Liu, 1996).

Limited research has been conducted to investigate this issue. Lopez and Gonzalez (1993) and Gonzalez et al. (1993) determined a critical limit for the degree of pore saturation, PS%, to be 45-50 %. Negligible corrosion rates occur if the PS% is below 35%. At a PS more than 70 %, corrosion rates start to decrease gradually due to the decrease in oxygen supply. Balabanic et al. (1996) reported the same limit (PS 45-50%) to induce maximum corrosion rates for a concrete mix that had a water/cement ratio of 0.4. Enevoldsen et al. (1994) concluded that if the internal humidity inside concrete drops below 85 %, high active corrosion rates cannot be maintained.

It should be mentioned that moisture availability in concrete is a controlling factor in other durability problems, besides corrosion, such as alkali- aggregate reactivity and freezing and thawing. Thus, it might be helpful to be able to determine the volumetric water content inside the concrete (θ_V). Time Domain Reflectometry (TDR) is a powerful technique that is used to determine the moisture content in soil, and it can be adapted to

be used for the determination of volumetric moisture content in concrete since both of them are porous media (Korhonen et al., 1997).

2.5.1 Time Domain Reflectometry (TDR)

Over the past three decades, the use of the TDR technique to measure soil moisture has increased until it has become the standard method of moisture content measurements second only to the thermo-gravimetric analysis (Topp and Reynolds, 1998). In this technique, an electromagnetic pulse is launched by a TDR signal generator and propagates through the soil or medium, guided by the conductors or the TDR probes. The TDR step pulse will travel along the probe length and be reflected when it hits the probe end. By measuring the arriving time of the reflected signal, the wave velocity can be calculated:

$$v = \frac{L_0}{\Delta t} \qquad [2.17]$$

where:

v = velocity of the signal (m/sec)

Δt = travel time through probe (sec)

L_0 = length of probe (m)

This velocity is inversely proportional to the square root of the dielectric constant of the medium:

$$v = \frac{c}{\sqrt{\varepsilon}} \qquad [2.18]$$

where c is the speed of light (3x 10^8 m/sec)

ε is the dielectric constant

Hence

$$\varepsilon = \left(\frac{\Delta t \; c}{L_0} \right)^2 \qquad [2.19]$$

Figure 2.12 shows a representative trace of a TDR signal for a two-rod, 20 cm probe (Topp and Reynolds, 1998). V_o is the voltage amplitude of the transmitted signal in Volts, V_f is the is the voltage amplitude of the reflected signal, and t_s is the travel time of the propagation signal in seconds (Δt).

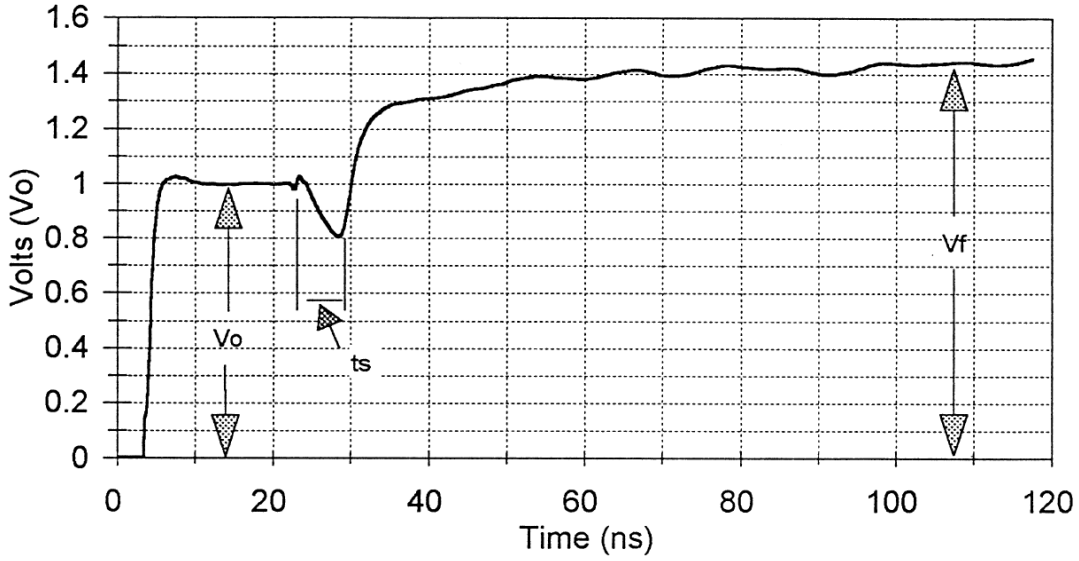

Figure 2.12 Typical TDR trace showing the travel time t_s (Topp and Reynolds, 1998)

By using Topp's formula (Topp and Davis, 1982), it is possible to calculate the volumetric moisture content for that medium

$$\theta_V = \frac{-530 + 292\varepsilon - 5.5\varepsilon^2 + 0.043\varepsilon^3}{10000} \qquad [2.20]$$

where:

θ_V = volumetric water content of the examined medium (m^3/m^3)

Equation [2.20] has been used by Van der Aa and Boer (1997) in their work on concrete and mortar. Recently Topp and Reynolds (1998) delivered a simpler equation to be used:

$$\theta_V = 0.114\sqrt{\varepsilon} - 0.176 \qquad [2.21]$$

However, Eq. [2.21] is only valid in soil applications. Korhonen et al. (1997) criticized the use of Eq. [2.20] with concrete, as it tends to overestimate the actual water content. They introduced the following second order polynomial equation to be used with concrete (Korhonen et al., 1997):

$$\theta_V = \frac{0.0001928\varepsilon^2 + 1.146\varepsilon - 4.425}{100} \qquad [2.22]$$

Also, knowing concrete's porosity Φ, the degree of pore saturation PS% can be calculated:

$$PS\% = \frac{\theta_V}{\Phi} \qquad [2.23]$$

2.6 Summary

In this chapter, an overview of the problem of rebar corrosion inside concrete and its main causes were introduced. In addition, corrosion-measuring techniques that are used in lab and field applications were explained. Also, the available literature on the corrosion behaviour of the metals under investigation in emulated concrete pore solution was reviewed. Finally, a brief introduction to the effect of moisture availability on rebar corrosion inside concrete and the use of Time Domain Reflectometry (TDR) technique to measure volumetric water content in concrete were presented.

CHAPTER 3

MATERIALS AND EXPERIMENTAL PROCEDURE

This project intended to investigate the electrochemical behaviour (i.e. critical chloride threshold and corrosion currents) of 316LN stainless steel and micro-composite steel (MMFX-2) in comparison with the behaviour of conventional carbon steel in synthetic solutions emulating both cases of fresh and carbonated concrete under chloride ion attack using direct current DC corrosion measurements techniques (open circuit potential E_{OC}, linear polarization R_P and potentiodynamic scan). The Electrochemical Impedance Spectroscopy (EIS) technique was used to investigate the change in the electrochemical properties of the passive film formed on the metal surface when immersed in fresh and carbonated concrete pore solution and subjected to incremental increases in the concentration of chloride ions. Furthermore, a set of carbon steel samples embedded in mortar and subjected to a chloride contamination of 5% of cement weight were tested to obtain the actual corrosion currents inside mortar. Finally, the effect of the presence of chloride ions on TDR measurements of volumetric water content in concrete was examined. The details of the experimental work are described in this chapter.

3.1 Experimental Details of Experiments Conducted in Synthetic Solutions

3.1.1 Composition of the concrete pore solutions used

Two different solutions were used in this study. Firstly, a solution of 0.2M NaCl + 0.6M KCl + 0.002M $Ca(OH)_2$ was used to emulate the fresh (non-carbonated) concrete pore solution. The initial pH measured was 13.7; however, it dropped to a value of 13.2±0.05 due to the chloride addition and possible carbonation from air during poring into the corrosion cells. Secondly, a solution of 0.05M $NaHCO_3$ that had a pH 8.5 was used to emulate the case of carbonated concrete. In order to

simulate the situation of chloride-contaminated concrete, various amounts of chloride ions Cl^- were added to both solutions in the form of NaCl. The NaCl concentrations ranged from 0.001M to 2M. All solutions were prepared using reverse osmosis water.

3.1.2 Sample size, shape and description of the corrosion cell

The corrosion cell used for the experiments is called the three electrodes cell. It consists of three electrodes that are immersed in the solution as follows:

- The reference electrode used was the saturated calomel electrode (SCE) to measure the potential of the working electrode. The saturated calomel electrode has a potential of + 0.241 V versus the standard hydrogen electrode (SHE).
- The counter electrode is used to complete the electrical circuit. A graphite counter electrode was used for testing.
- The working electrode is the tested sample itself. For carbon steel and 316LN stainless steel, samples were cut from rebars that had a diameter of 15 mm with length of 20 mm (exposed surface area =10.72 cm^2). For MMFX-2, samples with a diameter and length of 10 mm (exposed surface area =3.61 cm^2) were extracted from a 1.5 inch diameter rod. A threaded hole of 6.5 mm diameter and 13 mm depth was drilled in each sample in order to be attached to the sample holder. The sample holder was a threaded carbon steel rod that was covered with a Teflon tube to protect it from corrosion. A stainless steel nut was used to tighten the attachment. The electrolyte surface was kept all the time under the attaching point in order to prevent any possibility of crevice corrosion. This orientation enabled testing both of the rebar surface and the cross section. The same sample shape and orientation was used by Bautista et al. (2006) and Hurley (2007) in their work.

Figure 3.1 shows the reference, counter and working electrode used. Figure 3.2 shows carbon steel, 316LN stainless steel and micro-composite steel (MMFX-2) samples. The chemical compositions of the metals under investigation are shown in Tables 3.1 and 3.2. Table 3.3 shows the parameters used in corrosion rate calculations for the metals under investigation (Jones, 1996).

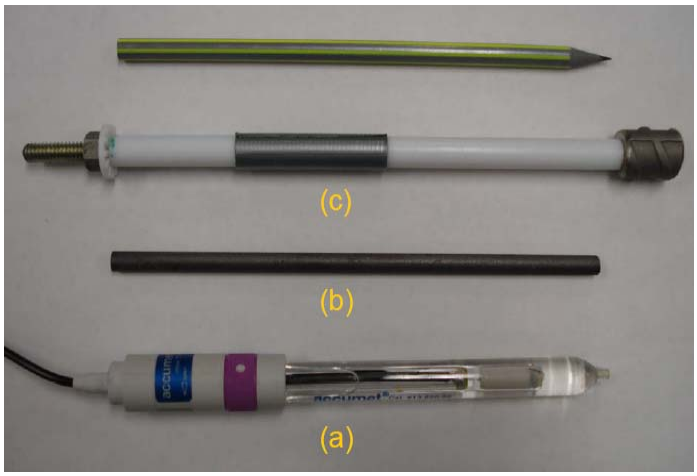

Figure 3.1 The electrodes used (a) Reference electrode (b) Counter electrode (c) Working electrode attached to its holder

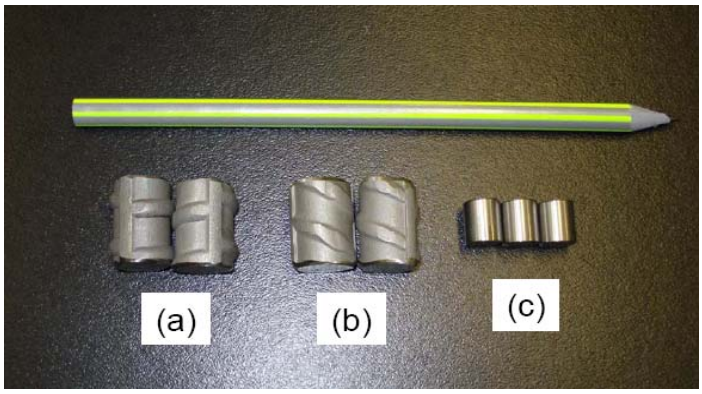

Figure 3.2 Samples used(a) Carbon steel (b) 316LN stainless steel (c) Micro-composite steel (MMFX-2)

Table 3.1 Chemical composition of carbon steel for concrete reinforcement (ASTM A706)

Metal	C% Max.	Mn% Max.	Si% Max.	S% Max.	P% Max.
CS	0.12	0.95	0.18	0.05	0.019

Table 3.2 Chemical composition of 316LN stainless steel and micro-composite steel MMFX-2

Metal	C%	Mn%	Si%	S%	P%	Cu%	Cr%	Ni%	Mo%	N_2
316LNSS*	0.03	2	1	0.015	0.045	-	18.5	14	3	0.22%
MMFX-2**	0.07	0.46	0.25	0.01	0.01	0.1	9.32	0.08	0.02	131ppm

* Reval Stainless Steel
** MMFX-2 Product Guide (2007)

Table 3.3 Parameters used in corrosion rate calculations

Parameter	Carbon Steel	MMFX-2	316LN SS
Density ρ (g/cm^3)	7.87	7.8	8
Equivalent Weight EW	27.92	26.5	25.65

Before testing, carbon steel and 316LN stainless steel samples were sand blasted in order to remove the mill scale (if any). While sand blasting of carbon steel resulted in the removal of its black surface layer, no visible change was observed on sand blasted 316LN stainless steel samples. Subsequently all samples were degreased in acetone, rinsed using distilled water, then dried in hot air and kept in a desiccator.

While the working electrode was immersed in the solution during the entire testing period, the reference and counter electrodes were immersed only when carrying out the measurements. Flasks of two different shapes were employed, as shown in Figure 3.3. The first type was the straight-sided glass jar that had a wide mouth covered with a plastic cap with three holes had been made in each cap to fit the three electrodes. This shape was used in DC corrosion measurements. The other type was the standard multi-necked electrochemical flask, which was used in EIS measurements to facilitate chloride addition without disturbing the sample. During testing, the three electrodes were attached to a GAMRY PC4^{TM} instrument. The instrument is equipped to conduct DC corrosion measurements, AC corrosion measurements, Electrochemical Noise measurements and Physical Electrochemistry measurements. The instrument is also equipped with an

ECM8^{TM} Electrochemical Multiplexer (see Figure 3.4). The instrument was upgraded and calibrated by the manufacturer in June 2007.

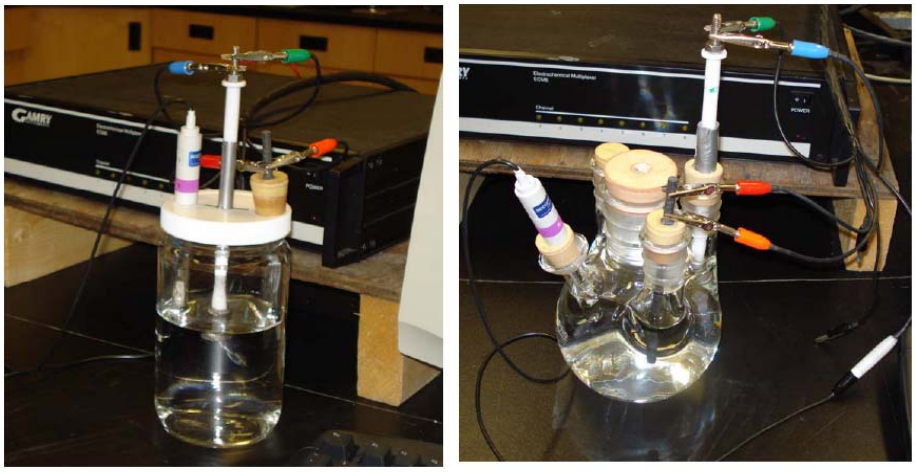

Figure 3.3 Corrosion cells used (a) straight sided jars (b) standard multi-necked electrochemical flask

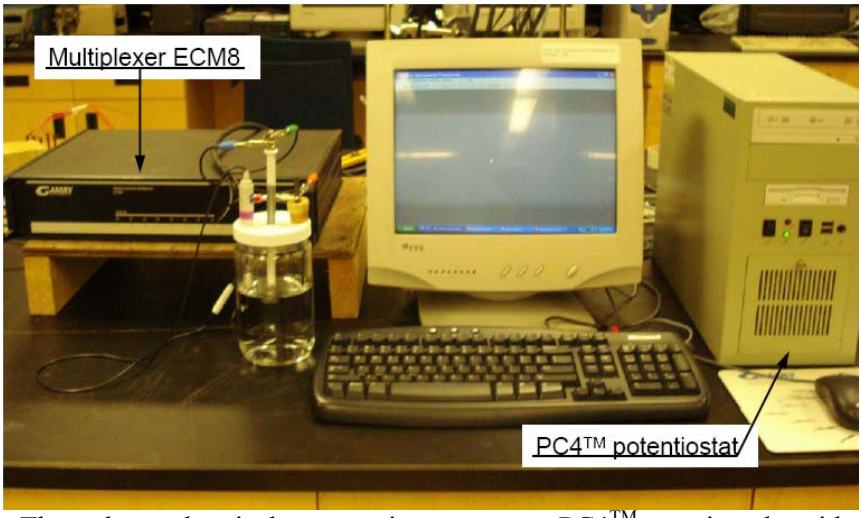

Figure 3.4 The electrochemical measuring system PC4^{TM} equipped with an ECM8 electrochemical multiplexer

3.2 Electrochemical Measurements

3.2.1 Direct Current (DC) measurements: Fixed chloride concentrations

In this experiment, fresh (non-carbonated) and carbonated concrete pore solutions were prepared and then different amounts of NaCl were added with concentrations

ranging between 0.001 M to 2 M. Each sample was immersed for a total period of 7 days in a solution that had fixed chloride concentration during the entire exposure time. Free corrosion potential measuring E_{OC}, linear polarization resistance LPR test and potentiodynamic scan were applied after 1 hour, 24 hours and 7 days of immersion. One sample from each metal was used per one chloride concentration. An estimation of the expected error in the results is provided in later in Section 4.2. Table 3.4 shows the tested chloride concentrations for the metals under investigation in both testing solutions.

Table 3.4 The tested chloride concentrations for DC measurements

Metal		Carbon Steel			MMFX-2			316LN SS		
Solution	Cl^-	1 hour*	24 hours	7 days	1 hour	24 hours	7 days	1 hour	24 hours	7 days
Fresh concrete pore solution pH 13.2	0.001	•	•	•	•	•	•	•	•	•
	0.01	•	•	•	•	•	•	•	•	•
	0.05	•	•	•	•	•	•	•	•	•
	0.1	•	•	•	•	•	•	•	•	•
	0.5	•	•	•	•	•	•	•	•	•
	0.75	•	•	-	•	•	•	-	-	-
	1	•	•	•	•	•	•	•	•	•
	2	•	•	•	•	•	•	•	•	•
Carbonated concrete pore solution pH 13.2	0.001	•	•	-	•	•	•	•	•	•
	0.005	•	•	-	•	•	•	•	•	•
	0.01	•	•	-	•	•	•	•	•	•
	0.05	•	•	-	•	•	•	•	•	•
	0.1	•	•	-	•	•	•	•	•	•
	0.5	•	•	-	•	•	•	•	•	•
	1	•	•	-	•	•	•	•	•	•
	2	•	•	-	•	•	•	•	•	•

• Sample tested at that concentration
- N/A
* E_{OC} and i_{corr} only

3.2.1.1 Open Circuit Potential Measurements E_{OC}

As mentioned earlier, the free corrosion potential is a good indication of the metal's tendency to corrode in a certain solution. The sample's potential was measured against the Saturated Calomel Electrode (SCE) for duration of 60 seconds. Having a

relatively fixed (not drifting) potential is an indication that the sample has stabilized in the solution. The test parameters are:

- The total time: this is the test duration in seconds. Test duration was 60 seconds.
- The sample period: this parameter determines the spacing between data points in seconds. The sample period was 1 second.
- The stability: that is used to tell the system the definition of a stable potential. When measuring the open circuit potential, if the drifting rate falls below the stability this will result in terminating the experiment immediately. This parameter has units of mV/sec. The stability was set to be zero mV/sec. This means that the test will be terminated only when the total time ends.
- Sample Area: the sample surface area in (cm^2) that is immersed in the solution.
- Conditioning: that is applying certain potential to the metal for a certain period in case it is needed to hold the metal surface in a certain state; i.e. make an oxide film grow or remove an oxide film. The conditioning potential is always expressed versus the reference electrode potential because the open circuit potential will not be measured until after conditioning has been completed. This option was turned off.
- IR Compensation: a high cell resistance will result in a voltage (IR) drop; fortunately, the GAMRY instrument is capable of compensating for this drop by turning on IR compensation. This option was not used in all experiments, as the solutions used were highly conductive due to the presence of many dissolved ions in the solution.

Figure 3.5 shows an example of the graphical output of the open circuit potential measurement.

3.2.1.2 Potentiodynamic Scans

For every sample, the potentiodynamic scan was applied after 1 hour, 24 hours and 7 days of exposure to determine the corrosion current density i_{corr} at that time. The test parameters are:

- Initial E: is the starting point for the potential sweep in Volts. The initial potential E was -0.15 V vs. E_{OC}.

- Final E: is the ending point for the potential sweep in Volts. The final potential E was +0.15 V vs. E_{OC}. This scan range (E_{OC} ± 0.15V) enabled the estimation of i_{corr}

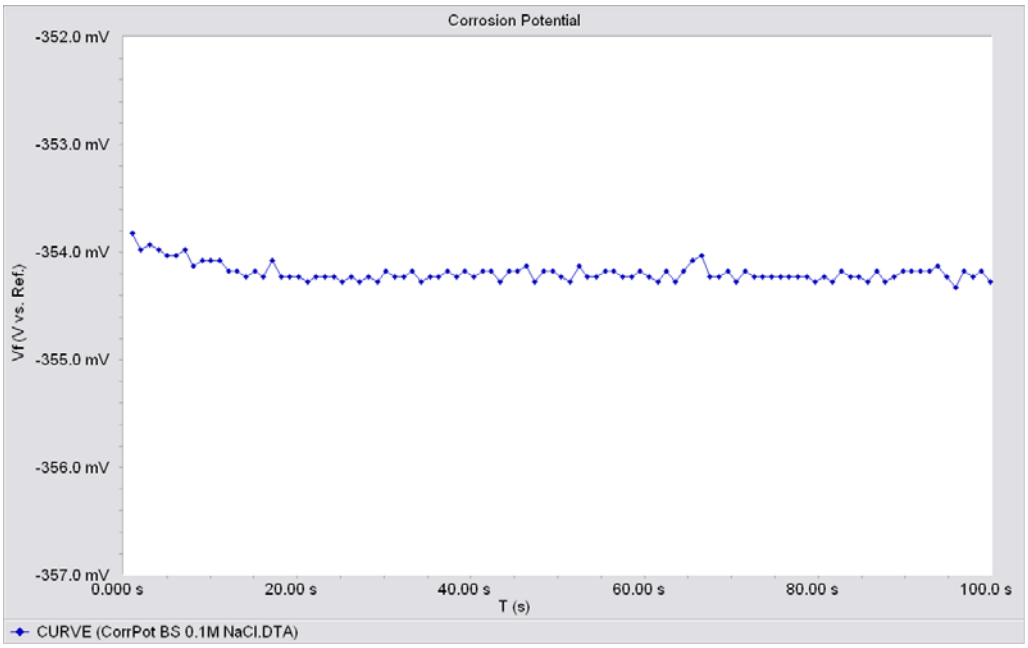

Figure 3.5 Example of the graphical output for open circuit potential E_{OC} measurement (carbon steel sample after 24 hours of immersion in non-carbonated concrete pore solution with Cl^- concentration of 0.1 M)

without destroying the sample. Testing further anodic potentials would force the sample to corrode (i.e., destructive testing).

- The sample period: the sample period was 1 second.
- Scan Rate: is the speed of the potential sweep during data acquisition. Its unit is mV/sec. Very high scan rates lead to unreliable data; however, very low scan rate elongate the test period. The applied scan rate was 0.5 mV/sec. No change in the shape of the curve was noticed when using slower scan rates (see Figure 3.6).
- Density: is the density of the metal tested in g/cm^3. This parameter is used for corrosion rate calculation.
- Equivalent Weight: is the theoretical mass of metal that will be lost from the sample after one Faraday of anodic charge has been passed. This parameter is used in corrosion rate calculations.

- Initial Delay: this option is used to allow the open circuit potential of the sample to stabilize prior to the potential scan. The delay time is the time that the sample will be held at its open circuit potential E_{OC} prior to the scan. The delay may stop

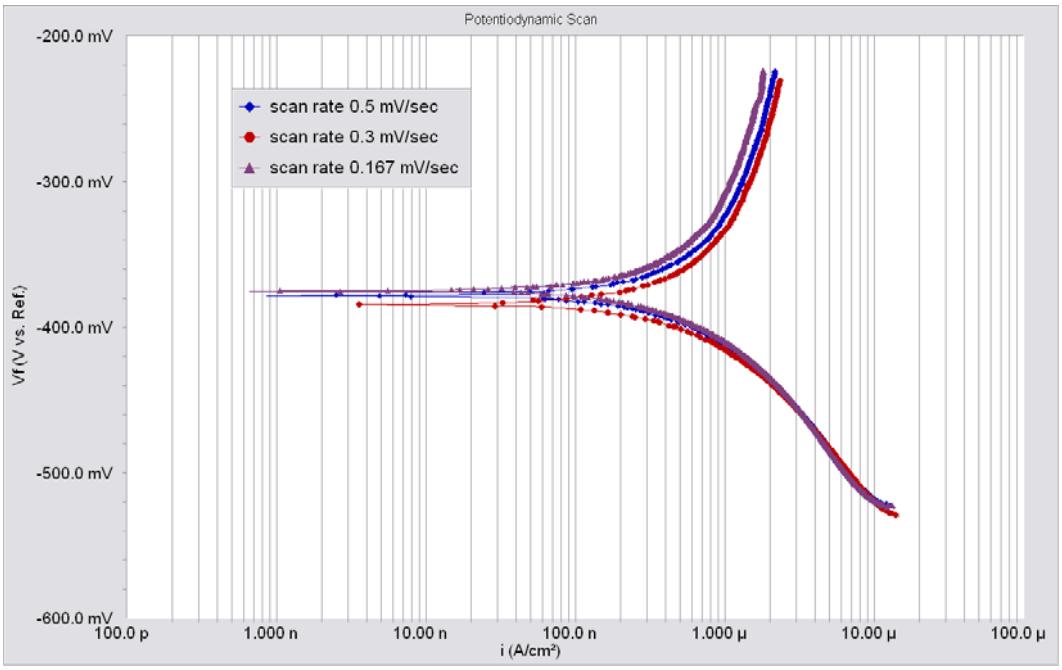

Figure 3.6 Potentiodynamic scans for carbon steel in non-carbonated concrete pore solution with Cl^- ion concentration of 0.1 M using three different scan rates.

prior to the delay time if the stability criterion for E_{OC} is met. The delay time parameter is active only if the initial delay is turned on. This option was turned off in all the experiments.

Extrapolation of the corrosion current density i_{corr} was made with the help of GAMRY Echem Analyst (v.1.35) software. Figure 3.7 shows an example of the graphical output of the potentiodynamic scan.

3.2.1.3 Linear Polarization Resistance

For every sample, the linear polarization test was applied after 1 hour, 24 hours and 7 days of exposure. The test parameters are:

- Initial E: is the starting point for potential sweep; initial E was -0.02 V vs. E_{OC}.
- Final E: is the ending point for potential sweep; final E was +0.02 V vs. E_{OC}.
- Scan Rate: is the scan rate was 0.1667 mV/ sec.
- The sample period: the sample period was 1 second.

- Beta An. and Beta Cat.: are the anodic and cathodic Tafel slopes in Volts. The default values for these parameters were accepted; however, the corrosion current density i_{corr} was calculated directly form the potentiodynamic scan.

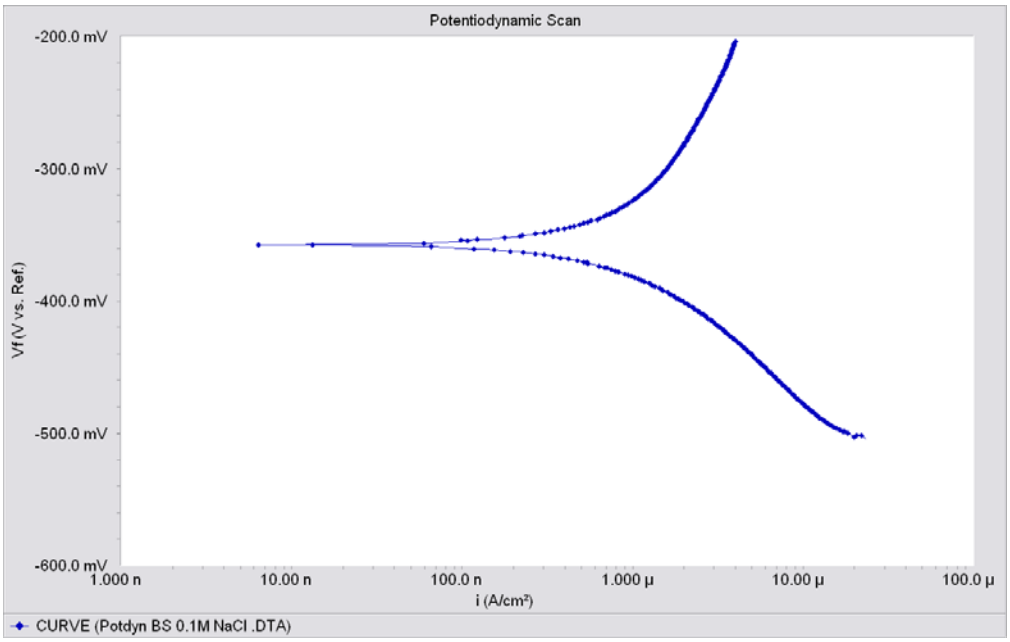

Figure 3.7 Example of the graphical output for Potentiodynamic scan test (carbon steel sample after 24 hours of immersion in non-carbonated concrete pore solution with Cl^- concentration of 0.1 M)

Extrapolation of the linear polarization resistance R_P was made with the help of GAMRY Echem Analyst (v.1.35) software. Figure 3.8 shows an example of the graphical output of the linear polarization test.

The linear polarization test was not used for calculating the corrosion current because of the ambiguity associated with Stern-Geary constant B. Trejo and Pillai (2003) found no agreement on its value when they reviewed four different studies. Qian et al. (2008) stated that Tafel slopes are often difficult to determine, especially when the steel surface is passive. Besides, no information was found in the literature about the value of B for 316LN stainless steel and micro-composite steel.

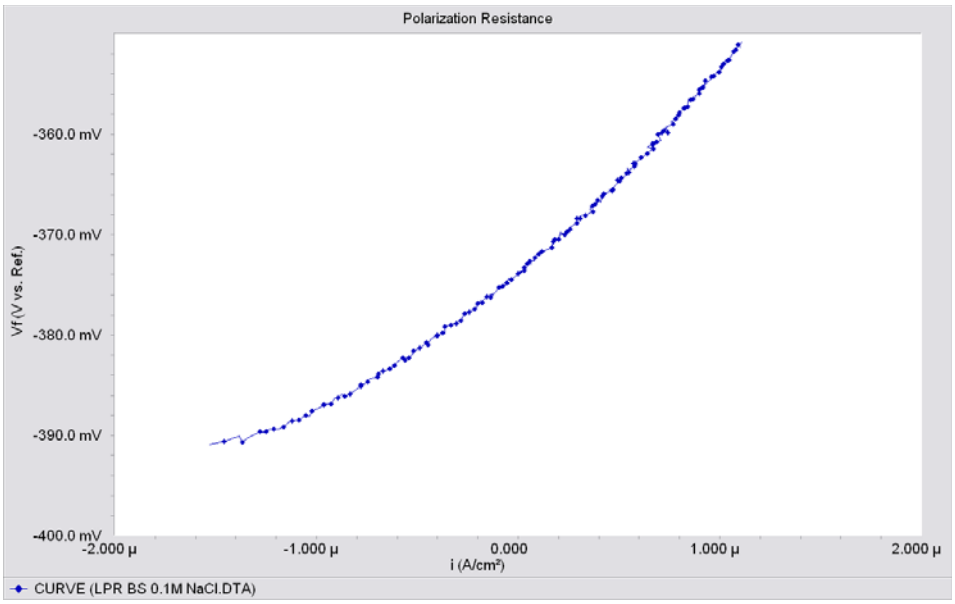

Figure 3.8 Example of the graphical output for linear polarization test (carbon steel sample after 24 hours of immersion in non-carbonated concrete pore solution with Cl^- concentration of 0.1 M)

3.2.2 Electrochemical Impedance Spectroscopy (EIS): Incremental chloride addition

In this experiment, the fresh (non-carbonated) and carbonated concrete pore solutions were prepared with zero chloride content at the beginning and then the sample was immersed and allowed a period of 24 hours to stabilize in the solution. Afterwards, a certain dose of NaCl was added every 24 hours to the solution until a maximum limit of 2 M was reached. EIS measurements were conducted every 24 hours before adding the next chloride dose. Each chloride dose was equal to the difference between the current

Table 3.5 The tested chloride concentrations and the exposure time for EIS measurements

Day	Cl^-	Carbon Steel		MMFX-2		316LN SS	
		pH 13.2	pH 8.5	pH 13.2	pH 8.5	pH 13.2	pH 8.5
1	0	-	-	-	-	-	-
2	0	•	•	•	•	•	•
3	0.01	•	•	•	•	•	•
4	0.05	•	•	•	•	•	•
5	0.1	•	•	•	•	•	•
6	0.5	•	-	•	•	•	•
7	1	•	-	•	•	•	•
8	2	•	-	•	•	•	•

• Sample tested at that concentration
- N/A

chloride concentration and the desired one. This procedure is very similar to the real life situation where chloride ions keep accumulating on the rebar surface until corrosion initiates. One sample from each metal was used for each solution. An estimation of the expected error in the results is provided in later in Section 4.2. Table 3.5 shows the tested chloride concentrations and the corresponding exposure time.

Literature on the applications of EIS shows that it has great advantages over other techniques in studying the passive film formation providing the use of low frequencies of AC signals (Pruckner, 2001). The test parameters are:

- Initial Frequency: is the starting point for the frequency sweep during the data acquisition phase. The frequency unit is Hertz. The initial frequency was 10^5 Hz.
- Final Frequency: is the ending point for the frequency sweep during the data acquisition phase. The final frequency was 10^{-2} Hz. Testing lower frequencies would make the test duration too long.
- Points/decade: is the number of data points in each decade frequency. The value used was the default value of 10 points per decade.
- AC Voltage: is the amplitude of the applied AC (alternated current) signal to the working electrode. The unit is in rms mV. The excitation AC signal should be small in order to keep in the linear region (i.e., the AC current response will be in the same frequency but with phase shift) and not to destroy the sample. The applied AC voltage was 10 mV rms.
- DC Voltage: is the applied DC (direct current) voltage on the working electrode. The purpose of the experiment was to study the properties of the passive film that is formed naturally on the metal surface. Thus, samples were held at their free corrosion potential E_{OC} (i.e., DC Voltage = 0.0 vs. E_{OC}).
- Estimated Z: is a rough estimate of the cell's impedance at the Initial Frequency entered. This value is used to minimize the number of trials that the system operates to calculate the cell's impedance at the first data point. After the first point, this value is not important as the system uses the last estimated value for Z to calculate the new Impedance with the new frequency.

Figure 3.9 shows a schematic of the equivalent circuit used in EIS data fitting. The circuit's components are the solution/electrolyte resistance R_{el}, the charge transfer resistance R_{ct}, double layer capacitance C_{dl}, and R_f and C_f which are the resistance and capacitance of the passive film, respectively. This circuit was used by Pruckner (2001), Saremi and Mahallati (2002), Joiret et al. (2002), Abreu et al. (2002), Sanchez et al. (2007), Sahoo and Balasubramaniam (2008), Xu et al. (2009) and Bautista et al. (2009) in their work to study passive film formation on carbon steel and stainless steel in alkaline solutions. GAMRY Echem Analyst (v.1.35) software was used in data fitting. The mathematical method used was Levenberg- Marquardt method. Figure 3.10 shows an example of the graphical output of EIS test (Nyquist plot of the impedance) and the curve fitting using the circuit shown in Figure 3.9.

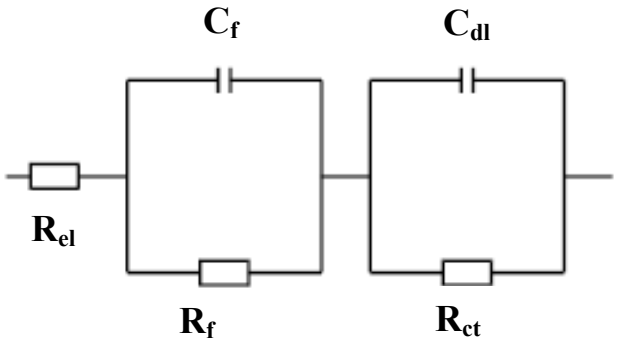

Figure 3.9 Representative circuit used to fit EIS results (Pruckner 2001)

The impedance Z of a resistor equals:

$$Z = R \qquad [3.1]$$

where R is the resistance in ohms.

The impedance of a capacitor equals:

$$Z = \frac{1}{jwC} \qquad [3.2]$$

where C is the capacitance in farads, j is $\sqrt{-1}$ and w is the angular frequency $w = 2\pi f$.

The total impedance of a system Z_{total} when the components are connected in series equals:

$$Z_{total} = Z_1 + Z_2 \qquad [3.3]$$

The total impedance of a system Z_{total} when the components are connected in parallel equals:

$$Z_{total} = \frac{Z_1 Z_2}{Z_1 + Z_2} \qquad [3.4]$$

Thus, for the circuit shown in Figure 3.9 the total impedance equals:

$$Z_{total} = \mathrm{R}_{e\,l} + \frac{R_f}{1 + R_f(j.w.C_f)} + \frac{R_{ct}}{1 + R_{ct}(j.w.C_{dl})} \qquad [3.5]$$

3.2.3 Cyclic polarization

Cyclic polarization scans were applied only on micro-composite steel (MMFX-2) samples to examine its pitting resistance in fresh and carbonated concrete pore solutions with the presence of chloride ions. Chloride ion concentration ranged between 0.01 M to 2 M. Each sample was allowed a period of 24 hours to stabilize in the solution before applying the test. The test parameters are:

- Initial E: is the initial potential was -0.15 V vs. E_{OC}
- Forward Scan: is the scan rate for the forward anodic polarization. The forward scan rate was 0.167 mV/sec
- Apex E: is the end potential for the anodic (upward) scan. Apex E (E_{rev}) is one of two conditions that will terminate the forward sweep and initiate the reversal scan if it is reached and the Apex I is not exceeded yet. Apex E was one V vs. E_{OC}.
- Reverse Scan: the scan rate for the reverse cathodic polarization. The reverse scan rate was 0.3 mV/sec.
- Final E: is the end for the reversal potential sweep. The final potential was 0.0 V vs. E_{OC}

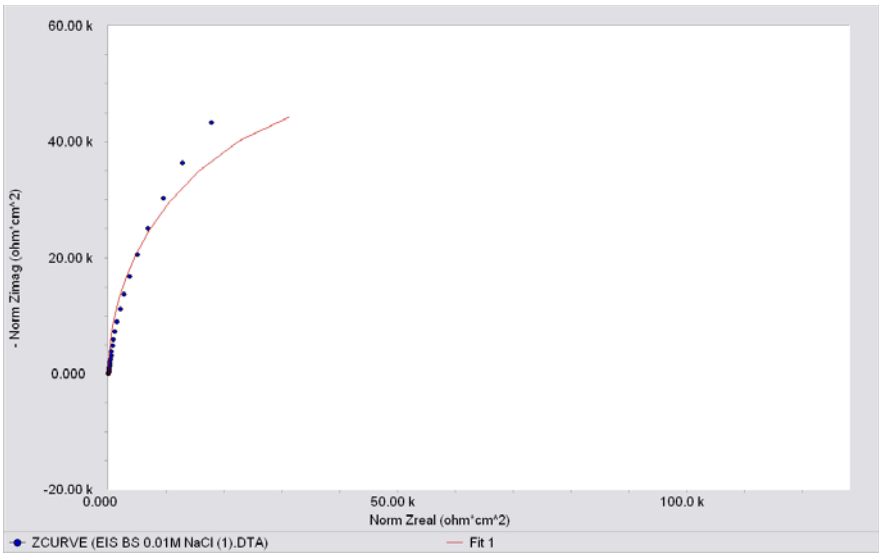

Figure 3.10 Example of Nyquist plot for EIS test (carbon steel sample immersed in non-carbonated concrete pore solution- Cl^- concentration = 0.01 M) - Data fitted using equivalent circuit shown in Figure 3.9

- Apex I: is the corrosion current density that is indicative of pitting initiation and it is one of two conditions that will terminate the forward sweep and initiate the reversal scan if it is exceeded by the absolute current of the sample. The Apex I was 1 mA/cm^2.

Figure 3.11 shows an example of the graphical output of the cyclic polarization scan.

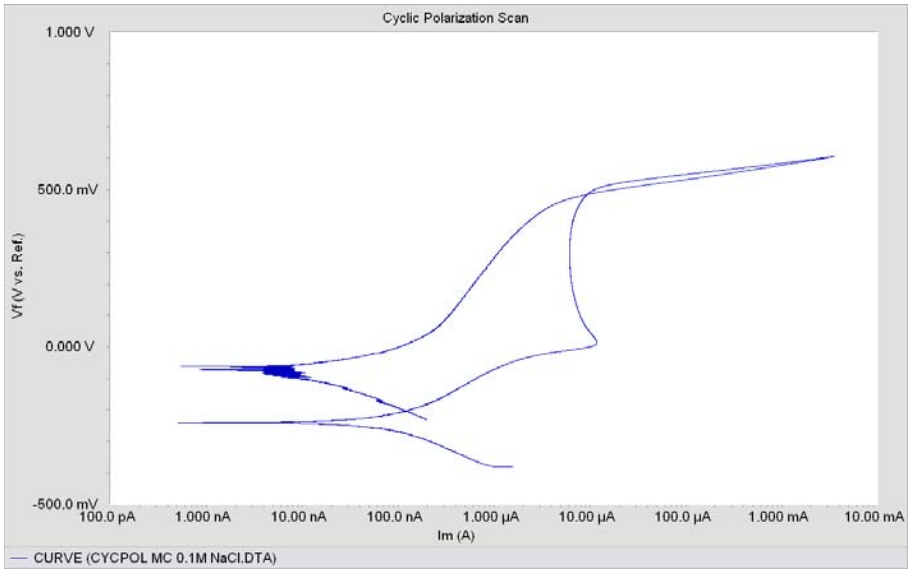

Figure 3.11 Example of the graphical output of the cyclic polarization scan (MMFX-2 sample after 24 hours of immersion in non-carbonated concrete pore solution with Cl^- concentration of 0.1 M)

3.3 Corrosion Current Measurements of Carbon Steel Samples Embedded in Mortar

In order to measure the actual corrosion currents in a concrete environment, a set of six carbon steel rebar samples embedded in mortar pre-contaminated with NaCl at 5% of cement weight were prepared. Samples had a water/cement ratio of 0.5 and a cement/sand ratio of 0.4. The cement used was Type 10 ordinary Portland cement. Sample dimensions were 20x 7x5 cm. A carbon steel rebar of 15 mm diameter and 100 mm length was embedded in each sample. The total exposed surface area was 47.12 cm^2. Each rebar sample had a threaded hole of 6.5mm diameter and 13mm depth in order to attach a 6.5mm stainless steel bolt to make an electrical connection to the embedded rebar sample. The bolt was to be attached only during testing. Before casting, rebar samples were degreased in Hexane for 15 minutes then rinsed with distilled water. Samples were cured for 14 days after demolding. The concentration of NaCl of 5% per cement weight was chosen to guarantee rebar corrosion initiation. In two literature surveys conducted by Glass and Buenfeld (1997) and Alonso et al. (2000) most values of reported chloride threshold level of carbon steel embedded in concrete or mortar were less than 5% per cement weight.

The potentiodynamic scan was used to measure corrosion current density, and then corrosion rate was calculated. The test was applied after 1, 3, 7, 14, 28 and 60 days of casting. The applied scan range and scan rate were 150 mV ± E_{OC} and 0.5mV/sec, respectively. A copper/copper sulphate electrode manufactured at the engineering shops at University of Saskatchewan was used as the reference electrode. The $Cu/CuSO_4$ had a potential of + 65 mV vs. SCE. The counter electrode was a stainless steel plate of 130x30mm dimensions. Prior to testing, the sample's surface was wiped with a wet sponge in order to decrease concrete electrical resistance. The test setup is shown in Figure 3.12. The change in the water content in mortar during the same period was monitored on samples described in the next section.

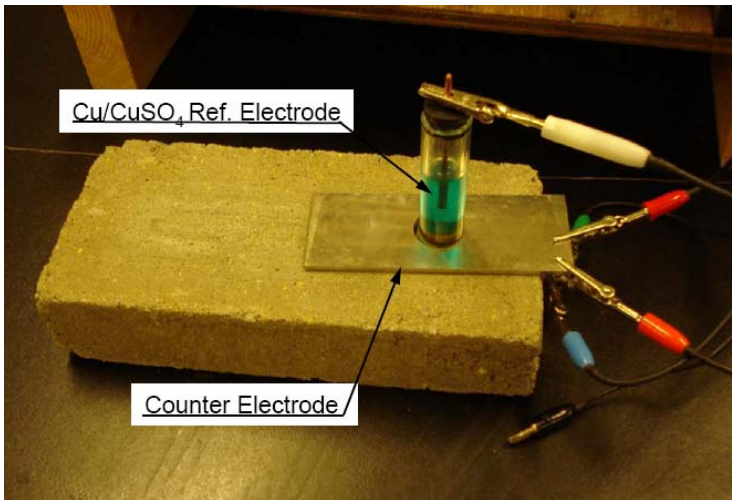

Figure 3.12 Test setup for corrosion current measurement of carbon steel in mortar

3.4 Measurements of Mortar Volumetric Water Content Using TDR Technique

For measuring the change in the water content inside mortar at early age and for determining the effect of the presence of chloride ions on TDR measurements of concrete moisture content, two sets of mortar samples (five samples in each set) were prepared. The first set was free of chlorides, while the other one was pre-contaminated with NaCl at 5% wt cement. Samples had a water/cement ratio of 0.5 and a cement/sand ratio of 0.4. The cement used was Type 10 ordinary Portland cement. Samples had a cylindrical shape of 7.5 cm diameter and 15 cm height. Two stainless steel probes of 14 cm length and 0.2cm diameter were embedded in each sample during casting, with only 1 cm extending out of the sample in order to attach it to the TDR cable. A portable metallic cable tester Tektronix 1502B was used as the signal generator. Samples were cured for 14 days after demolding. Figure 3.13 shows the test setup. According to Equation [2.19], the dielectric constant ε equals:

$$\sqrt{\varepsilon} = \frac{\Delta t.c}{L_0} = \frac{c.t_2 - c.t_1}{L_0} = \frac{L_2 - L_1}{L_0} = \frac{\Delta L}{L_0} \qquad [3.6]$$

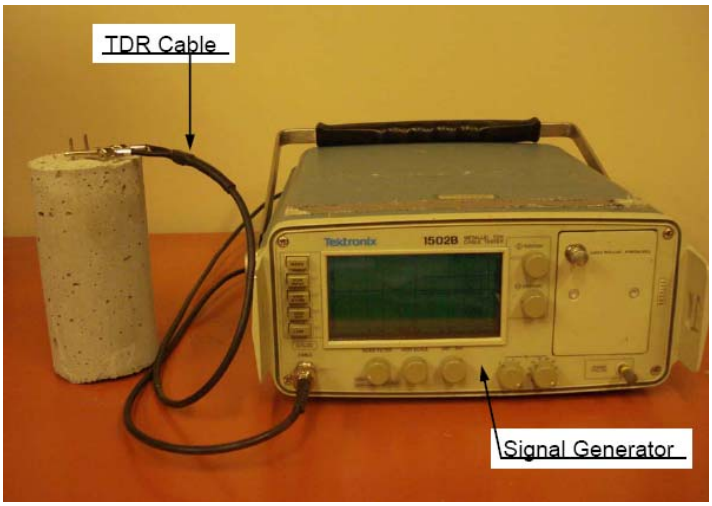

Figure 3.13 Test setup for concrete volumetric water content measurement using TDR technique

where c is the speed of light (3x 10^8 m/s)

t_1 and t_2 are the time when signal enters and leaves the sample, respectively

L_0 = length of probe inside the sample, which is 13 cm.

The values of L_1 and L_2 can be read directly from the screen of the instrument. Then the volumetric water content θ_V was calculated using Equation [2.22].

To calculate the degree of pore saturation (PS), the porosity Φ was measured after 60 days. The average measured porosity was 23±0.2. The water saturation method was used to measure the porosity:

$$\Phi = \frac{W_s - W_D}{V} \qquad [3.7]$$

where W_s is the weight of the fully saturated sample

W_D is the weight of the dried sample

V is the volume of the sample

Full saturation was obtained by immersing the samples in water in a desiccator for 3 days. Samples were dried in the oven under a temperature of 80^o C and a pressure of -77.2 mm of mercury for 3 days.

3.5 Summary

In this chapter, the information on the chemical composition of the solutions used, samples' size, shape and preparation and the corrosion cells used was presented. In addition, the information about the parameters used in the electrochemical techniques and the testing procedure was presented. Finally, a description of the prepared mortar samples for measuring corrosion currents of steel embedded in mortar and for TDR measurements of moisture content inside chloride free and chloride contaminated samples was presented.

CHAPTER 4
RESULTS AND DISCUSSION

4.1 Introduction

This chapter presents the experimental results with a discussion of their significance. As was discussed earlier, the main objective of this research was to study the corrosion behaviour in terms of the chloride threshold level and corrosion currents of carbon steel, micro-composite steel, and 316LN stainless steel in synthetic concrete pore solutions emulating fresh and carbonated concrete under chloride ion attack using direct current DC corrosion measurement techniques. The second objective was to study the effect of increasing chloride concentration in the solution on the electrochemical properties of the passive film formed on the metal surface using the Electrochemical Impedance Spectroscopy (EIS) technique. Firstly, results of a statistical study conducted to define the 95 % confidence intervals of the measured corrosion parameters for six micro-composite steel samples immersed in the non-carbonated solution with 0.1 M Cl^- ions contamination are presented. Then, results of the applied DC and EIS corrosion evaluation techniques are introduced in graphical form with a detailed discussion of their meanings. Results of corrosion current measurements of carbon steel embedded in mortar specimens pre-contaminated with NaCl at 5% of cement weight are also presented. Finally, results of TDR measurements of volumetric water content of chloride free and chloride contaminated mortar specimens are presented.

4.2 Repeatability of Electrochemical Corrosion Measurements

As was discussed earlier (Section 2.3.1), when using artificial concrete pore solutions in studying the corrosion behaviour of metals in a concrete environment, the data obtained are more reliable and less scattered, as the test environment (unlike

concrete or mortar samples) is homogenous and greater control is gained over the Cl^-/OH^- ratio. In the current project, a study on the repeatability of both DC and EIS corrosion measurements was conducted. However, due to time constraints, the repeatability study was conducted only on one metal type subjected to one chloride concentration (micro-composite steel in the non-carbonated pore solution contaminated with 0.1M Cl^-).

Results showed that the error range was small and it can be tolerated, especially for DC corrosion measurements. Since the test procedure and the surface treatment are identical, the same error range can be expected for other metals subjected to different chloride concentrations. The Student's t distribution was used to determine the expected error in corrosion test results for a 95 % confidence limit. This test is used when the sample size is small and the population (corrosion test results) standard deviation is unknown. In the current study, the sample size was six test samples for uncertainty calculations for both DC and EIS experiments. The standard error of the mean S_X is calculated using Eq. [4.1]

$$S_X = \frac{S}{\sqrt{N}} \qquad [4.1]$$

where:
S is the sample standard deviation, and
N is the number of samples

Then, the random uncertainty P can be calculated from Eq [4.2]

$$P = t.S_X \qquad [4.2]$$

where t is the two-tailed value of the Student *t* distribution taken at the 95% confidence level. This number t depends on the number of degrees of freedom, which equals (N-1). For a 95% confidence level and a degree of freedom of 5, t = 2.57 (Haldar and Mahadevan 2000) for a double sided test. For a very small number of samples, the value

of t will be quite large and will result in a large random uncertainty. Thus, increasing the number of measurements will generally decrease the random uncertainty.

4.2.1 DC measurements

Figures 4.1 through 4.3 show the 95% lower and upper confidence limits for the mean of the open circuit potential E_{OC}, polarization resistance R_P and corrosion current density i_{corr} (obtained from potentiodynamic scans) of six micro-composite steel samples. Samples were immersed in an emulated fresh concrete pore solution contaminated with 0.1 M of NaCl. Measurements were applied after 1 hour, 24 hours and 7 days of immersion. The error in the measured open circuit potential E_{OC} was only a few mVolts (± 9 mV) around the mean value after 7 days of exposure (see Figure 4.1). In the same period, the error in the calculated polarization resistance was 10 % about the mean value (see Figure 4.2), while that of the corrosion current density i_{corr} was 7.35 % about the mean value (see Figure 4.3).

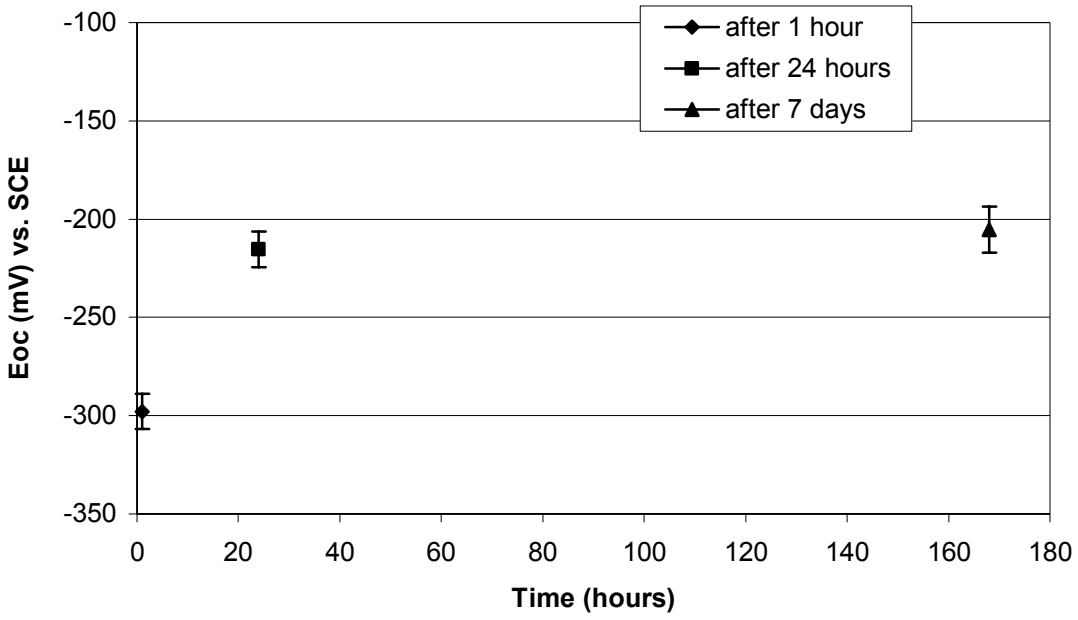

Figure 4.1 The 95% lower and upper confidence limits for the mean of open circuit potential E_{OC} after 1 hour, 24 hours and 7 days (MMFX-2 in the non-carbonated solution- Cl^- = 0.1M).

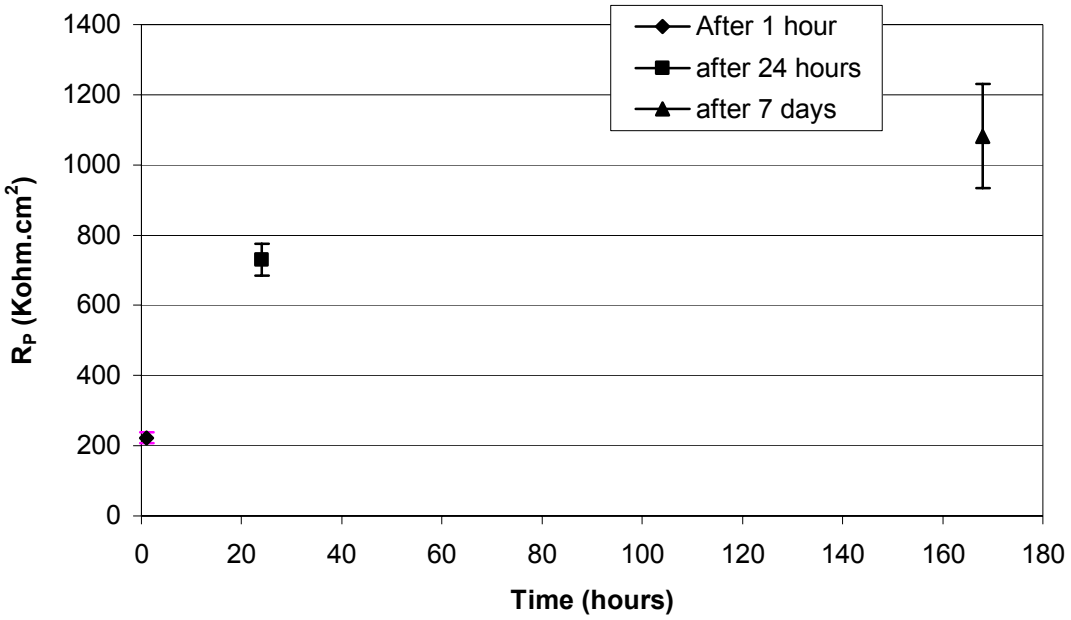

Figure 4.2 The 95% lower and upper confidence limits for the mean of polarization resistance R_P after 1 hour, 24 hours and 7 days (MMFX-2 in the non-carbonated solution- Cl^- = 0.1M).

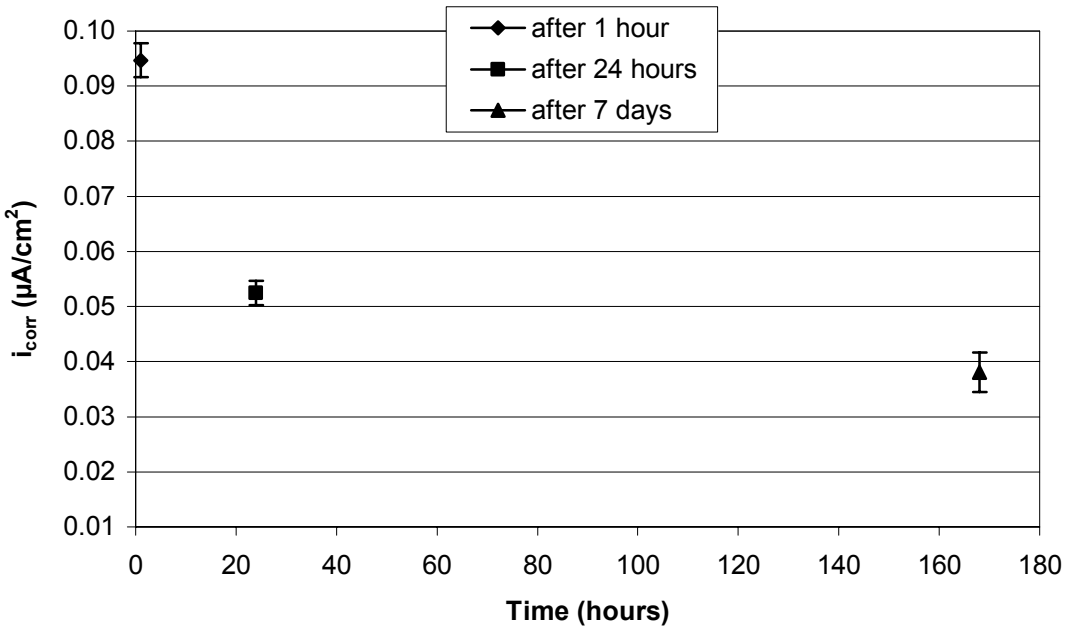

Figure 4.3 The 95% lower and upper confidence limits for the mean of corrosion current density i_{corr} after 1 hour, 24 hours and 7 days (MMFX-2 in the non-carbonated solution- Cl^- = 0.1M).

4.2.2 EIS measurements

Table 4.1 shows the mean value and the 95% confidence intervals ($t.S_x$) of EIS test results performed on six micro-composite steel samples immersed in fresh concrete pore solution after 24 hours (Cl^- 0.05M) and 48 hours (Cl^- 0.1 M) of immersion. Data were fitted using the circuit shown in Figure 3.9.

Table 4.1 Values of the parameters of the representative electrical circuit and their 95% confidence intervals (MMFX-2 in the non-carbonated solution).

	R_{el} ohm.		R_{ct} Kohm		R_f mohm		C_{dl} µF		C_f µF	
Cl^- M	Mean value	$t.S_x$	Mean value	$t.S_x$	Mean value	$t.S_x$	Mean value	$t.S_x$	Mean value	$t.S_x$
0.05	4.24	0.13	759	96.1	32.7	1.91	67.3	16.34	111	25.12
0.1	4.10	0.13	886	147	33.3	1.25	59.6	12.68	177	41.45

4.3 Results of Carbon Steel Immersed in Synthetic Solutions Emulating Concrete under Chloride Ion Attack

4.3.1 Fresh (non-carbonated) concrete pore solution

4.3.1.1 Open circuit potential and polarization resistance

Figures 4.4 and 4.5 show the open circuit potential and polarization resistance obtained from linear polarization tests for carbon steel samples immersed in non-carbonated synthetic concrete pore solution with a fixed amount of chlorides added to the solution after 1 hour, 24 hours and 7 days of immersion. A drop in the corrosion potential (Hausmann, 1967 and Li and Sagues, 2001) or the polarization resistance (Trejo and Pillai, 2003 and 2004 and Qian et al., 2008) was used by other researchers as an indication of reaching the critical chloride limit. In this study, the chloride concentration of 0.05 M seems to be critical for carbon steel and acts as a separation point between passive and active state. At chloride concentrations lower than 0.05 M, the metal was able to increase its passivity with time (i.e. nobler potential and higher polarization

resistance). At chloride concentrations greater than 0.05 M active corrosion processes took place with decreased potentials and polarization resistances with time.

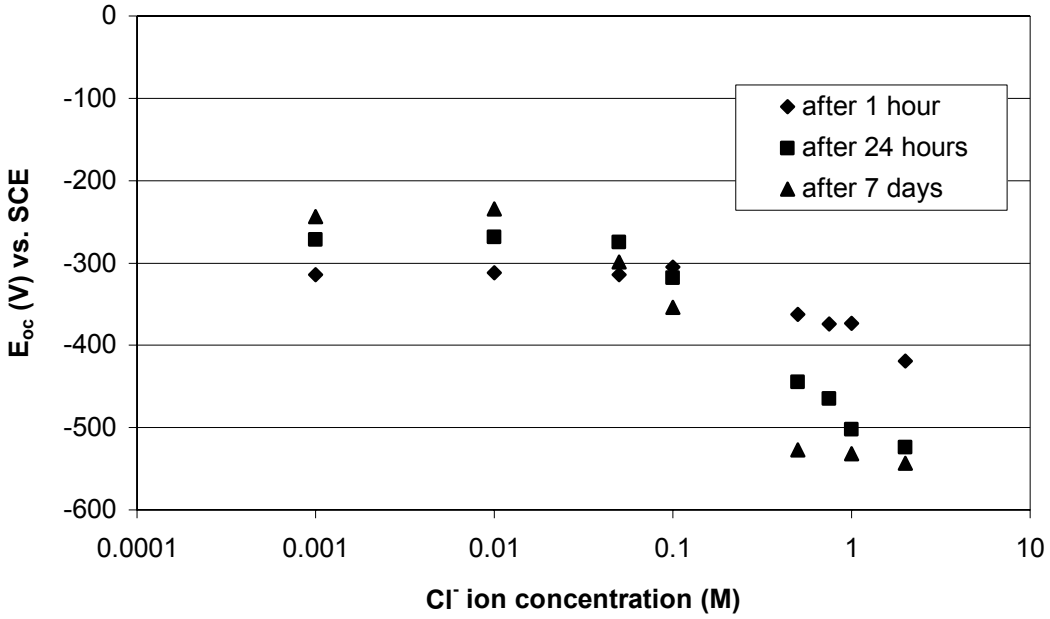

Figure 4.4 Open Circuit Potentials (E_{OC}) of Carbon Steel samples immersed in synthetic concrete pore solution with various amounts of NaCl added, after 1 hour, 24 hours and 7 days of immersion.

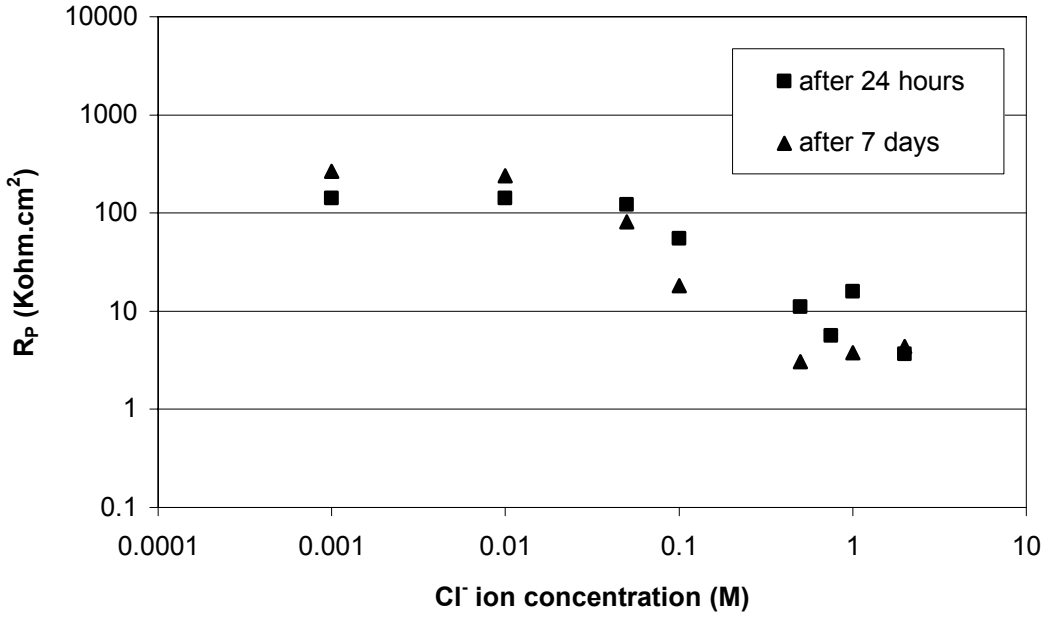

Figure 4.5 Polarization Resistance (R_P) of Carbon Steel samples immersed in synthetic concrete pore solution with various amounts of NaCl added, after 1 hour, 24 hours and 7 days of immersion.

The corresponding Cl^-/OH^- ratio is 0.32 (see Appendix B). This value of chloride threshold level (CTL) is in agreement with values reported by other researchers. Haussmann (1967) and Gouda and Halaka (1970) reported CTL values for the Cl^-/OH^- ratio of 0.6 and 0.35, respectively, for carbon steel samples immersed in $Ca(OH)_2$ solution, while Goni and Andrade (1990) reported a range between 0.25 and 0.8 in alkaline solutions. Andrade and Page (1986) reported a range between 0.15 and 0.69 for carbon steel samples embedded in mortar with Cl^- added as a mixture. This was later confirmed by Alonso et al. (2000), Izquierdo et al. (2004), and Hurley (2007).

4.3.1.2 Corrosion current density

Figure 4.6 shows the corrosion current density i_{corr} obtained from applying potentiodynamic scans on carbon steel samples after 1 hour, 24 hours and 7 days of immersion in non-carbonated synthetic concrete pore solution with fixed amount of chlorides added to the solution. A limit of 0.1- 0.2 $\mu A/cm^2$ for corrosion current density was set to identify initiation of the active corrosion process. The significance of that limit was discussed earlier in section 2.3.2.

The limit of 0.1 $\mu A/cm^2$ was exceeded at chloride concentration of 0.1 M (Cl^-/OH^- = 0.63), which is slightly higher than was determined by a drop in E_{OC} and R_P previously, but still in agreement with the reported values in the literature. The corrosion current density at 0.05 M was 0.088 $\mu A/cm^2$ (~ 0.1 $\mu A/cm^2$). Corrosion current densities obtained after 1 hour of immersion were not considered to be indicative of the metal's tendency either to passivate or corrode in its certain solution as each sample needed enough time to whether develop its passivation layer or actively corrode. A period of 24 hours was enough for samples to stabilize; corrosion currents did not change significantly after 7 days.

4.3.1.3 EIS measurements

The equivalent circuit used for data fitting was presented earlier in Figure 3.9. It is believed that this circuit introduces a reasonable explanation of the ongoing electrochem-

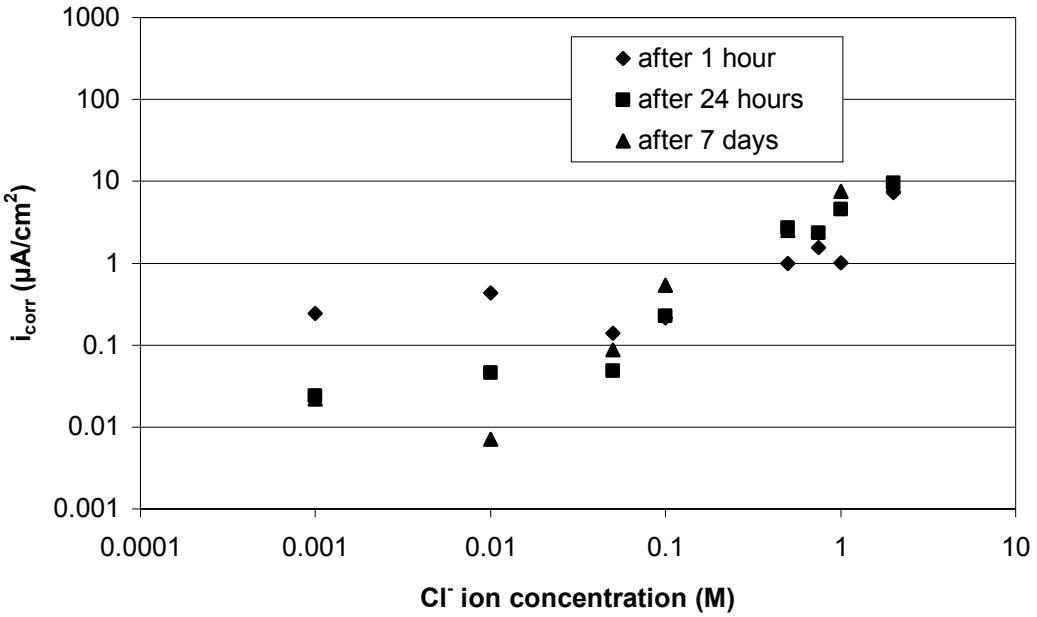

Figure 4.6 Corrosion Current Density (i_{corr}) of Carbon Steel samples immersed in synthetic concrete pore solution with various amounts of NaCl added, after 1 hour, 24 hours and 7 days of immersion.

-ical process on the metal surface immersed in a high alkaline solution. It consists of the solution ohmic resistance R_{el} connected in series to two loops. The first loop represents the double layer capacitance C_{dl} and the charge transfer resistance R_{ct}. The other loop represents the passive film formed on steel surface in the high alkaline solutions where C_f and R_f are the faradic capacitance and the ohmic resistance of the film, respectively. Since the capacitance (C) equals the charge built up in the capacitor (q) divided by the potential (V) (the free corrosion potential in this case), a metal in a passive state (i.e. less metal dissolution-less charge transfer between the metal surface and the electrolyte) will have less capacitance than an actively corroding metal. In other words, for a constant exposed area an active corrosion process will lead to an increase in the total charge transfer, which leads to increased film capacitance (Sahoo and Balasubramaniam 2007).

Figure 4.7 shows a Nyquist plot of the impedance of carbon steel immersed in fresh concrete pore solution with various amounts of NaCl added incrementally to the solution in a period of 7 days. It can be noticed that the low frequency portion of the impedance spectra (on the right hand side) decreases with an increase in chloride ion

concentration in the solution with a drastic change after the chloride concentration exceeds 0.05 M, as a sign of passivity break down.

Figure 4.8 shows the change of the parameters related to the passive film formation with chloride addition to the solution. Basically, the passive film has a high resistivity; however, it decreased with an increase in the chloride ion concentration in the solution due to the penetration of Cl^- ions (Saremi and Mahallati 2002) into the film. Thus, a decrease in the sum of the charge transfer resistance and the film resistance (R_{ct}+ R_f) was observed (from $6.91x10^4$ to $7.29x10^3$ ohm.cm^2 at chloride concentrations of 0.0 to 2 M respectively). The faradic capacitance of the passive film C_f increased with an increase in chloride ion concentration in the solution due to the increase of charge transfer at the metal/electrolyte interface. It is remarkable that the film capacitance increased by about six times from the beginning of the experiment (C_f 2.83 μF/cm^2) until a chloride concentration in the solution of 1 M (C_f 18.3 μF/cm^2). C_f at a chloride concentration of 2 M was too high, so it was not plotted.

4.3.2 Carbonated concrete pore solution

4.3.2.1 Open circuit potential and polarization resistance

The 1 hour, 24 hour and 7 day readings of open circuit potentials and linear polarization obtained from the linear polarization test of carbon steel samples immersed in carbonated concrete pore solution with fixed amounts of chlorides in the solution are shown in Figures 4.9 and 4.10, respectively. Comparison of these figures with Figures 4.4 and 4.5 shows the difference between carbon steel behaviour in fresh and carbonated concrete pore solutions. In carbonated solutions, carbon steel did not show any sign of passivity or corrosion resistance even in the solution that had the lowest chloride concentration (Cl^- = 0.001). Increasing the amount of chlorides in the solution had no effect on the corrosion potential or the polarization resistance. Low corrosion potentials (~ -740 mV vs. SCE) and polarization resistances ($1x10^3$ ohm.cm^2) were maintained all the time.

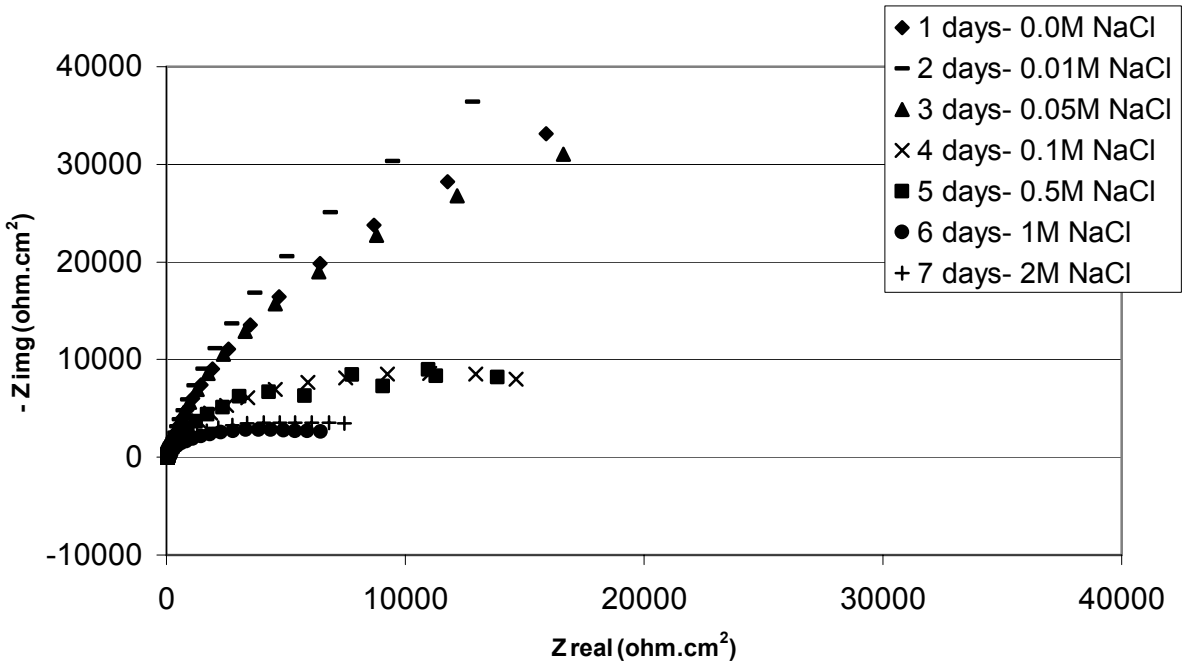

Figure 4.7 Nyquist plot of the impedance of the carbon steel immersed in emulated fresh concrete pore solution with various chloride amounts as measured by EIS.

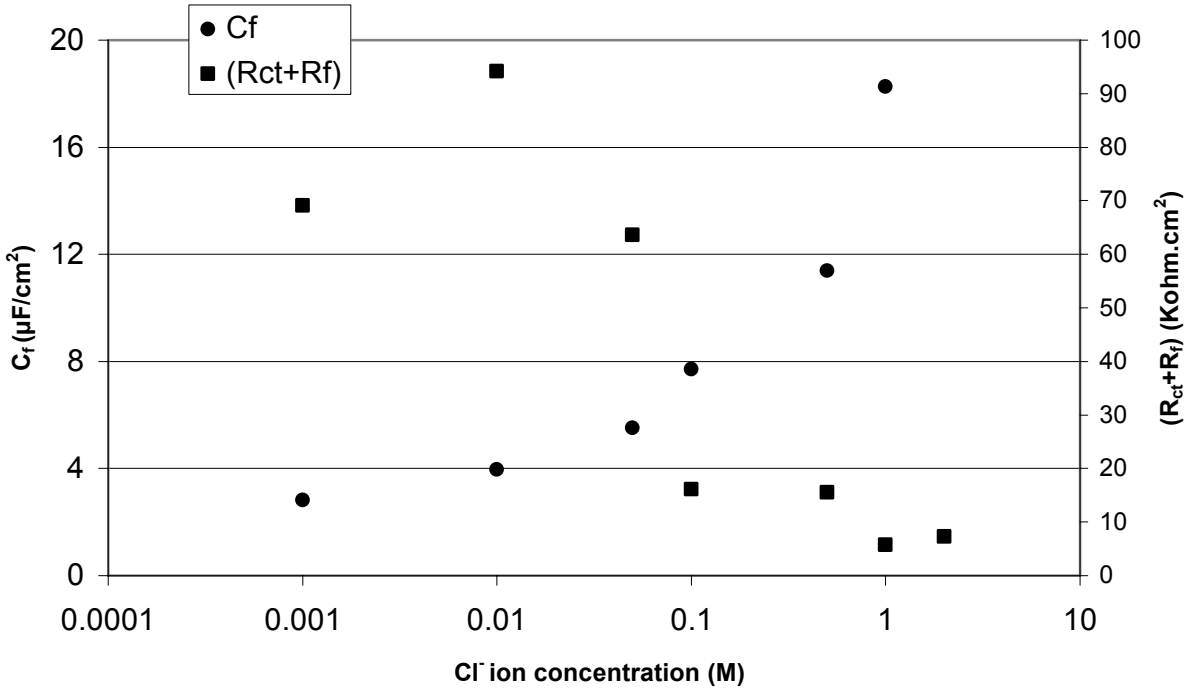

Figure 4.8 Change of the faradic capacitance of the passive film C_f and the sum of the charge transfer resistance R_{ct} and the passive film resistance R_f of carbon steel immersed in fresh concrete pore solution with various chloride amounts

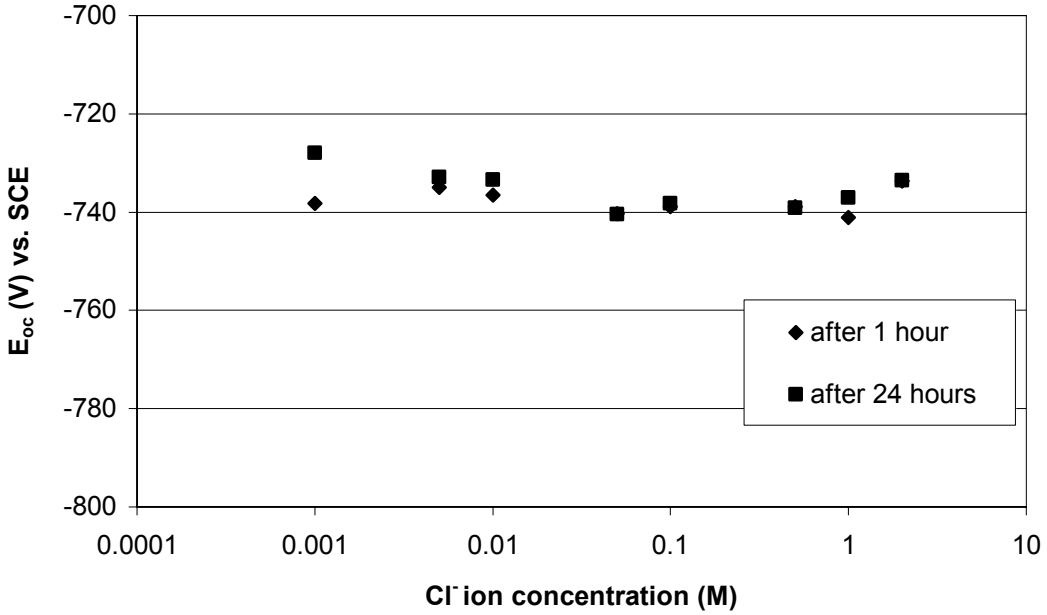

Figure 4.9 Open Circuit Potentials (E_{OC}) of Carbon Steel samples immersed in synthetic carbonated concrete pore solution with various amounts of NaCl added, after 1 hour and 24 hours of immersion.

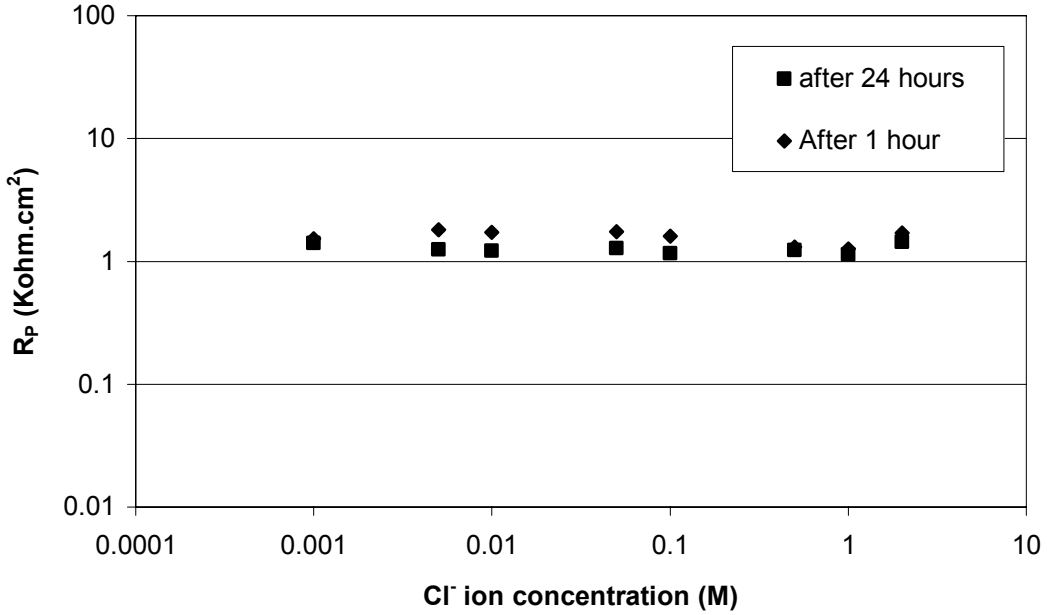

Figure 4.10 Polarization Resistance (R_P) of Carbon Steel samples immersed in synthetic carbonated concrete pore solution with various amounts of NaCl added, after 1 hour and 24 hours of immersion.

The values of polarization resistance were comparable to those obtained from samples immersed in the non- carbonated solution with high chloride content ($Cl^- \geq 1$ M) after 7 days of exposure (R_P = 1-10x10^3 ohm.cm^2). This is evidence of ongoing active corrosion. This was also supported by the visual inspection. After only a few hours, the whole exposed area was covered with rust, regardless the amount of chlorides in the solution. The experiment was terminated after only 24 hours.

4.3.2.2 Corrosion current density

Figure 4.11 shows the corrosion current density i_{corr} obtained when applying the potentiodynamic scan on carbon steel samples immersed in carbonated concrete pore solution with different amounts of chlorides added to the solution after 1 hour and 24 hours of immersion. It is clear that the amount of chlorides in the solution had no effect on the corrosion currents. All the obtained corrosion currents were too high (i_{corr} ~ 22 $\mu A/cm^2$ >> 0.1 $\mu A/cm^2$). This value is in good agreement with previous research. Garces et al. (2005) reported corrosion current density ranged between 5-40 $\mu A/cm^2$ for carbon steel immersed in a solution of 9.5 pH. A slightly lower value of 7 $\mu A/cm^2$ was reported by Moreno et al. (2004) for carbon steel immersed in emulated carbonated concrete pore solution with chloride amounts in the solution ranged between 0-0.1 % after 7 days of exposure. A slight decrease in the corrosion currents obtained after 24 hours was noticed. This can be explained by a slowdown in the corrosion process due to rust formation on the surface, which acts as a barrier for dissolved oxygen preventing it from reaching the surface and being reduced.

4.3.2.3 EIS measurements

Very low impedance spectra (compared to the spectrum obtained in the fresh concrete pore solution(see Figure 4.7) were obtained from carbon steel immersed in the carbonated concrete pore solution with various amounts of chloride ions added incrementally to the solution, as shown in Figure 4.12. The amount of chlorides in the solution had no effect on the impedance. It has to be mentioned that the graphical output from this experiment could not be fitted with the chosen equivalent circuit. This can be explained by the absence of any passive film on the sample's surface.

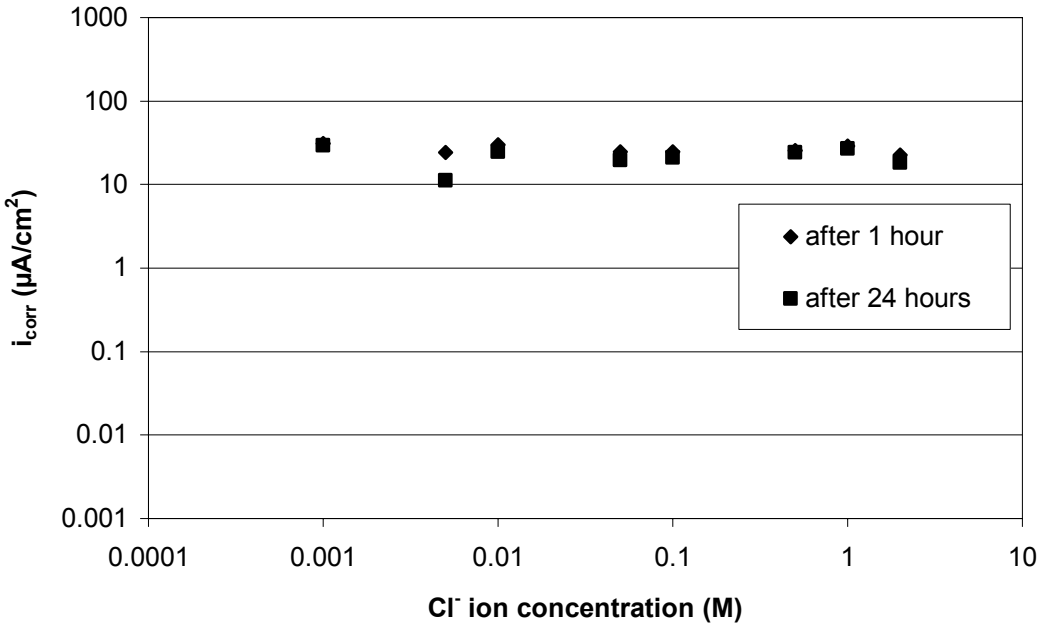

Figure 4.11 Corrosion Current Density (i_{corr}) of Carbon Steel samples immersed in synthetic carbonated concrete pore solution with various amounts of NaCl added, after 1 hour and 24 hours of immersion.

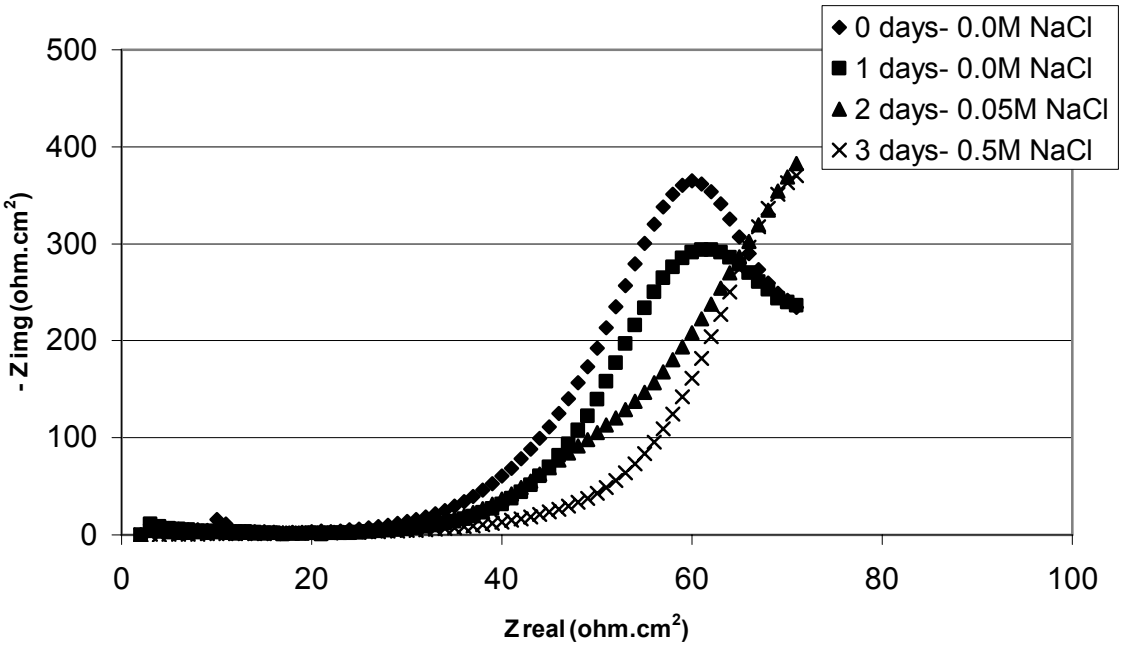

Figure 4.12 Nyquist plot of the impedance of carbon steel immersed in emulated carbonated concrete pore solution with various chloride amounts as measured by EIS.

4.4 Results of Micro-Composite Steel (MMFX-2) Immersed in Synthetic Solutions Emulating Concrete under Chloride Ion Attack

4.4.1 Fresh (non-carbonated) concrete pore solution

4.4.1.1 Open circuit potential and polarization resistance

Figures 4.13 and 4.14 show the open circuit potential and the polarization resistance obtained from linear polarization tests for micro-composite samples immersed in non-carbonated synthetic concrete pore solutions with fixed amounts of chlorides added to the solution after 1 hour, 24 hours and 7 days of immersion. A drop in the free corrosion potential E_{OC} and polarization resistance R_P can be noticed between chloride concentrations of 0.1 M and 0.5 M. The corresponding Cl^-/OH^- ratio is between 0.63 and 3.16. At chloride concentrations ≤ 0.1 M both E_{OC} and R_P were not affected by the increase in Cl^- concentration.

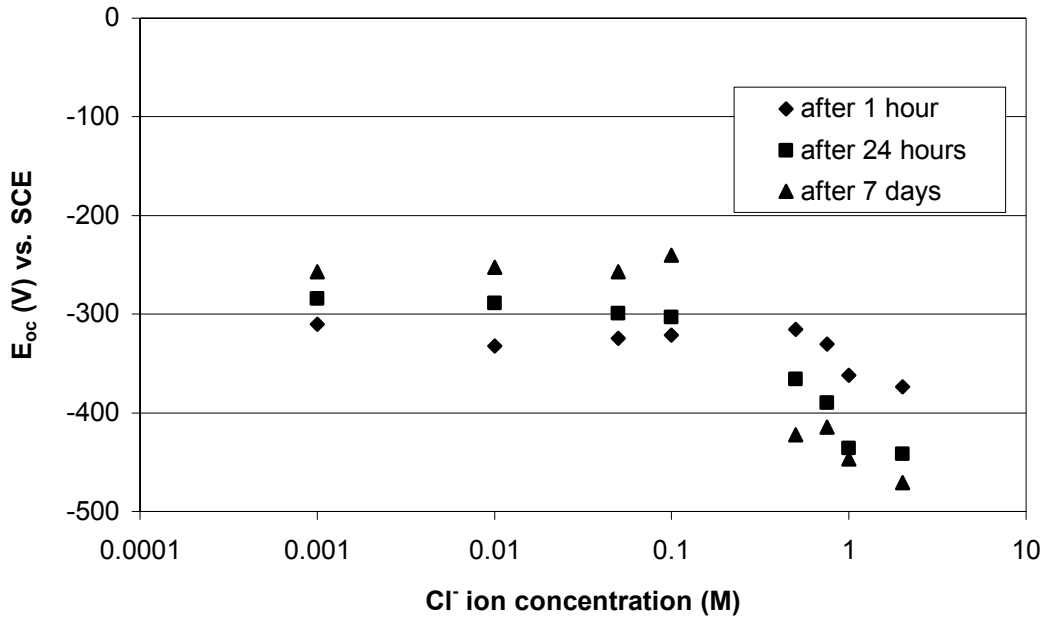

Figure 4.13 Open Circuit Potentials (E_{OC}) of Micro-Composite Steel samples immersed in fresh concrete pore solution with various amounts of NaCl added, after 1 hour, 24 hours and 7 days of immersion.

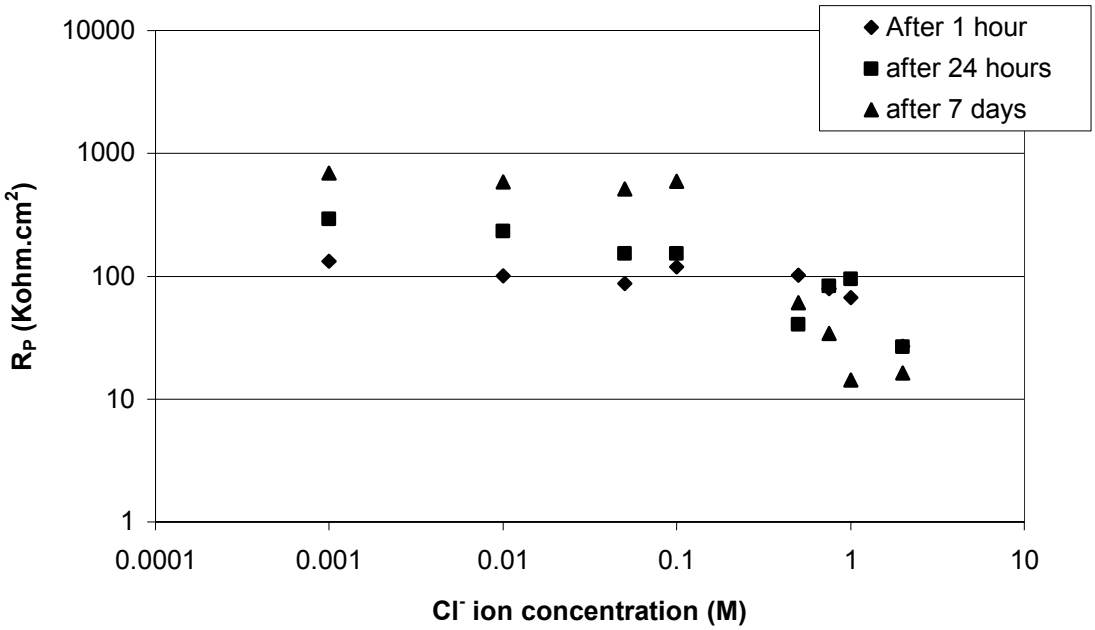

Figure 4.14 Polarization Resistance (R_P) of Micro-Composite Steel samples immersed in synthetic concrete pore solution with various amounts of NaCl added, after 1 hour, 24 hours and 7 days of immersion.

With time, nobler (i.e. more positive) potentials and increased polarization resistance were achieved as a sign of passivity increasing. At chloride concentrations of 0.5 M or higher, E_{OC} and R_P reached very low values (E_{OC} < -400 mV vs. SCE and R_P = 10-100 Kohm.cm^2) after 7 days of immersion. However, these values were higher than those of carbon steel at the same chloride concentrations (E_{OC} < -500 mV vs. SCE and R_P = 1-10 Kohm.cm^2). These results suggest that the chloride threshold level for micro-composite steel in fresh concrete pore solution is somewhere between 0.1-0.5 M (Cl^-/OH^- = 0.63-3.16). This chloride threshold value is 2 to 10 times higher than the carbon steel threshold level. This finding is in good agreement with the published literature. Hurely (2007) reported a Cl^-/OH^- threshold ratio of 3.7 for micro-composite steel immersed in the full saturated $Ca(OH)_2$ solution using the anodic polarization technique (6 times higher than carbon steel). For samples embedded in mortar, Trejo and Pillai (2004) reported a Cl^-/OH^- threshold ratio of 3.02 ± 0.65 (9 times higher than ASTM A615 carbon steel). A slightly higher range (Cl^-/OH^- = 4.7 to 6) was reported by Clemena and Virmani (2004) for samples embedded in concrete.

4.4.1.2 Corrosion current density

The corrosion current density i_{corr} obtained from potentiodynamic scans of micro-composite samples after 1 hour, 24 hours and 7 days of immersion in fresh concrete pore solution are shown in Figure 4.15. The i_{corr} limit ($i_{corr} > 0.1$ μA/cm^2) was exceeded at the chloride concentration of 0.5 M ($Cl^-/OH = 3.16$). While indeed corrosion current density increased with the increase in chloride concentration in the solution after reaching the threshold value, the increasing rate was low compared to carbon steel (see Figure 4.6). The corrosion current density (μA/cm^2) after 7 days of exposure for carbon steel increased from 0.54 μA/cm^2 at Cl^- concentration of 0.1 M to 8.81 μA/cm^2 at Cl^- concentration of 2 M (see Figure 4.6), while that of micro-composite steel increased from 0.41 μA/cm^2 to be only 2 μA/cm^2 at Cl^- concentrations of 0.5 M and 2 M, respectively. This suggests that even if the chloride threshold limit is exceeded, severe loss of the rebar cross section is not expected for micro-composite steel rebars inside non-carbonated concrete. This is valid until a Cl^-/OH^- ratio of 12.62. Higher chloride concentrations are not practically expected in concrete.

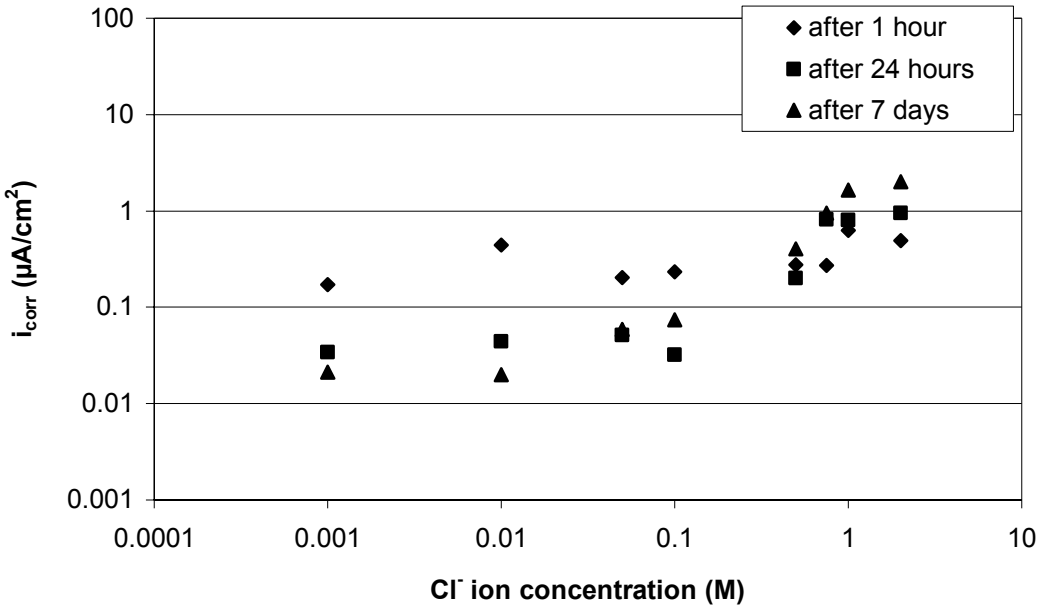

Figure 4.15 Corrosion Current Density (i_{corr}) of Micro-Composite Steel samples immersed in synthetic concrete pore solution with various amounts of NaCl added, after 1 hour, 24 hours and 7 days of immersion.

4.4.1.3 EIS measurements

Figure 4.16 shows a Nyquist plot of the impedance of micro-composite steel immersed in the fresh concrete pore solution with various amounts of NaCl added incrementally to the solution in a period of 7 days. The low frequency portion of the impedance spectra decreases gradually with the increase of chloride ion concentration in the solution. This behaviour is similar to that of carbon steel in the same solution; however, no sudden decrease in the impedance spectra can be noticed.

Figure 4.17 shows the change of the parameters related to the passive film formation with chloride addition to the solution. With the increase of chloride amounts in the solution, a decreased sum of charge transfer resistance and passive film resistance (R_{ct} + R_f) was observed and, similar to carbon steel, the film capacitance C_f increased as a sign of increased corrosion rates. However, the rate of the increase of C_f was very

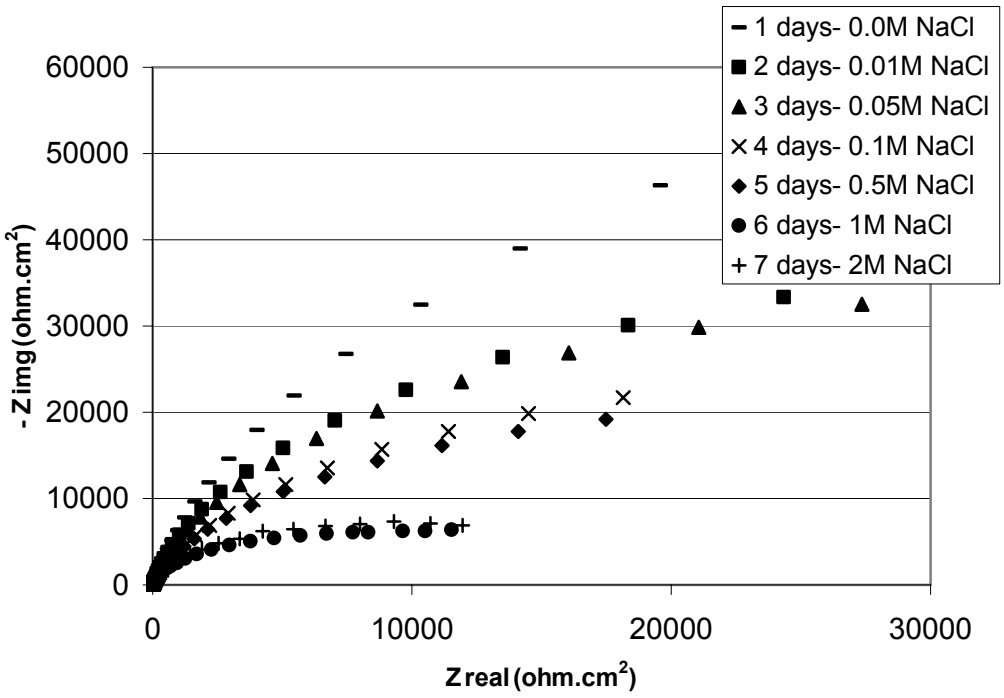

Figure 4.16 Nyquist plot of the impedance of micro-composite steel immersed in emulated fresh concrete pore solution with various chloride amounts as measured by EIS.

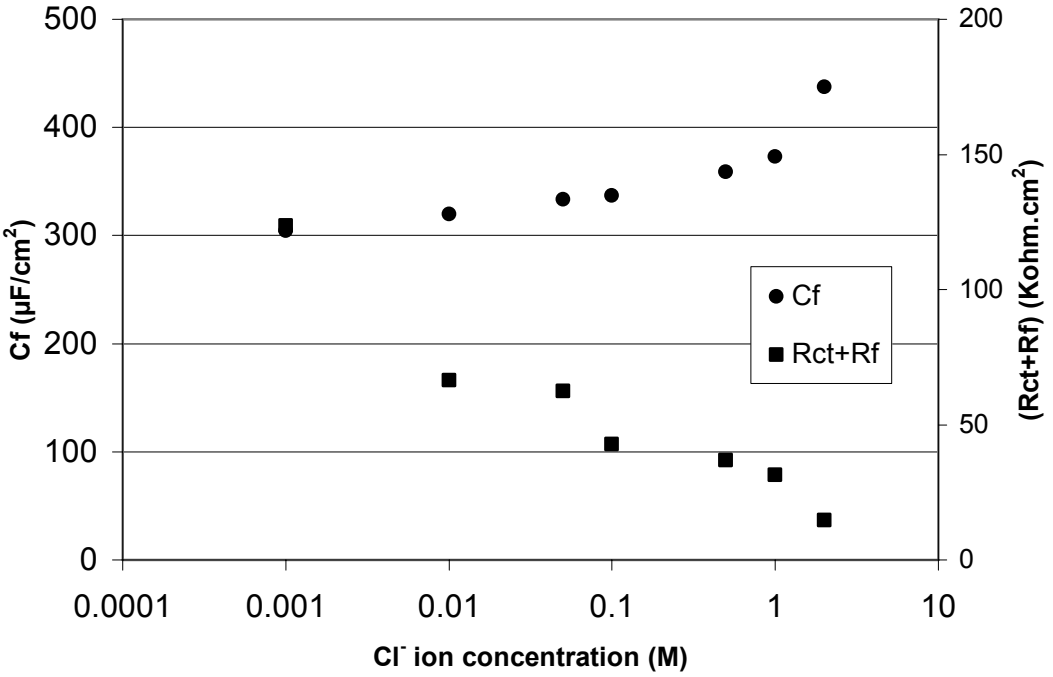

Figure 4.17 Change of the faradic capacitance of the passive film C_f and the sum of the charge transfer resistance R_{ct} and the passive film resistance R_f of micro-composite steel immersed in fresh concrete pore solution with various chloride amounts.

small (C_f = 300 µF/cm^2 at 0 chloride concentration, C_f = 437 µF/cm^2 at Cl^- concentration of 2 M) compared to that of carbon steel in the same solution. This supports the previous finding, that even at high chloride concentrations (up to 2 M) severe corrosion is not expected to occur for micro-composite steel in fresh concrete pore solution.

4.4.1.4 Cyclic polarization curves

As mentioned earlier, the cyclic polarization scan is used to examine the metal's tendency to pit in a certain environment. Figure 4.18 shows the cyclic polarization curves for micro-composite steel samples immersed in the fresh concrete pore solution at different chloride concentrations after 24 hours of exposure. It can be noticed that the metal had a passive region (increased applied over potential and same current density) that started immediately after the Tafel area (E_{OC} ± 150 mV) and continued until E_{pit} was reached. This applies for all the tested chloride concentrations. However, the effect of the

amount of chloride ions in the solution can be noticed in the decreasing value of E_{pit} with the increase of chloride concentration in the solution. E_{pit} had the same value of +500 mV vs. SCE in the 0.01, 0.1 and 0.5 M solutions.

In these solutions, the hysteresis loop was unnoticeable and both E_{pit} and E_{prot} had the same value, which is an indication that the metal is able to resist pitting corrosion at these chloride levels. In addition, it can be noticed that in the 0.5 M solution, although E_{pit} and E_{prot} had the same value as were obtained in the lower chloride concentration solutions, the recorded i_{corr} in the reverse scan was higher. Perhaps a longer exposure time in that solution (Cl^- 0.5 M) was needed to reduce the pitting resistance of the metal. At higher chloride concentrations of 1 and 2 M, the pitting potential E_{pit} decreased to be 315 and 128 mV vs. SCE, respectively, and the hysteresis loop did not close. This is an indication of the breakdown of the passive film and that the metal was not able to repassivate (was not able to heal) at these chloride concentrations.

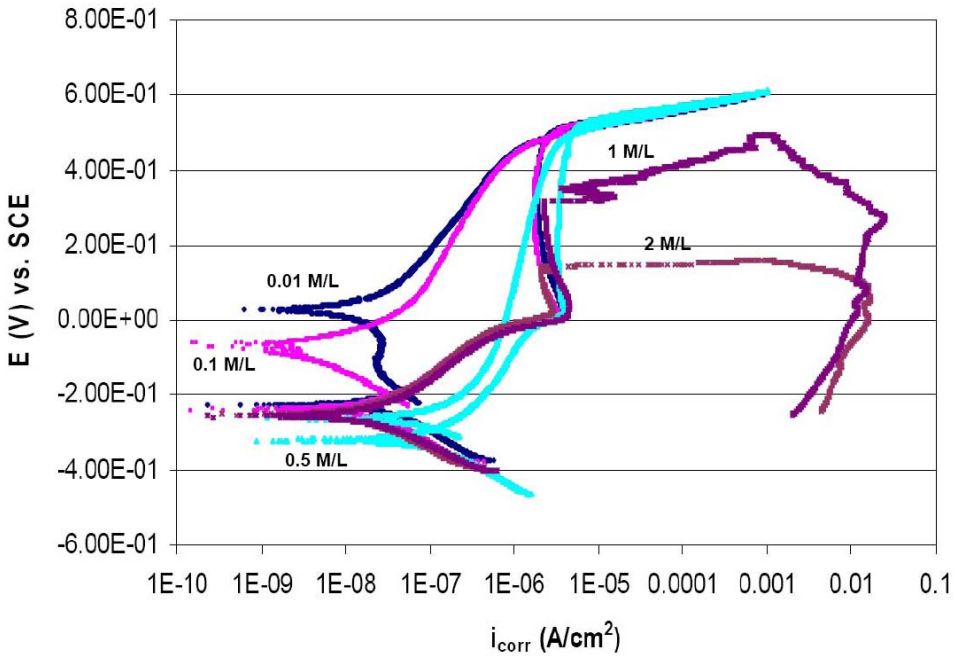

Figure 4.18 Cyclic polarization curves of micro-composite steel after 24 hours of immersion in non-carbonated concrete pore solution with different chloride levels in the solution

This behaviour can be explained by the competitive action of both Cl^- and OH^- ions in the solution. At low chloride ion concentrations ($Cl^- \leq 0.5$ M) and after pitting initiated at E_{pit} = +500 mV vs. SCE the high alkalinity of the solution (high concentration of OH^-) will help the metal to repassivate (heal) when the applied potential is decreased. On the other hand, at high chloride ions concentrations ($Cl^- > 0.5$M) Cl^- ions will overcome OH^- ions and prevent the process of repassivation after pitting is initiated (Benture et. al., 1997 and Saremi and Mahallati, 2002).

4.4.2 Carbonated concrete pore solution

4.4.2.1 Open circuit potential and polarization resistance

The corrosion behaviour of micro-composite steel samples immersed in the carbonated concrete pore solution was significantly different from that of carbon steel samples immersed in the same solution. While carbon steel exhibited active corrosion ($i_{corr} >> 0.1$ $\mu A/cm^2$) regardless the chloride concentration in the solution, micro-composite steel exhibited increasingly active corrosion with the increase of chloride concentration in the solution. This behaviour was similar to its behaviour in the fresh concrete pore solution.

The open circuit potential and polarization resistance obtained from linear polarization tests for micro-composite samples immersed in carbonated synthetic concrete pore solution after 1 hour, 24 hours and 7 days of immersion are shown in Figures 4.19 and 4.20, respectively. From these figures, a gradual decrease of the open circuit potential E_{OC} and the polarization resistance R_P with the increase of chloride concentration in the solution after 7 days of immersion can be noticed beyond a chloride concentration of 0.01 M. However, this decrease became more significant after a chloride concentration of 0.1 M was exceeded. At a chloride concentration $\leq$ 0.01 M, noble potentials and high polarization resistance were maintained until the end of the exposure time.

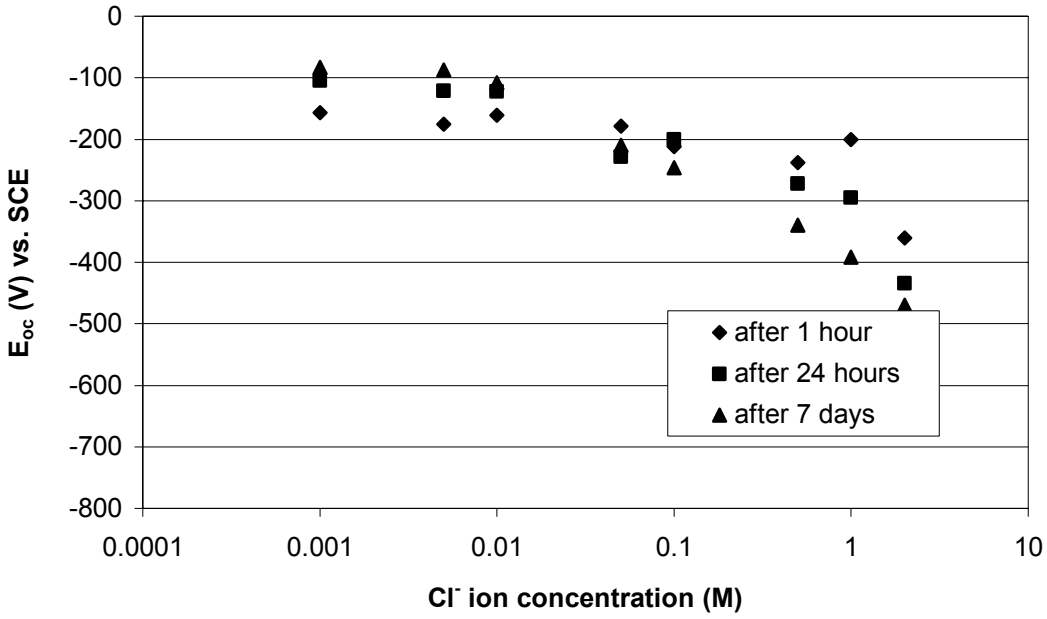

Figure 4.19 Open Circuit Potentials (E_{OC}) of Micro-Composite Steel samples immersed in synthetic carbonated concrete pore solution with various amounts of NaCl added, after 1 hour, 24 hours and 7 days of immersion.

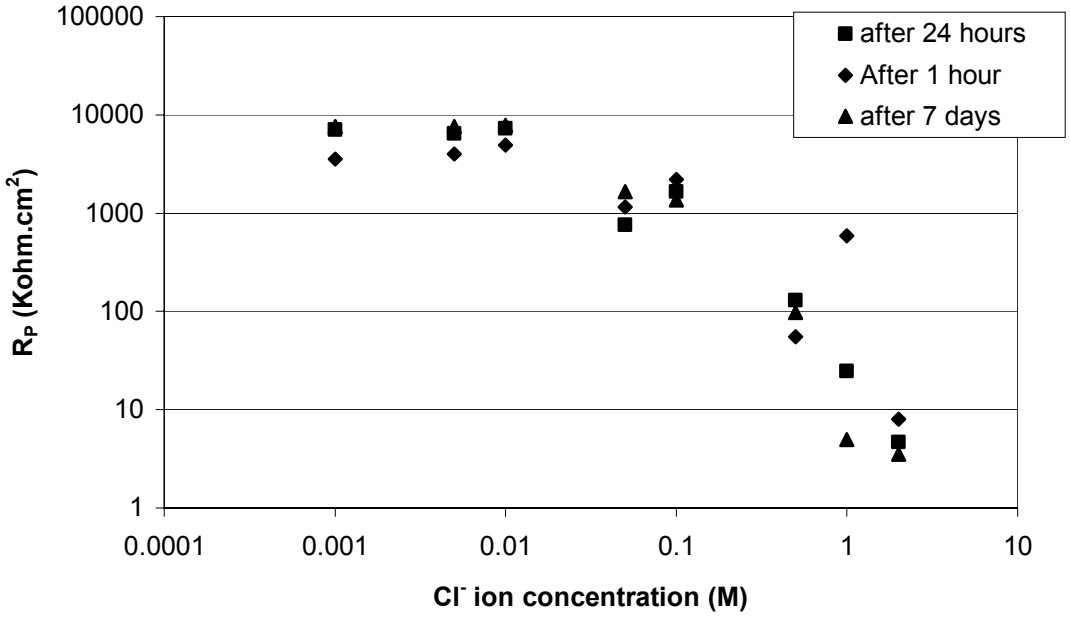

Figure 4.20 Polarization Resistance (R_P) of Micro-Composite Steel samples immersed in synthetic carbonated concrete pore solution with various amounts of NaCl added, after 1 hour, 24 hours and 7 days of immersion.

4.4.2.2 Corrosion current density

The corrosion current density i_{corr} obtained from potentiodynamic scans of micro-composite samples after 1 hour, 24 hours and 7 days of immersion in carbonated concrete pore solution are shown in Figure 4.21. Although lowering corrosion potentials and polarization resistance occurred at a chloride concentration of 0.01 M, the i_{corr} limit (i_{corr} > 0.1 μA/cm^2) was not exceeded until a chloride concentration of 0.5 M. This is the same chloride threshold concentration for micro-composite steel in the fresh (non-carbonated) solution. After that limit, increased corrosion currents were obtained. This behaviour highlights the beneficial effect of chromium addition to the alloy, which led to the extension of the passivity region to lower pH values (pH = 8.5). However, the metal's passivity started to deteriorate when the chloride concentration in the solution reached 0.5M in both cases of fresh and carbonated concrete pore solution. It is worth noting that although corrosion currents obtained at high chloride concentrations (Cl^- = 0.5-2M) were high and unacceptable from a durability point of view (i_{corr} > 0.1 μA/cm^2), they were significantly lower than those of carbon steel were in the same solution.

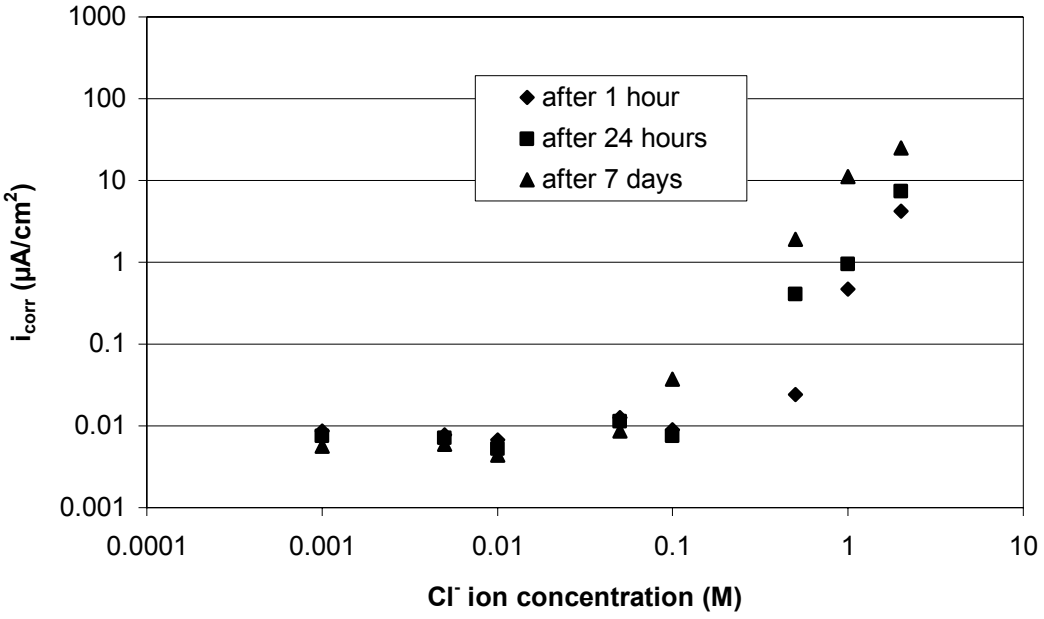

Figure 4.21 Corrosion Current Density (i_{corr}) of Micro-Composite Steel samples immersed in synthetic carbonated concrete pore solution with various amounts of NaCl added, after 1 hour, 24 hours and 7 days of immersion.

4.4.2.3 EIS measurements

Figures 4.22 and 4.23 show the Nyquist plot of the impedance of micro-composite steel immersed in carbonated concrete pore solution with various amounts of NaCl added incrementally to the solution in a period of 7 days and the change of the parameters related to the passive film formation with chloride addition to the solution, respectively. Data were fitted using the representative circuit shown in Figure 3.9. In agreement with the DC experiment findings, the impedance spectrum decreased constantly with chloride addition to the solution. The impedance almost vanished at Cl^- concentration of 1 M and 2 M. This was accompanied by a decrease in the sum of the charge transfer resistance and film resistance ($R_{ct} + R_f$) ($R_{ct} + R_f$ decreased from $1.72x10^6$ to be $0.06\ x10^6$ ohm.cm^2 at 0.0 and 2 M respectively) and an increase of the faradic capacitance of the film C_f (C_f increased from 8.55 to be 236 μF/cm^2 at 0.0 and 2 M respectively). It was noticeable that these parameters changed significantly when chloride concentration in the solution exceeded 0.1 M as a sign of a weakened passive film.

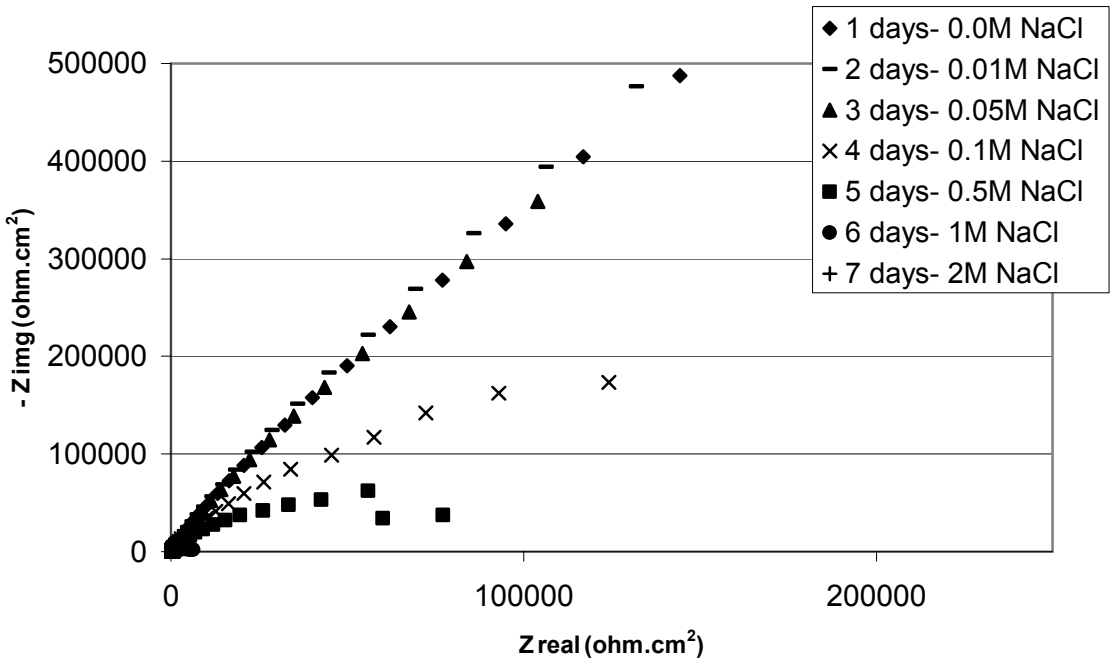

Figure 4.22 Nyquist plot of the impedance of micro-composite steel immersed in emulated carbonated concrete pore solution with various chloride amounts as measured by EIS.

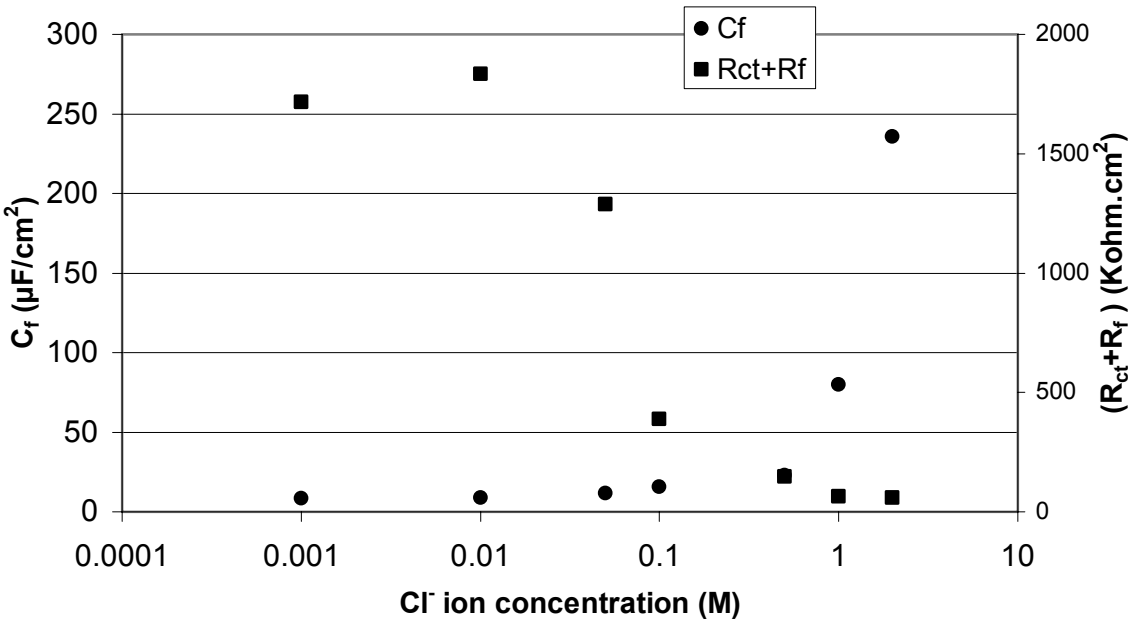

Figure 4.23 Change of the faradic capacitance of the passive film C_f and the sum of the charge transfer resistance R_{ct} and the passive film resistance R_f of micro-composite steel immersed in carbonated concrete pore solution with various chloride amounts.

4.4.2.4 Cyclic polarization curves

Figure 4.24 shows cyclic polarization curves for micro-composite steel samples immersed in the carbonated concrete pore solution at different chloride concentrations after 24 hours of immersion. From this figure, it can be noticed that the metal was unable to repassivate (no hystresis loop) after decreasing the applied overvoltage at all the chloride concentrations tested. This can be attributed to the shortage of OH^- ions in the solution. The pitting potential decreased with the increase of chloride ions concentration in the solution. At a chloride concentration of 0.01 M the metal was able to resist pitting until a relatively high potential (E_{pit} = +300 mV vs. SCE); however, at 0.1 M and 0.5 M E_{pit} decreased to be only 0.0 mV vs. SCE. The metal resistance to pitting corrosion almost vanished in 1 M and 2 M solutions.

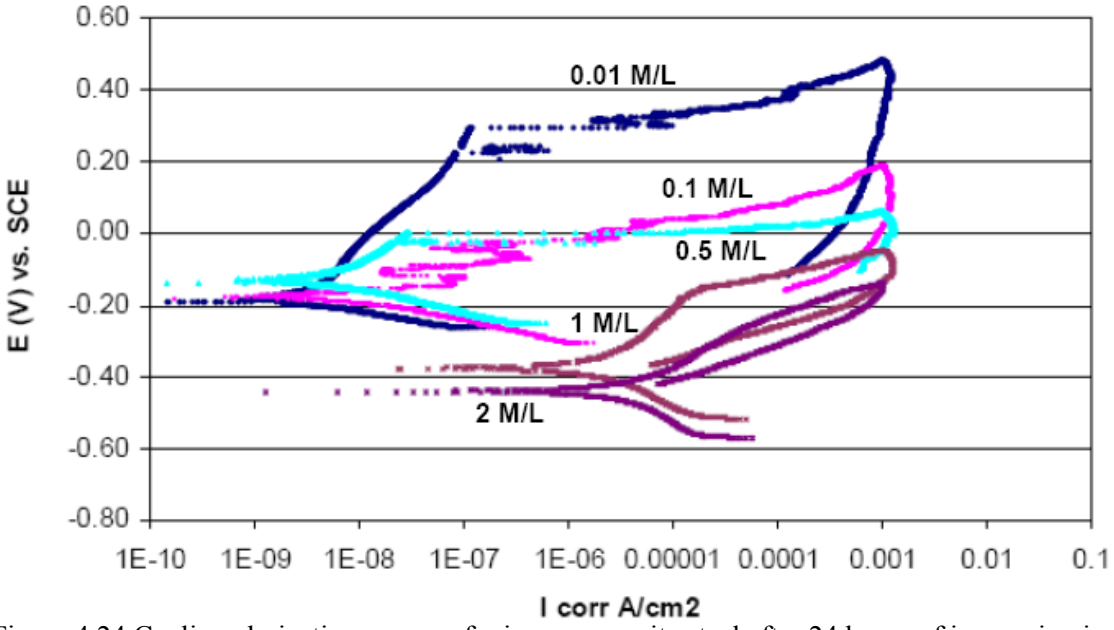

Figure 4.24 Cyclic polarization curves of micro-composite steel after 24 hours of immersion in carbonated concrete pore solution with different chloride levels in the solution.

4.5 Results of 316LN Stainless Steel Immersed in Synthetic Solutions Emulating Concrete under Chloride Ion Attack

4.5.1 Fresh (non-carbonated) concrete pore solution

4.5.1.1 Open circuit potential and polarization resistance

Figures 4.25 and 4.26 show the open circuit potential and polarization resistance obtained from linear polarization tests for 316LN stainless steel samples immersed in a non-carbonated synthetic concrete pore solution with fixed amount of chlorides added to the solution after 1 hour, 24 hours and 7 days of immersion. The amount of chloride ions in the solution does not seem to have any effect on the free corrosion potential or the polarization resistance for a chloride concentration up to 2 M (Cl^-/OH^- = 12.62). In fact, nobler potentials and increased polarization resistance were achieved after 7 days of exposure at chloride concentrations tested. This suggests that the chloride threshold ratio Cl^-/OH^- of 316LN stainless steel is greater than 12.62. This finding is in good agreement with the previous research conducted by others. Bertolini et al. (1996) found that AISI

316L stainless steel immersed in saturated $Ca(OH)_2$ solution will exhibit pitting at a chloride concentration of 5% (Cl^-/OH^- ~ 21.4). Hurley and Scully (2002) reported a chloride threshold ratio Cl^-/OH^- greater than 100 for 316LN stainless steel in saturated $(CaOH)_2$ solution polarized at -200 mV vs. SCE, dropping to be 24 at polarization of +200 mV vs. SCE. Terjo and Pillai (2004) found a threshold ratio Cl^-/OH^- of 28.92 ± 8.27 for 316LN stainless steel samples embedded in mortar.

4.5.1.2 Corrosion current density

Figure 4.27 shows the corrosion current density i_{corr} for 316LN stainless steel samples after 1 hour, 24 hours and 7 days of immersion in non-carbonated synthetic concrete pore solution with fixed amount of chlorides added to the solution. As expected, the corrosion current density was not affected by the increase in the chloride concentration in the solution. After 7 days of exposure, the corrosion current density was as low as 0.01-0.04 $\mu A/cm^2$ regardless of the chloride concentration in the solution. It was noticeable that the corrosion currents decreased by about an order of magnitude after 7 days of exposure as an evidence of further growth of the metal's passive layer

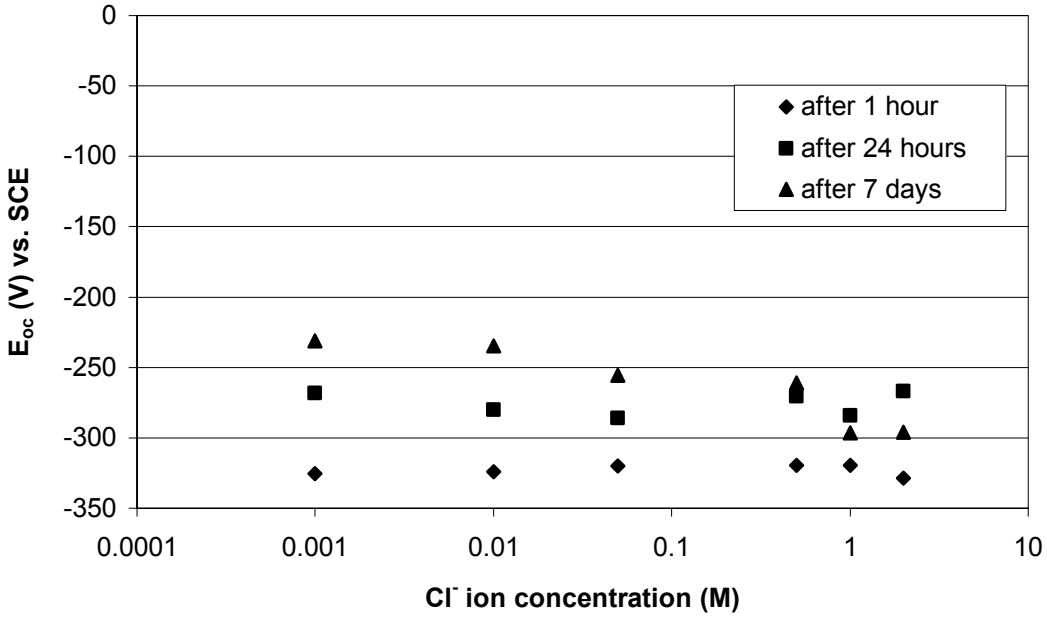

Figure 4.25 Open Circuit Potentials (E_{OC}) of 316LN Stainless Steel samples immersed in synthetic concrete pore solution with various amounts of NaCl added, after 1 hour, 24 hours and 7 days of immersion.

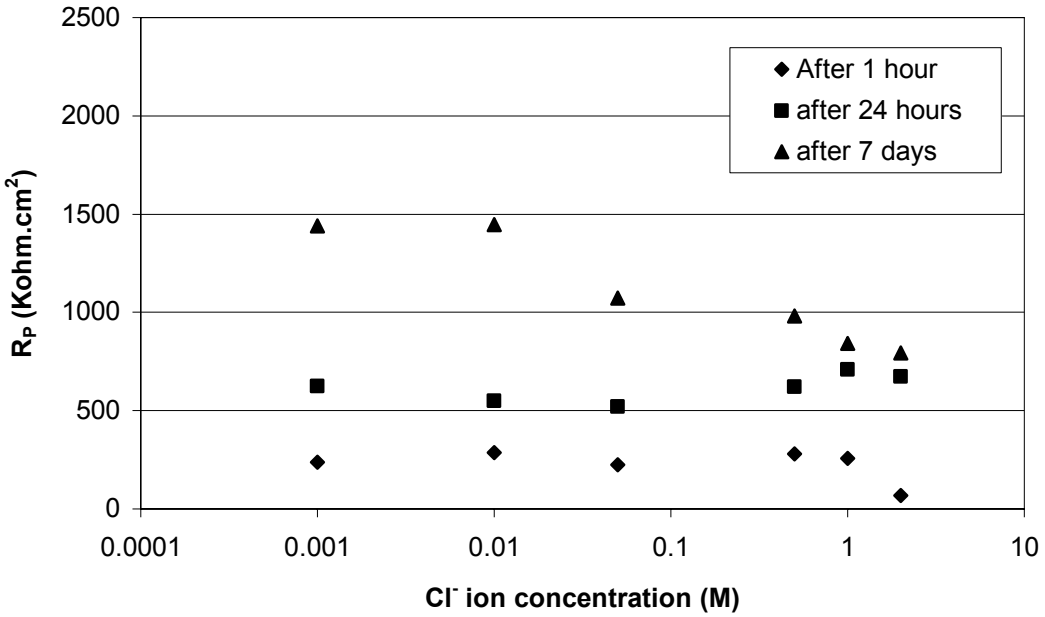

Figure 4.26 Polarization Resistance (R_P) of 316LN Stainless Steel samples immersed in synthetic concrete pore solution with various amounts of NaCl added, after 1 hour, 24 hours and 7 days of immersion.

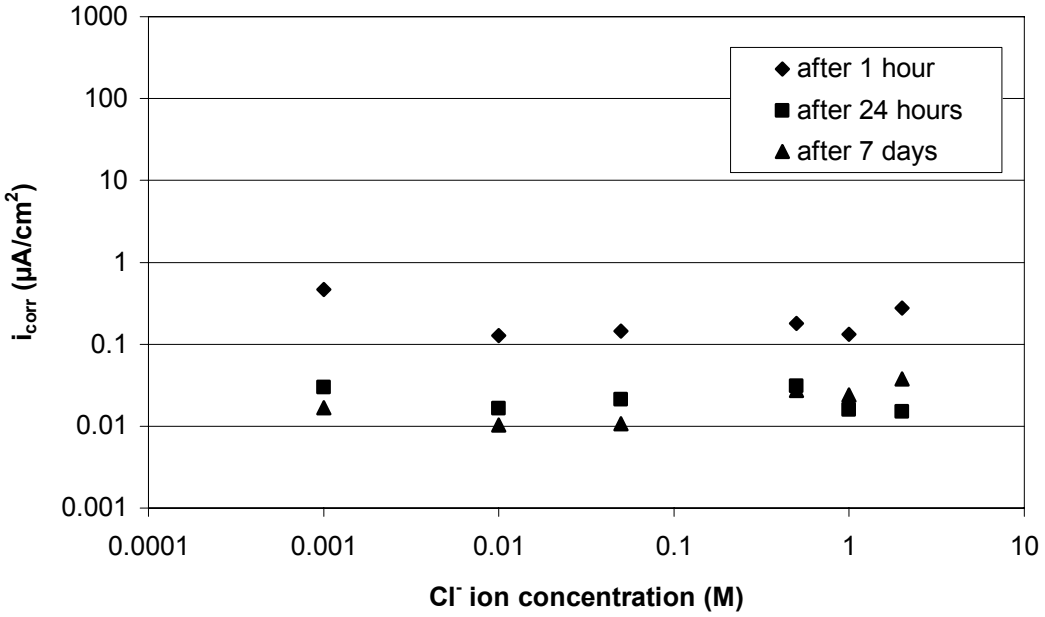

Figure 4.27 Corrosion Current Density (i_{corr}) of 316LN Stainless Steel samples immersed in synthetic concrete pore solution with various amounts of NaCl added, after 1 hour, 24 hours and 7 days of immersion.

Escudero et al. (2002) reported similar corrosion currents between 0.1μA/cm^2 and 0.01 μA/cm^2 for 316 stainless steel after 48 hours of immersion in the fully saturated $Ca(OH)_2$ solution with chloride concentration of 3.5% (Cl^-/OH^- = 15).

4.5.1.3 EIS measurements

Figures 4.28 and 4.29 show the Nyquist plot of the impedance of 316LN stainless steel immersed in fresh concrete pore solution with various amounts of NaCl added incrementally to the solution in a period of 7 days and the change of the parameters related to the passive film formation with chloride addition to the solution, respectively. The EIS results showed a good agreement with the DC measurements. A mainly high impedance spectrum was maintained until the Cl^- concentration reached 2 M. However, it was noticeable that the impedance limit, especially at the low frequency range, had lower values at that concentration than other concentrations. This was also accompanied by a slight decrease in the sum of (R_{ct} + R_f) (2.65x10^5 ohm.cm^2 to 1.06x10^5 ohm.cm^2 at Cl^- concentration of 0.0 and 2 M respectively) and an increase in the faradic capacitance

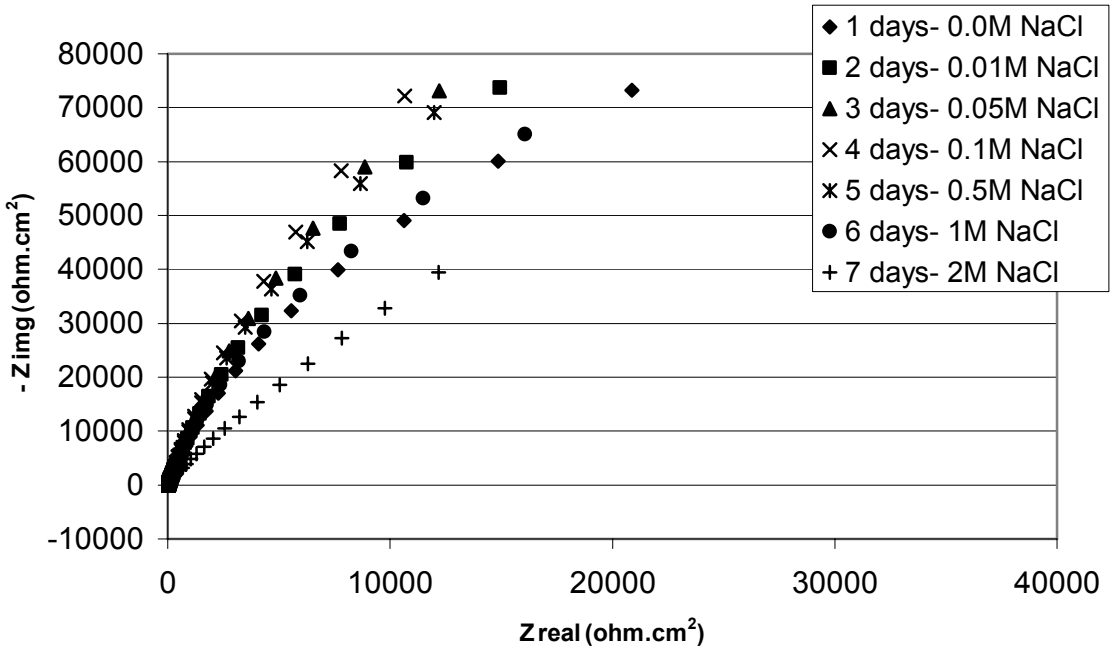

Figure 4.28 Nyquist plot of the impedance of 316LN stainless steel immersed in emulated fresh concrete pore solution with various chloride amounts added as measured by EIS.

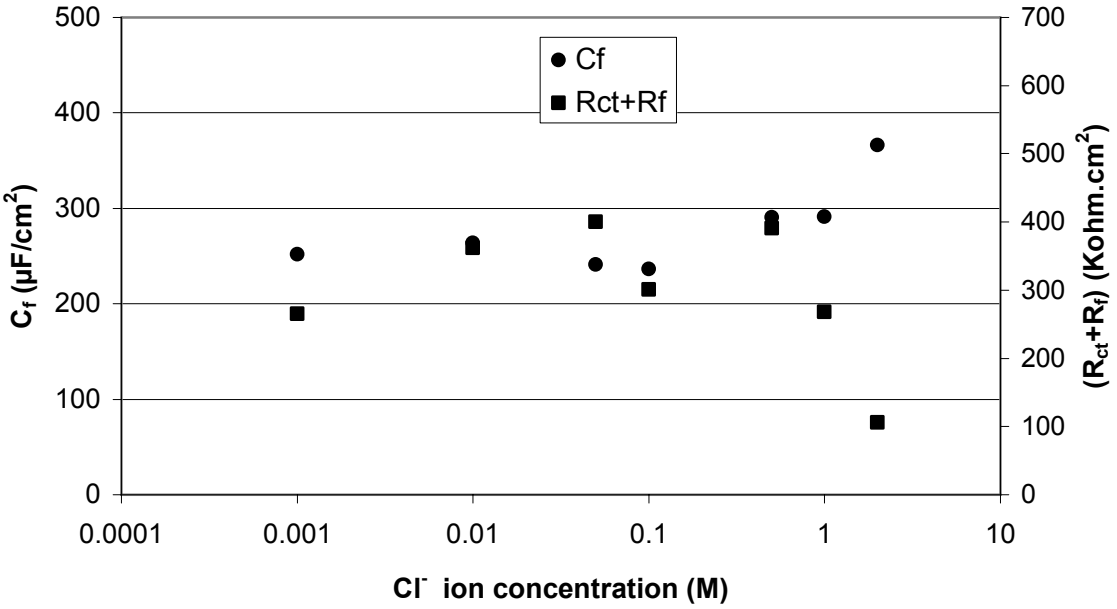

Figure 4.29 Change of the faradic capacitance of the passive film C_f and the sum of the charge transfer resistance R_{ct} and the passive film resistance R_f of 316LN stainless steel immersed in fresh concrete pore solution with various chloride amounts

of the passive film C_f (2.52×10^{-4} F/cm^2 to 3.66×10^{-4} F/cm^2 at Cl^- concentration of 0.0 and 2 M respectively). This indicates the beginning of chloride ions penetration to the passive film and suggests that the chloride threshold of the metal does exist at Cl^-/OH^- ratios higher than 12.6.

4.5.2 Carbonated concrete pore solution

4.5.2.1 Open circuit potential and polarization resistance

Similar to its behaviour in the high pH (pH = 13.2) fresh concrete pore solution, 316LN stainless steel did not show any sign of passivity break down in the low pH (pH = 8.5) carbonated concrete pore solution even at the highest chloride level in the solution (Cl^- = 2 M). Both free corrosion potential E_{OC} and polarization resistance values were almost the same within the tested chloride range (0.001 – 2 M) after 7 days of immersion, as shown in Figures 4.30 and 4.31.

Two important observations have to be highlighted here. Firstly, both E_{OC} and R_P values did not increase with time (in contrast with the metal's behaviour in the high pH solution (see Figures 4.25 and 4.26)). This observation suggests the importance of the high alkaline medium (i.e. high OH^- ions concentration) for strengthening the metal's passive film overtime. Secondly, E_{OC} values, although they did not increase with time of exposure, their values were, surprisingly, higher than those obtained when the metal was immersed in the high pH solution, especially after 1 hour of immersion. The same observation was reported by Blanco et al. (2006).

4.5.2.2 Corrosion current density

The corrosion current density i_{corr} obtained from potentiodynamic scans of 316LN stainless steel samples after 1 hour, 24 hours and 7 days of immersion in carbonated concrete pore solution are shown in Figure 4.32. After 7 days of exposure, the critical i_{corr} limit of 0.1 $\mu A/cm^2$ was not exceeded even at chloride concentration as high as 2 M. However, unlike its behaviour in the non-carbonated solution, the metal's corrosion current did not decrease with the increase of exposure time.

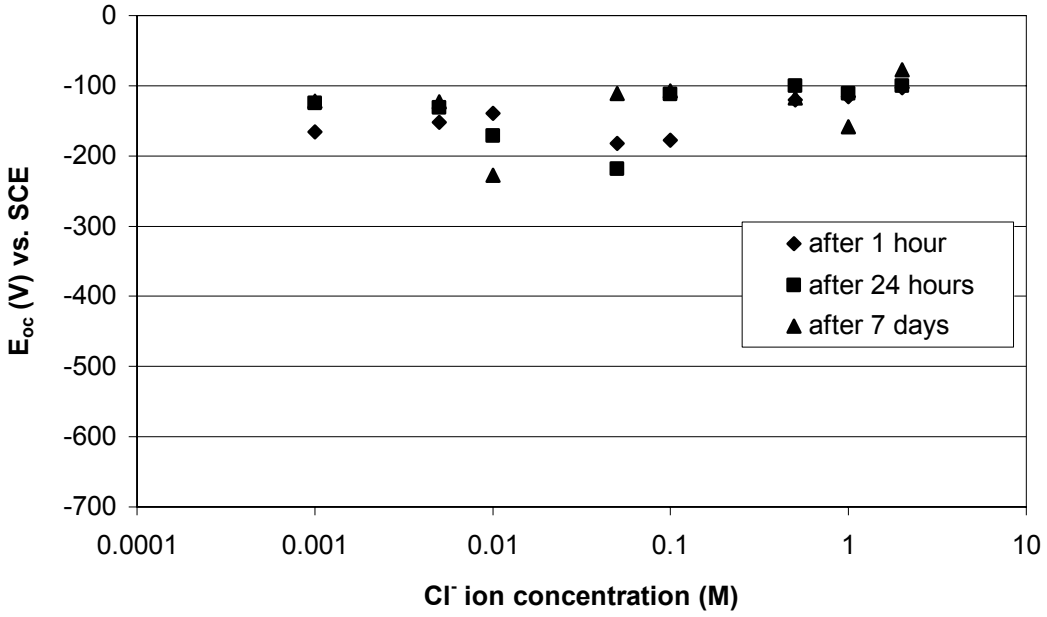

Figure 4.30 Open Circuit Potentials (E_{OC}) of 316LN Stainless Steel samples immersed in synthetic carbonated concrete pore solution with various amounts of NaCl added, after 1 hour, 24 hours and 7 days of immersion.

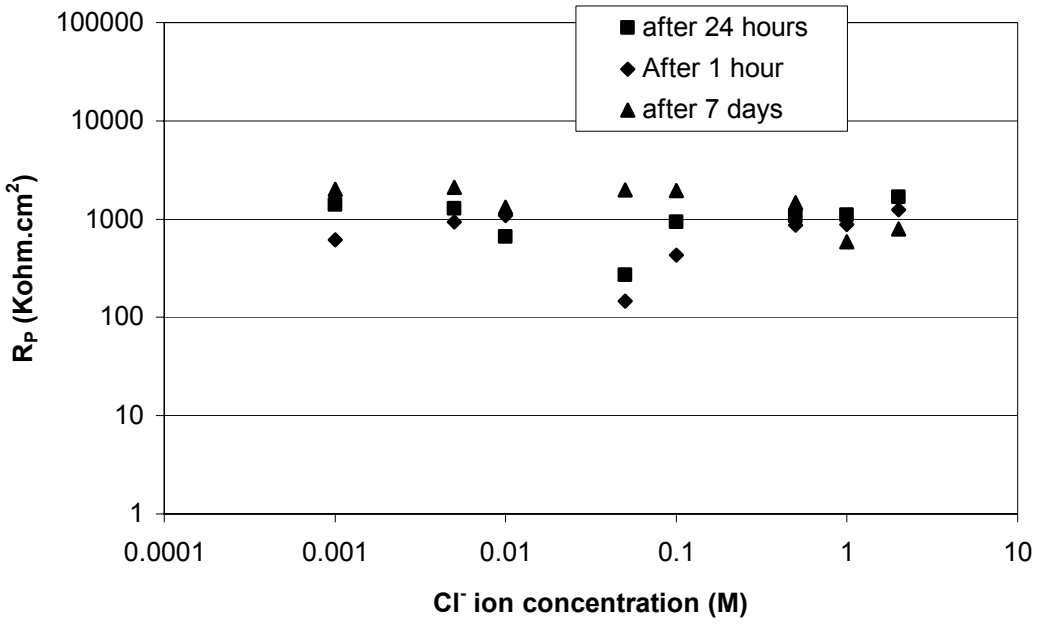

Figure 4.31 Polarization Resistance (R_P) of 316LN Stainless Steel samples immersed in synthetic carbonated concrete pore solution with various amounts of NaCl added, after 1 hour, 24 hours and 7 days of immersion.

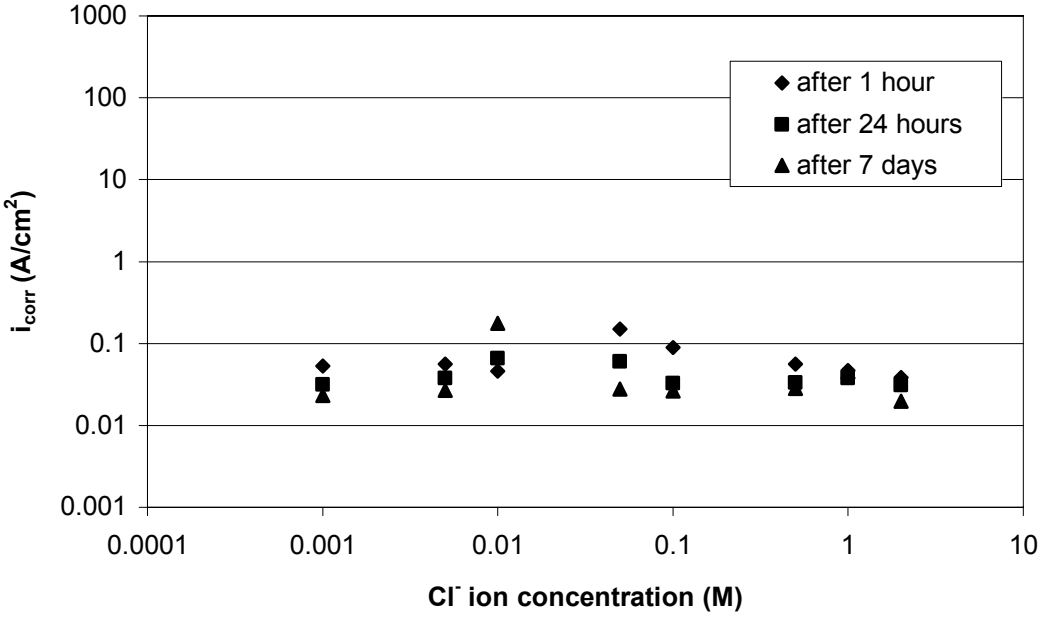

Figure 4.32 Corrosion Current Density (i_{corr}) of 316LN Stainless Steel samples immersed in synthetic carbonated concrete pore solution with various amounts of NaCl added, after 1 hour, 24 hours and 7 days of immersion.

4.5.2.3 EIS measurements

Figures 4.33 and 4.34 show the Nyquist plot of the impedance of 316LN stainless steel immersed in the carbonated concrete pore solution with various amounts of NaCl added incrementally to the solution in a period of 7 days and the change of the parameters related to the passive film formation with chloride addition to the solution, respectively. Similar to its behaviour in the non-carbonated solution, the metal maintained a high impedance spectrum at the tested chloride concentrations except when the concentration of Cl^- reached the limit of 2 M. At that limit, the impedance was significantly lower than at other tested concentration with increased film capacitance C_f and decreased ($R_{ct} + R_f$) parameter. This is a sign of degradation of the passive film. It has to be mentioned here that this does not mean that the metal is corroding yet (i_{corr} obtained from DC measurements at the same chloride concentration was lower than 0.1 $\mu A/cm^2$ after 7 days of exposure (see Figure 4.32)). Also, it was noticeable that the rate of change of C_f ($1.09x10^{-10}$ F/cm^2 to $1.14x10^{-8}$ F/cm^2 at Cl^- concentration of 0.0 and 2 M respectively) and ($R_{ct} + R_f$) ($2.48x10^5$ $ohm.cm^2$ to $1.16x10^4$ $ohm.cm^2$ at Cl^- concentration of 0.0 and 2

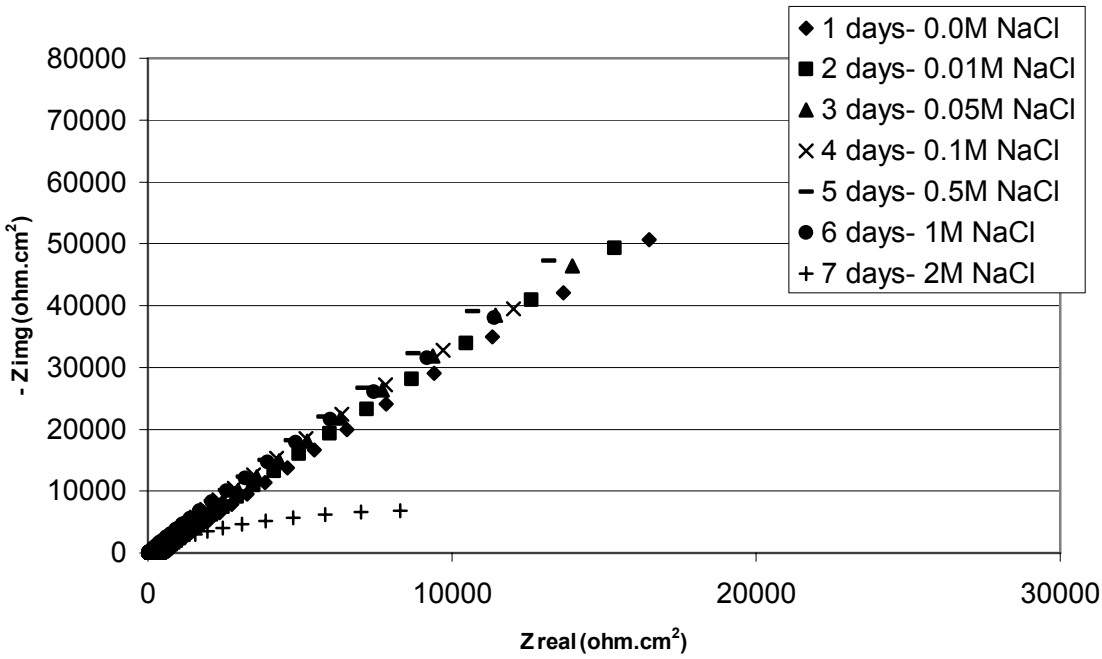

Figure 4.33 Nyquist plot of the impedance of 316LN stainless steel immersed in emulated carbonated concrete pore solution with various chloride amounts added as measured by EIS.

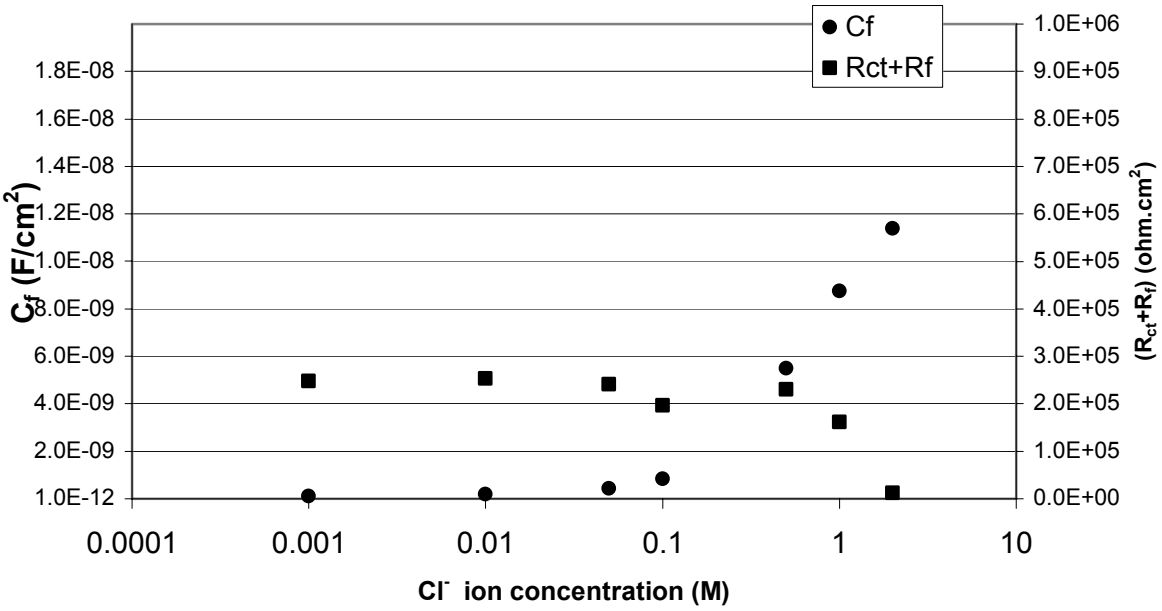

Figure 4.34 Change of the faradic capacitance of the passive film C_f and the sum of the charge transfer resistance R_{ct} and the passive film resistance R_f of 316LN stainless steel immersed in carbonated concrete pore solution with various chloride amounts.

M, respectively) with the increase of Cl^- ion concentration in the solution, was greater in the carbonated solution than in the non-carbonated one. Very recently, Bautista et al. (2009) reported the same observation for 304 stainless steel tested in the non-carbonated (pH 12.6) and carbonated (pH 9) $Ca(OH)_2$ solution. The possible explanation was that the chemical composition of the passive layer of austenitic stainless steels (304 and 316) formed in the carbonated solution had less chromium content than that formed in the non-carbonated solution, thus; it is more sensitive to the increase of the chloride concentration in the carbonated solution than the fresh one (Bautista et al., 2009).

4.6 Cross Section Loss and Service Life Prediction

With the help of the measured corrosion current densities, the corrosion rates (rate of thinning or cross section loss) in μm /year of metals under investigation can be calculated. Equation [2.12] is used to calculate the corrosion rates. Hence, an empirical relation between the chloride ion concentration (mole) at the rebar level and the cross section loss (μm /year) can be established. Since the corrosion currents of 316LN

stainless steel did not change significantly with the change of the chloride ion concentration in the solution, average constant corrosion currents of 0.02 μA/cm^2 and 0.03 μA/cm^2 (corrosion rates of 0.2 μm/yr and 0.3 μm/yr) were taken for that metal in the non-carbonated and the carbonated concrete, respectively. The corrosion rates of carbon steel in the carbonated concrete pore solution were too high (average i_{corr} 22 μA/cm^2 or corrosion rate of 255 μm/yr) and independent of the chloride concentration. With such rates, the cracking of the concrete cover would be expected to take place within only a few weeks after the carbonation front reaches the rebar level.

Figure 4.35 shows the relation between the chloride ion concentration and the corresponding corrosion rates for carbon steel in the non-carbonated concrete pore solution. Figures 4.36 and 4.37 show the relation between the chloride ion concentration and the corresponding corrosion rates for micro-composite steel in the non-carbonated and carbonated concrete pore solution, respectively. Corrosion rates were calculated using the corrosion current densities measured at the end of the exposure period, which was 7 days.

Since the diffusion of chloride ion through concrete can be assumed to follow Fick's second law (Liu, 1996), the concentration of the chloride ion at the rebar level can be calculated using Eq 4.3:

$$\frac{C_s - C_x}{C_s - C_0} = erf\left[\frac{X}{\sqrt{(4D_e.t)}}\right] \qquad [4.3]$$

where Cs is the chloride ion concentration at the surface,

C_x is the chloride ion concentration at the depth X,

C_0 is the initial chloride ion concentration at the surface, assumed nil,

D_e is the diffusion coefficient of concrete, and

t is time

According to Broomfield (1997), the depth of the carbonation front will follow the basic equation:

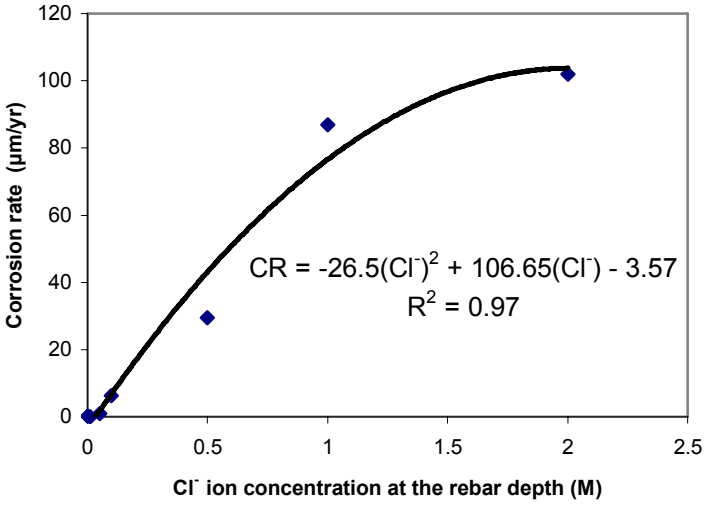

Figure 4.35 Corrosion rates of carbon steel in the non-carbonated concrete pore solution at different chloride concentrations.

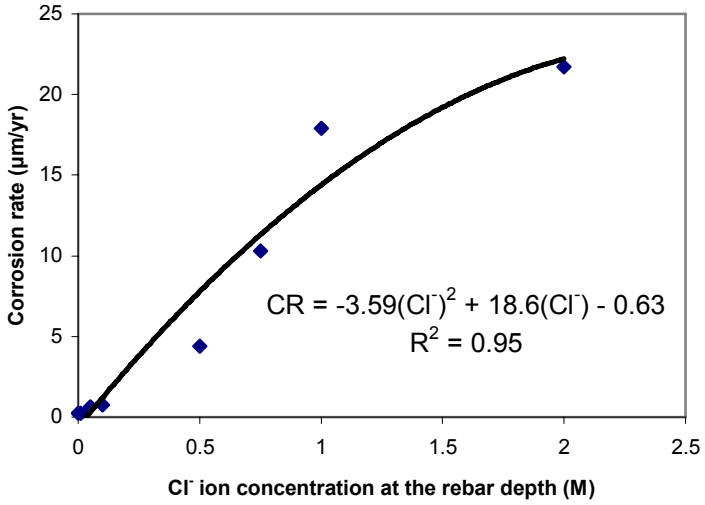

Figure 4.36 Corrosion rates of micro-composite steel in the non-carbonated concrete pore solution at different chloride concentrations.

$$X = At^{0.5} \qquad [4.4]$$

where X is the carbonation depth,

A is the diffusion coefficient of carbon dioxide in concrete, and

t is the time in years,

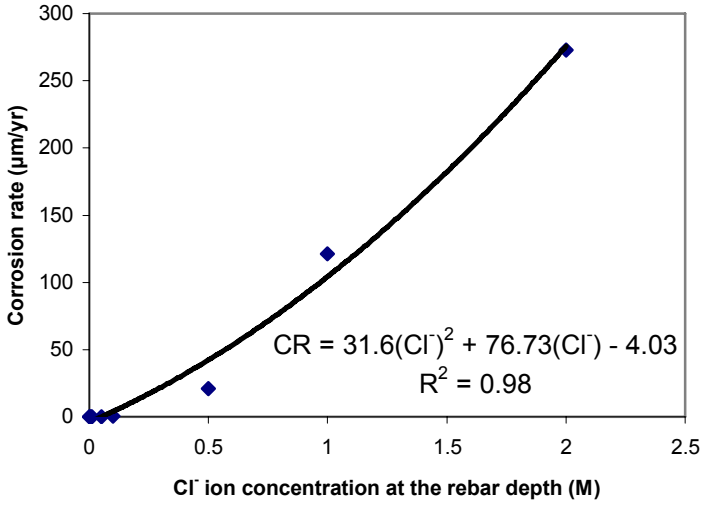

Figure 4.37 Corrosion rates of micro-composite steel in the carbonated concrete pore solution at different chloride concentrations.

Combining Equations [4.3] and [4.4] with the fitted expressions for corrosion rate as a function of chloride ions shown on Figures 4.35-4.37, one can easily estimate the evolution of corrosion rate as a function of time. Integrating the obtained corrosion rate (µm/yr) over a given period provides an estimate of the corrosion depth over that period. This procedure was implemented in Excel and allows an estimation of the service life, in years, as a function of rebar depth X, chloride diffusion coefficient in concrete De, diffusion coefficient of carbon dioxide in concrete A, and the chloride ion concentration at the surface Cs.

Figure 4.38 shows the change in the corrosion rates of metals under investigation with time when concrete is subjected to chloride ion attack. Figure 4.39 shows the change in the corrosion rates of metals under investigation with time when concrete is subjected to both carbonation and chloride ion attack. Figures 4.38 and 4.39 were obtained by assuming that the rebar depth X was 5 cm and a constant chloride ion concentration on the surface of the concrete member of 0.25M. The assumed chloride diffusion coefficient in concrete was D_e is 9.4×10^{-12} m^2/s (for a concrete mix of 0.45 water/cement ratio, 0.675-volume fraction of aggregate, and 5 % air content, Bentz et

al., 1999) and the diffusion coefficient of carbon dioxide in concrete A was assumed to be 7 $mm/yr^{0.5}$ (poor quality concrete).

The total cross section loss (μm) at a certain time t (years) can be estimated by calculating the area under the corrosion rate vs. time curve (see Figures 4.40 and 4.41). A wide range of the amount of the rebar cross section loss that is necessary to cause cracking of the concrete cover has been reported in the literature. Table 4.2 shows a summary of these values (adapted after Liu, 1996). This amount is dependant on the thickness of the concrete cover, concrete properties, and properties of the rust products (Liu, 1996).

Table 4.2 Available literature on the metal loss required for concrete cracking

Author	Required cross section loss for concrete cover cracking
Spellman and Stratfull (1968)	2.54 μm (laboratory experiment) 734 μm (Field Experiment)
Clear (1989)	94 μm
Bazant (1979)	7.87 μm
Hladky et al. (1989)	16 to 32 μm
Gonzalez et al. (1995)	10-50 μm
Broomfield (1997)	10 μm
Pfeifer (2000)	25.4 μm

In the current study, for the sake of comparison, a limit of 50 μm cross section loss was chosen to be enough to cause cracking of the concrete cover and hence, the time when the first repair is necessary. In a non-carbonated concrete under chloride ion attack of 0.25M at the surface of the concrete member, assuming X=5cm and D_e is $9.4x10^{-12}$ m^2/s, the use of micro-composite steel as the reinforcement material instead of carbon steel will increase the service life from 10 to 30 years, as can be seen in Figure 4.40. If the chloride ion concentration at the surface increased to 1M, the time until cracking occurs is expected to be 5 years in the case of using carbon steel, extended to 10 years

in the case of using micro-composite steel. If the chloride concentration at the surface dropped to 0.1M the time until cracking occurs increases to 25 years and 80 years for carbon steel and micro-composite steel, respectively.

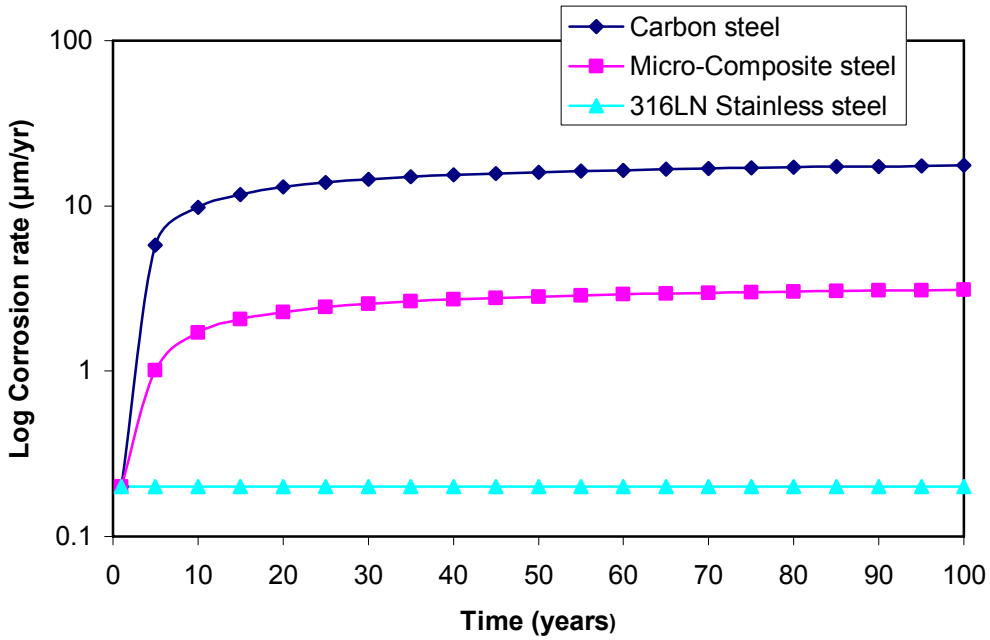

Figure 4.38 Change in the corrosion rate of the metals under investigation with time when subjected to a chloride contamination at the surface of 0.25 M in a non-carbonated concrete (rebar depth is 5 cm and $D_e = 9.4x10^{-12}$ m^2/s).

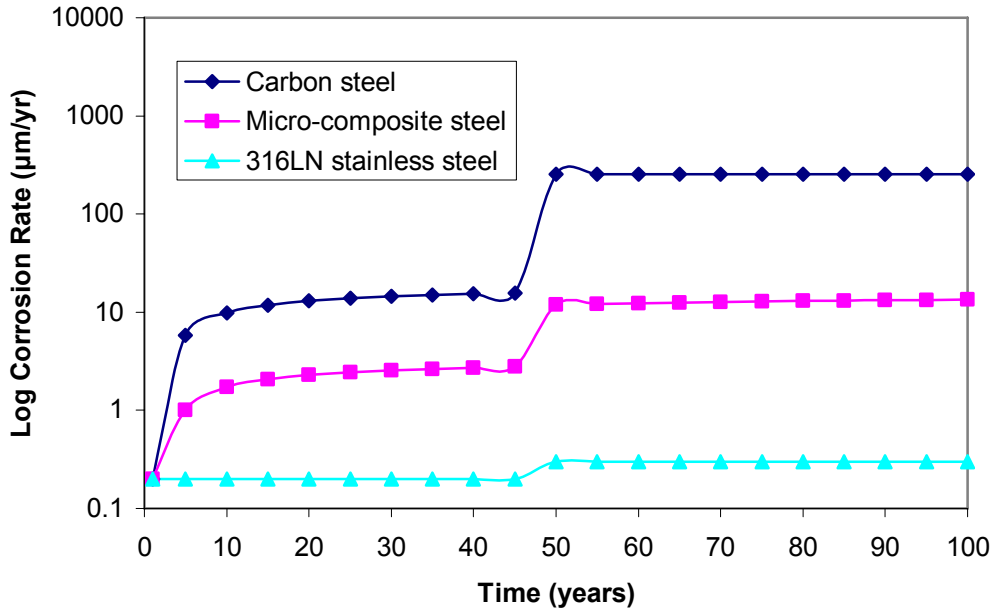

Figure 4.39 Change in the corrosion rate of the metals under investigation with time when subjected to both a chloride contamination at the surface of 0.25 M and carbonation (rebar depth is 5 cm, D_e = of $9.4x10^{-12}$ m^2/s, and A= $7mm/yr^{0.5}$).

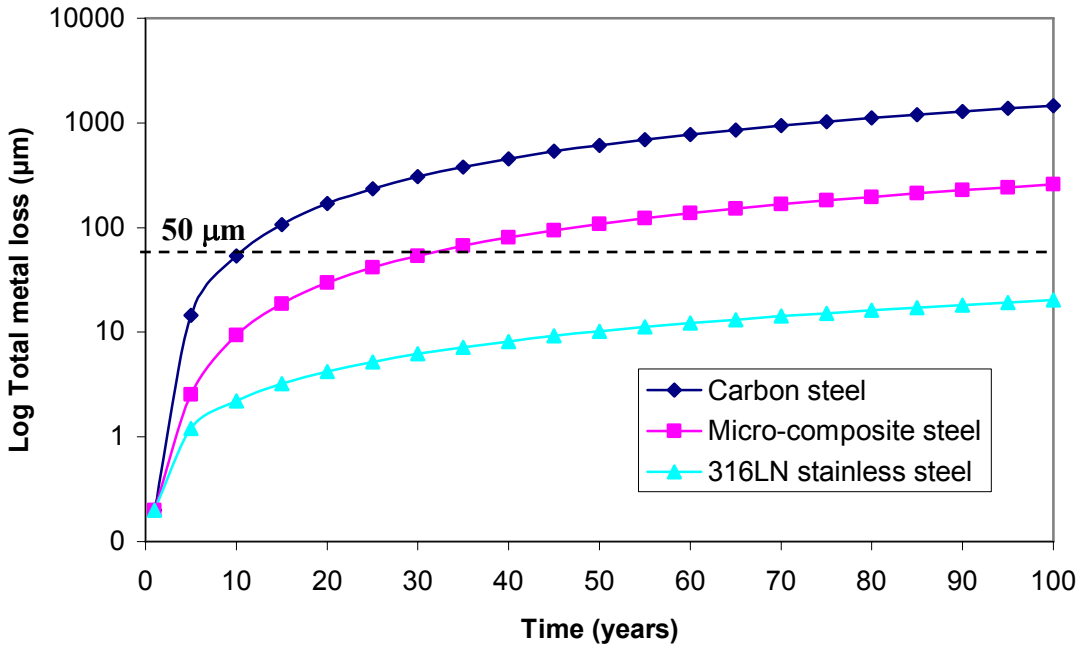

Figure 4.40 Total metal loss as function of time for the metals under investigation when subjected to a chloride contamination at the surface of 0.25 M in a non-carbonated concrete.

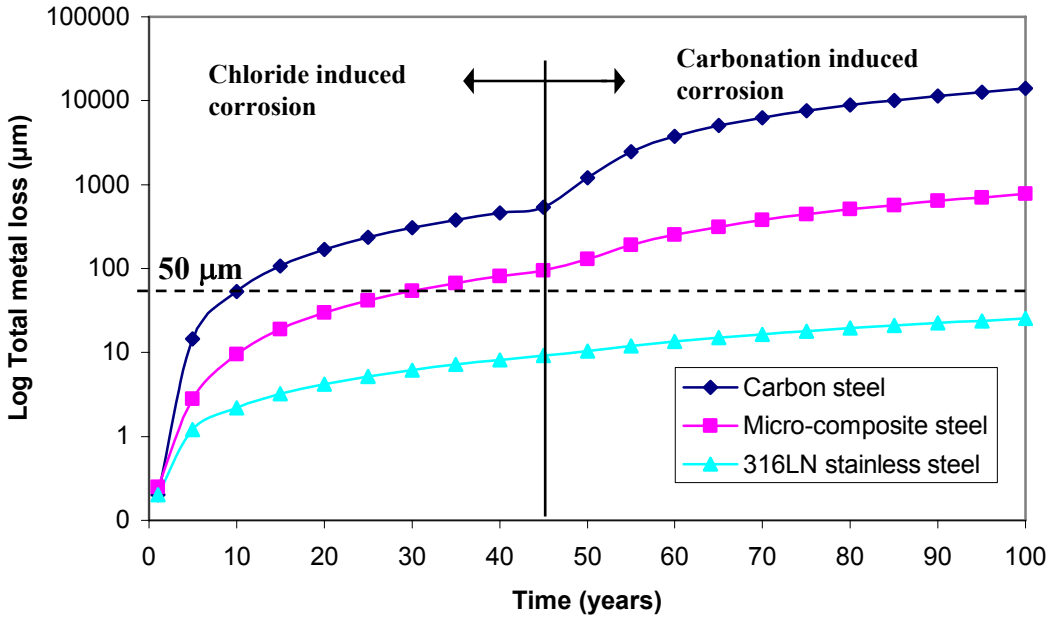

Figure 4.41 Total metal loss as function of time for the metals under investigation when subjected to both a chloride contamination at the surface of 0.25 M and carbonation.

If the concrete becomes carbonated, the service life of a structure that contains carbon steel as the reinforcement material is expected to be only a few weeks after the carbonation front reaches the rebar level. However, even for a poor concrete, the carbonation front may take 50 years or more to reach a 5 cm depth, depending on the diffusion coefficient of carbon dioxide in concrete. If the concrete is under both chloride ion attack and carbonation, the chlorides will cause corrosion long before carbonation (Broomfield, 1997). This can be noticed in Figure 4.41. For both carbon steel and micro-composite steel, the limit of total cross-section loss that will cause cracking of the concrete cover (50 μm) will be exceeded due to chloride-induced corrosion before the carbonation front reaches the rebar level.

In both non-carbonated and carbonated concrete, when using 316LN stainless steel as the reinforcement material, service life is not expected to be less than 100 years. This is true until a chloride concentration of 2M at the rebar depth.

4.7 Corrosion current density of Carbon Steel Embedded In Mortar Samples

Figure 4.42 shows the change in both the corrosion current density i_{corr} of carbon steel samples embedded in mortar and contaminated with NaCl at 5% wt cement and the water content inside mortar measured by the TDR technique over time. For this set of samples, it was found that the average corrosion current density was high, i_{corr} = 3.8 μA/cm^2 (i_{corr} > 0.1 μA/cm^2) 24 hours after casting. However, average i_{corr} decreased with time to 0.06 μA/cm^2 after 60 days. The water content measured at the same ages was also decreasing. Certainly, the water content decreased because of water consumption due to the cement hydration process. Corrosion currents decreased with time due to a couple of reasons. Firstly, the amount of the free chlorides (chloride ions that are able to take part in the corrosion process) decreased due to chemical (the reaction with tri calcium aluminates C_3A) and physical (adsorption within the C-S-H gel) binding in the cement paste. With time, the pore system became more developed and less chloride ions were available at the rebar surface. Secondly, since the

availability of moisture is essential for the corrosion process to take place, when the water content decreased due to the hydration process, the corrosion currents also decreased.

Figure 4.43 shows the change in corrosion current density as a function of the change of the degree of pore saturation PS during the first 60 days after casting. The degree of pore saturation, PS, was calculated using Equation [2.23]. The average porosity Φ was 23.04%, measured after 60 days of casting. Regardless the high chloride content, the corrosion current density was negligible (i_{corr} = 0.06 μA/cm^2) when the PS dropped to about 20% after 60 days. This is in agreement with Gonzalez et al. (1993). They reported that corrosion rates would be negligible if PS ≤ 35%.

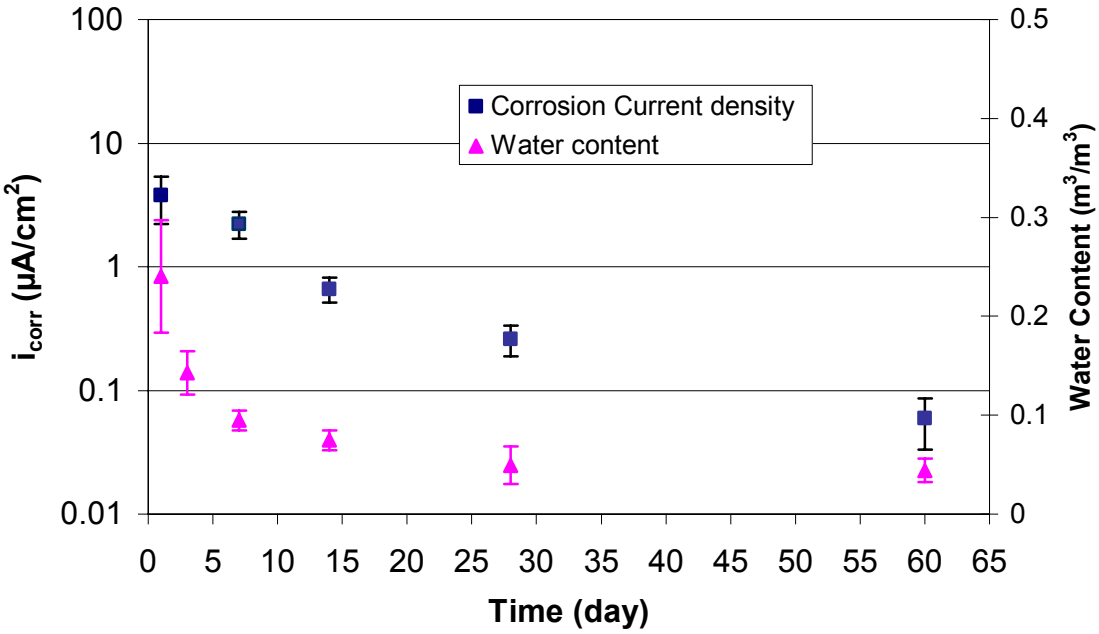

Figure 4.42 The corrosion current density of carbon steel embedded in mortar with 5% NaCl added to the mix at and the volumetric water content versus time.

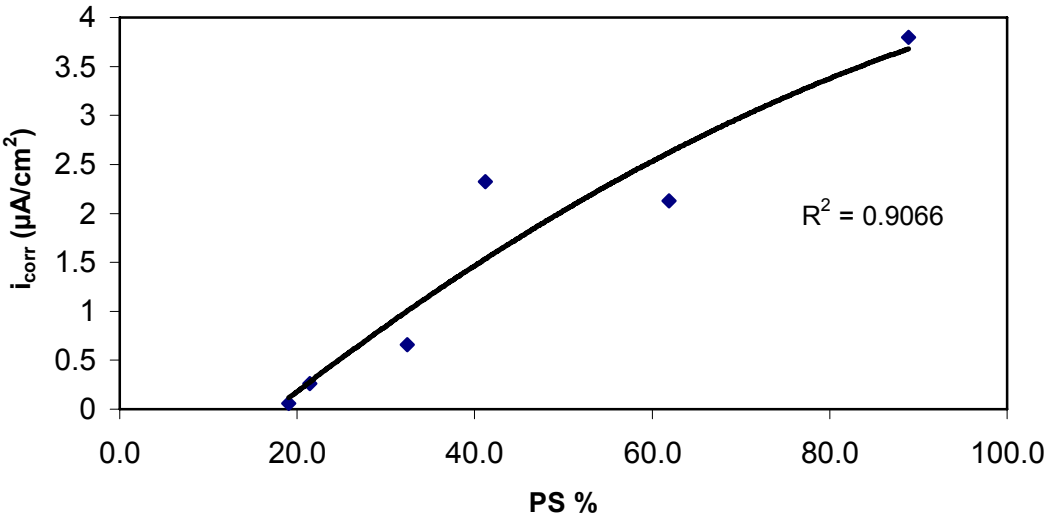

Figure 4.43 The change in the corrosion current density of carbon steel embedded in mortar with 5% NaCl added to the mix with the change of the degree of pore water saturation PS%.

4.8 Effect of the Presence of Chloride Ions on TDR Measurements of Moisture Content in Mortar

Although several studies have been conducted to investigate the effect of salinity on the TDR measurements of moisture content in soil, a disagreement between the various authors still exists. Nadler et al. (1999) conducted a literature survey of 22 studies, which dealt with that issue. Of the 22 studies, four found that the volumetric water content θ_V in soil was not affected by the soil's salinity, three found underestimation, six found overestimation and nine found both underestimation and overestimation of θ_V depending on the actual water content determined using gravimetric studies (Nadler et al., 1999). The inconsistency in the data reported was attributed to the presence of both clay particles and salinity.

The effect of the presence of Cl^- ions on TDR measurements of moisture content in concrete or mortar has not been investigated yet. Therefore, two sets of mortar specimens, with five samples in each set for a total of ten, were prepared to examine this issue. The first set was chloride free while the other one was contaminated with NaCl at of 5% wt cement.

Figure 4.44 shows the average of the measured values of dielectric constant of both sets at different ages. The measured value of ε for the chloride free set was 21.6 after 1 day of casting and decreased to 7.69 after 60 days. Clearly, the value of the dielectric constant decreased due to the increase in the resistivity of mortar due to the consumption of water in the process of cement hydration. These values are in agreement with published data on the dielectric constant of mortar and concrete. Korhonen et al. (1997) reported ε values of 13 and 3.9 for saturated surface-dry and oven dry mortar samples, respectively, and 12 and 5.4 for saturated surface-dry and oven dry concrete samples.

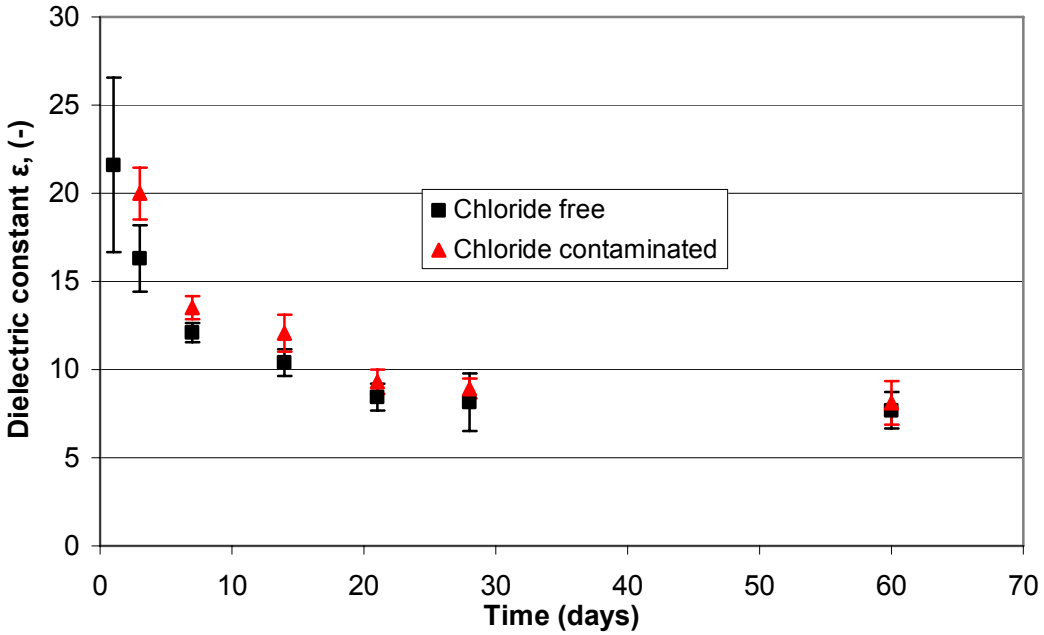

Figure 4.44 Dielectric constant of chloride free and chloride-contaminated mortar samples at different ages

Shi et al. (2003) found that mortar had a dielectric constant of 16 after 1 day of casting, decreasing gradually to ≤ 10.5 after 10 days. In addition, they observed a dielectric constant of concrete of 20 after 1 day, which decreased to ≤ 13 after 20 days. Sun (2008) reported dielectric constant values of 14, 7 and 2 after 1, 25 and 50 days of casting, respectively.

In Figure 4.44, it seems that the presence of chloride ions causes an overestimation of the measured dielectric constant ε; however, this effect decreased with time. The overestimation in the readings that were taken after 3 days was about 23 % of the actual dielectric constant, and dropped to 5.5 % after 60 days. Consequently, the same observation can be noticed on the calculated volumetric water content θ_V (see Figure 4.45). Equation [2.22] was used to calculate the water content with using the measured value of the dielectric constant ε. The difference in the calculated θ_V between the chloride free and chloride-contaminated samples was about 30% after 3 days of casting. This difference decreased to 11% after 60 days. The dielectric constant of the chloride-contaminated samples after 1 day was unreasonably high, so it was not plotted.

The decreasing effect of the presence of chloride ions on TDR measurements can be explained as follows. After only one day of casting, the process of cement hydration is still incomplete and lots of free water exists in the pore system of mortar. Such water

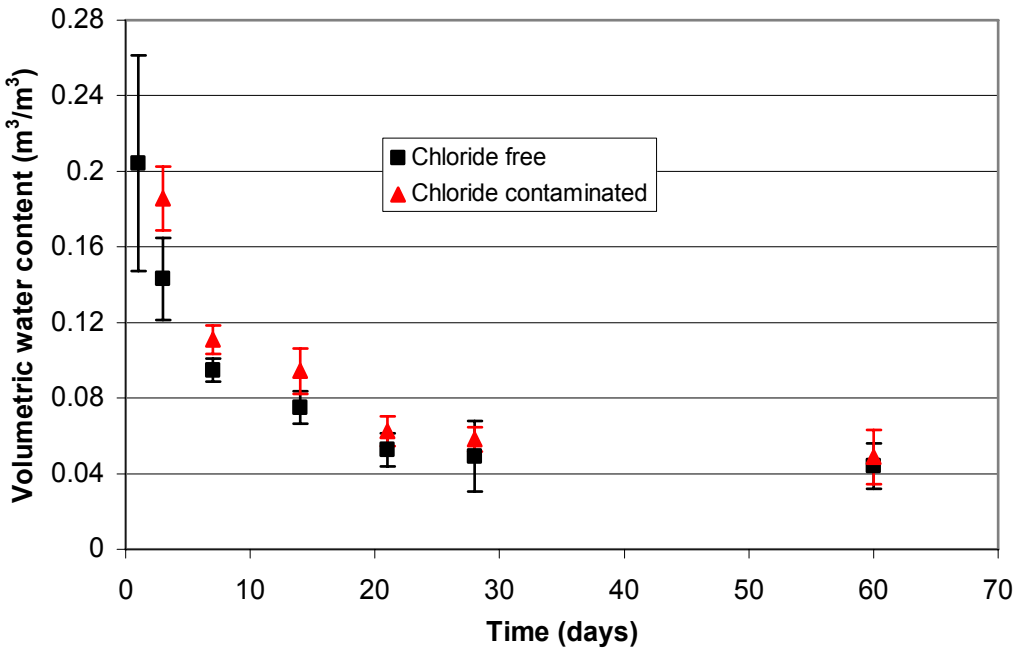

Figure 4.45 Volumetric water content of chloride free and chloride contaminated mortar samples at different ages

facilitates the movement of different ion species in the matrix (i.e. Cl^- and OH^-) and that leads to increased conductivity and high values of the dielectric constant (even excessively high values may occur). With time, some of that free water is consumed in the hydration process and any ions present will become less mobile. Also, with time, a portion of the chloride ions in the matrix will get bound either physically or chemically to cement hydration products.

4.9 Summary

In this chapter, the experimental results were presented and discussed. It was found that 316LN stainless steel had much higher corrosion resistance than carbon steel and micro-composite steel (MMFX-2) in both the non-carbonated (pH 13.2) and carbonated (pH 8.5) concrete pore solutions. In both solutions, the increase of chloride ion concentration (up to 2 M) did not cause any change to the free corrosion potential or the polarization resistance, which suggests that the chloride threshold level of 316LN stainless steel is higher than 2 M. The corrosion current density of 316LN stainless steel can be tolerated, from a durability point of view ($i_{corr} < 0.1$ μA/cm^2), at all tested chloride concentrations. However, it was found that the parameters associated with the passive film formed on the metal's surface were more sensitive to chloride ion addition in the carbonated solution than the non-carbonated one.

Micro-composite steel (MMFX-2) showed better performance than carbon steel in both of the testing environments. In the fresh concrete pore solution, the chloride concentration threshold of MMFX-2 was found to be between 0.1 and 0.5 M (Cl^-/OH^- = 0.63 to 3.16). This is 2 to 10 times higher than the chloride threshold of carbon steel (Cl^- = 0.05 M, Cl^-/OH^- = 0.32). In the carbonated concrete pore solution, the corrosion currents of MMFX-2 exceeded the 0.1 μA/cm^2 limit at the same range of Cl^- concentration of 0.1-0.5 M. However, the corrosion currents at Cl^- concentration ≥ 0.5 M were very severe ($i_{corr} >> 0.1$ μA/cm^2). Thus, the use of MMFX-2 rebars is not

recommended in the highly aggressive environments (i.e. low pH, high Cl^- concentrations).

The chloride threshold level measured for carbon steel ($Cl^-/OH^- = 0.32$) was in agreement with the published literature. Once the chloride concentration in the solution exceeded the threshold level, unacceptable corrosion rates were obtained ($i_{corr} >> 0.1$ $\mu A/cm^2$). It was also found that carbon steel would suffer severe corrosion in the carbonated solution regardless the chloride ion concentration in the solution.

For carbon steel samples tested in mortar pre-contaminated with chloride ions at 5% of cement weight, although the measured corrosion current was high in the first three days after casting, the corrosion current decreased continuously with time after two months of casting. This was attributed to the decrease of free chloride ions in the paste and to the decrease in the degree of pore saturation, due to water consumption in the hydration process.

Finally, it was found that the effect of the presence of chloride ions in concrete on the TDR measurements for volumetric water content, although it decreased significantly after 3 days of casting, caused an overestimation of about 11% of that of the chloride free samples after 60 days of casting.

CHAPTER 5

CONCLUSIONS

5.1 Summary

In this study, the effect of the presence of chloride ions in both fresh and carbonated synthetic concrete pore solutions on the corrosion behaviour of carbon steel, micro-composite steel (MMFX-2) and 316LN stainless steel was investigated using direct current corrosion measurements and electrochemical impedance spectroscopy techniques. In addition, the effect of the presence of chloride ions on the TDR measurements of volumetric moisture content inside mortar was investigated. Following are the conclusions of this study.

5.2 Conclusions

1. In the non-carbonated concrete pore solution, it was found that the chloride threshold level CTL of carbon steel is 0.05M. In the carbonated concrete pore solution it was found carbon steel will corrode in very high currents ($i_{corr} >> 0.1$ $\mu A/cm^2$) regardless the concentration of chloride ions in the solution.

2. For micro-composite steel (MMFX-2), in both the non-carbonated and the carbonated concrete pore solution, it was found that the CTL is between chloride concentrations of 0.1 to 0.5 M. However, in the carbonated solution and at chloride concentration $\geq$ 0.5 M, the corrosion currents measured were significantly higher than those obtained at the same chloride concentration in the non-carbonated solution.

3. For 316LN stainless steel, the CTL was not reached even at chloride concentration of 2M in both the non-carbonated and the carbonated concrete pore solution.

4. For all the metals under investigation EIS results showed that, generally, the increase of the chloride ion concentration in the solution would reduce the resistance of the passive film ($R_{ct} + R_f$) and increase its faradic capacitance (C_f). That change becomes more noticeable when the chloride concentration in the solution exceeds the metal's threshold level. EIS data of carbon steel in the carbonated concrete pore solution could not be fitted using the chosen representative circuit. This was explained by the absence of any passive film on the metal surface in that solution.

5. It was found that the corrosion currents of carbon steel embedded in mortar contaminated of NaCl at 5% per cement weight, would decrease due to the decrease in the degree of pore saturation PS. Regardless the high chloride content, the corrosion current was as low as 0.06 $\mu A/cm^2$ when PS dropped to about 20% after 60 days.

6. Finally, it was found that the presence of chloride ions in mortar would cause an overestimation in the measured dielectric constant using the TDR technique of about 5.5 % of that of the chloride free samples after 60 days of casting. The overestimation in the calculated volumetric water content (using equation 2.22) was 11 % of that of the actual water content after 60 days of casting.

LIST OF REFERENCES

Abreu, C. M., Cristóbal, M. J., Montemore, M. F., Novoa, X. R., Pena, G., and Perez, M. C. (2002). "Galvanic coupling between carbon steel and austenitic stainless steel in alkaline media." Electrochimica Acta, 47(13), 2271.

Alonso, C., Andrade, C., Castellote, M., and Castro, P. (2000). "Chloride threshold values to depassivate reinforcing bars embedded in a standardized OPC mortar." Cement and Concrete Research, 30(7), 1047.

Alonso, C., Castellote, M., and Andrade, C. (2002). "Chloride threshold dependence of pitting potential of reinforcements." Electrochimica Acta, 47(21), 3469.

Alonso, M.C. andrade, C. (1989). "Electrochemical behaviour of steel reinforcements in Na_2CO_3 and $NaHCO_3$ solutions in relation to stress corrosion cracking." Corrosion Science, 29(9), 1129.

Alvarez, M.G. and Galvele, J. A. (1984). "The mechanism of pitting of high purity iron in NaCl solutions." Corrosion Science, 24(1), 27.

Andrade, C. and Page, C. L. (1986). "Pore Solution Chemistry and Corrosion in Hydrated Cement Systems Containing Chloride Salts: A Study of Cation Specific Effects." British Corrosion Journal, 21(1), 49.

Andrade, M.C. and Gonzalez, J. A. (1977). Mat. Const., Vol: 168, page 1 (Cited in Alonso et al. 2002).

Ann, K.Y. and Song, H. W. (2007). "Chloride threshold level for corrosion of steel in concrete." Corrosion Science, 49(11), 4113.

Anstice, D. J., and Page,C.L. and Page, M. M. (2005). "The pore solution phase of carbonated cement pastes." Cement and Concrete Research, 35(2), 377.

Arya C. and Newman J.B. (1990). "Problem of predicting risk of corrosion of steel in chloride contaminated concrete." ICE Proceedings, 88 875.

ASTM Standard A706M. (2008).“Standard Specification for Low-Alloy Steel Deformed and Plain Bars for Concrete Reinforcement." ASTM International, West Conshohocken, PA, 2004, DOI: 10.1520/A0706_A0706M-08A, Www.Astm.Org.,.

ASTM Standard C1152M. (2004). "Standard Test Method for Acid-Soluble Chloride in Mortar and Concrete." ASTM International, West Conshohocken, PA, 2004, DOI: 10.1520/C1152_C1152M-04E01, Www.Astm.Org., .

ASTM Standard C1218M. (2008). "Standard Test Method for Water-Soluble Chloride in Mortar and Concrete." ASTM International, West Conshohocken, PA, 2008, DOI: 10.1520/C1218_C1218M-99R08, Www.Astm.Org., .

ASTM Standard C876-91. (1999). "Standard Test Method for Half-Cell Potentials of Uncoated Reinforcing Steel in Concrete." ASTM International, West Conshohocken, PA, 1999, DOI: 10.1520/C0876-91R99, Www.Astm.Org., .

Balabanić, G., and Bicanic, N. and Durekovic, A. (1996). "The influence of w/c ratio, concrete cover thickness and degree of water saturation on the corrosion rate of reinforcing steel in concrete." Cement and Concrete Research, 26(5), 761.

Barneyback Jr.,R.S. and Diamond, S. (1981). "Expression and analysis of pore fluids from hardened cement pastes and mortars." Cement and Concrete Research, 11(2), 279.

Bautista, A., Blancoa, G., and Velasco, F. (2006). "Corrosion behaviour of low-nickel austenitic stainless steels reinforcements: A comparative study in emulated pore solutions." Cement and Concrete Research, 36(10), 1922.

Bautista, A., Blancoa, G., Velascoa, F., Gutiérrezb, A., Soriano, L., Palomaresc, F. J., and Takenoutid, H. (2009). "Changes in the passive layer of corrugated austenitic stainless steel of low nickel content due to exposure to emulated pore solutions." Corrosion Science, 51(4), 785.

Bazant Z. P. (1979). “Physical Model for Steel Corrosion in Sea Structures-Applications,” Journal of the Structural Division, June, pp. 1155-1166 (cited in Liu, 1996).

Beddoes, J. (1999.). Introduction to stainless steels. ASM International, Materials Park, OH.

Bentur, A. (1997). Steel corrosion in concrete :fundamentals and civil engineering practice. E & FN Spon, London ;.

Bentz,D., Garboczi, E., and Lagergren, E. (1998). "Multi-Scale Microstructural Modeling of Concrete Diffusivity: Identification of Significant Varibles." Cement, Concrete and Aggregates, 20(1), 129.

Bertolini, L., Bolzoni, F., Pastore, T., and Pedeferri, P. (1996). "Behaviour of stainless steel in emulated concrete pore solution." British Corrosion Journal, 31(3), 218.

Blanco, G., Bautista, A., and Takenouti, H. (2006). "EIS study of passivation of austenitic and duplex stainless steels reinforcements in emulated pore solutions." Cement Concrete Composites, 28(3), 212.

Broomfield, J. P. (1997.). Corrosion of steel in concrete :understanding, investigation, and repair. E & FN Spon, London ;.

Brown, M. C. (2002). "Corrosion Protection Service Life of Epoxy Coated Reinforcing Steel in Virginia Bridge Decks." PhD thesis, Virginia Polytechnic Institute and State University, Blacksburg, Virginia, USA.

Castellote, M., Alonso, C., Andrade, C., Castro, P., and Echeverria, M. (2001). "Alkaline leaching method for the determination of the chloride content in the aqueous phase of hardened cementitious materials." Cement and Concrete Research, 31(2), 233.

Chaussadent, T., and Arliquie, G. (1999). "AFREM test procedures concerning chlorides in concrete: Extraction and titration methods." Materials and Structures, 32(217), 230.

Clear, K. (1992). “Measuring Rate of Corrosion of Steel in Field Concrete Structure,” Transportation Research Record, No. 1211, pp. 28-38 (cited in Liu, 1996).

Clementa, G. G., Jackson D. R., and Crawford G. C. “Use of Rebar Corrosion Rates in Condition Surveys of Concrete Bridge Decks,” an unpublished paper (cited in Liu, 1997).

Clemena, G. G. and Virmani, Y. P. (2004). "Comparing the chloride resistances of reinforcing bars: Evaluating new, economical metallic reinforcement for its ability to withstand high salt concentrations." Concrete International, 26 39.

Corbo, J., and Farazam, H. (1989). "Influence of three commonly used inorganic compounds on pore solution chemistry and their possible implications to the corrosion of steel in concrete." ACI Materials Journal, 86(5), 498.

Dehwah, H. A. F., Maslehuddin, M., and Austin, S. A. (2002). "Effect of cement alkalinity on pore solution chemistry and chloride-induced reinforcement corrosion." ACI Materials Journal, 99(3), 227.

Enevoldsen, J. N., Hansson, C. M., and Hope, B. B. (1994). "The influence of internal relative humidity on the rate of corrosion of steel embedded in concrete and mortar." Cement and Concrete Research, 24(7), 1373.

Enos, D. G., and Scribner, L. (1997). "The potentiodynamic polarization scan, A Division of Solartron Group Ltd." Rep. No. 33, .

Escudero, M. L., García-Alonso, M. C., Capilla, F., and González, J. A. (2002). "Study of the corrosion resistance of stainless steel in solution emulating concrete." .

Esmaeilpoursaee, A. (2007). "An Analysis of the Factors Influencing Electrochemical Measurements of the Condition of Reinforcing Steel in Concrete Structures." PhD thesis, University of Waterloo, Waterloo, Canada.

Freire, L., Nóvoa, X. R., Montemor, M. F., and Carmezim, M. J. (2009). "Study of passive films formed on mild steel in alkaline media by the application of anodic potentials." Materials Chemistry and Physics, 114(2-3), 962.

Gaal, G.C.M. (2004). "Prediction of Deterioration of Concrete Bridges Corrosion of Reinforcement due to Chloride Ingress and Carbonation." PhD thesis, Technical University at Delft, Delft, Netherland.

GAMRY Instruments (2005) Electrochemical Impedance Spectroscopy Primer. An Application Note from GAMRY Instruments, pp. 11 – 16.

Garces, P., Andrade, M. C., Saez, A., and Alonso, M. C. (2005). "Corrosion of reinforcing steel in neutral and acid solutions emulating the electrolytic environments in the micropores of concrete in the propagation period." Corrosion Science, 47(2), 289.

Glass, G. K., Reddy, B., and Buenfeld, N. R. (2000). "The participation of bound chloride in passive film breakdown on steel in concrete." Corrosion Science, 42(11), 2013.

Glass, G. K., and Buenfeld, N. R. (1997). "Presentation of the chloride threshold level for corrosion of steel in concrete." Corrosion Science, 39(5), 1001.

Gong, L., Darwin, D., Browning, J. P., and Locke, C. E. (2004). "Evaluation of Mechanical and Corrosion Properties of MMFX Reinforcing Steel for Concrete." Rep. No. FHWA-KS-02-8, KANSAS DEPARTMENT OF TRANSPORTATION, USA.

Goni, S. l., and Andrade, C. (1990). "Synthetic concrete pore solution chemistry and rebar corrosion rate in the presence of chlorides." Cement and Concrete Research, 20(4), 525.

Gonzalez, J. A., Andrade, C., Alonso, C., and Feliu, S. (1995). "Comparison of rates of general corrosion and maximum pitting penetration on concrete embedded steel reinforcement." Cement and Concrete Research, 25(2), 257.

Gonzalez, J. A., Lopez, W., and Rodriguez, P. (1993). "Effects of moisture availability on corrosion kinetics of steel embedded in concrete." Corrosion, 49(12), 1004.

Gouda, V. K., and Halaka, W. Y. (1970). "Corrosion and corrosion inhibition of reinforcing steel- 2." British Corrosion Journal, 5(5), 204.

Guidoni, G., and Vazquez, M. (2004). "An evaluation of rust conversion coatings in emulated reinforced concrete pore solutions." Anti - Corrosion Methods and Materials, 51(1), 18.

Guilbaud, J. P., Chahbazian, G., Derrien, F., and Raharinaivo, A. (1994). "Electrochemical behaviour of steel under cathodic protection in medium emulating concrete, Corrosion and Corrosion Protection of Steel in Concrete." 1382-1391.

Gutierrez, M. (1995) "Estudio de la corrosion de armaduras provocada por cloruros. Limite umbral de despasivacion Cl^-/OH^-". Small Thesis Univ. Compl. de Madrid. (Cited in Alonso et al. 2002)

Haldar, A., and Mahadevan, S. (2000.). Probability, reliability, and statistical methods in engineering design. John Wiley, New York.

Hausmann, D. A. (1967). "Steel corrosion in concrete - How does it occur." Materials Protection, 6(11), 19.

Hausmann, D.A. (1968) 24th Conference of NACE, Cleveland, 1968. (Cited in Alonso et al. 2002)

Hausmann, D. A. (2007). "Three myths about corrosion of steel in concrete." Materials Performance, 46(8), 70.

Hladky, K. et al. (1989). “Development in Rate of Corrosion Measurements for Reinforced Concrete Structures,” Corrosion *89*, No. 169, NACE, Houston, TX (cited in Liu, 1996).

Hope, B. B., Page, J. A., and Poland, J. S. (1985). "The determination of the chloride content of concrete." Cement and Concrete Research, 15(5), 863.

Hou, J., Fu, X., and Chung, D. D. L. (1997). "Improving both bond strength and corrosion resistance of steel rebar in concrete by water immersion or sand blasting of rebar." Cement and Concrete Research, 27(5), 679.

Hurley, M. F., and Scully, J. R. (2002). "Corrosion 2002, NACE International." Chloride threshold levels in clad 316L and solid 316LN stainless rebar, Denver, Co, .

Hurley, M. F. (2007). "Corrosion initiation and propagation behaviour of corrosion resistant concrete reinforcing materials." PhD thesis, University of Virginia, USA.

Hurley, M. F. (2006). "Threshold chloride concentrations of selected corrosion-resistant rebar materials compared to carbon steel." Corrosion, 62(10), 892.

Hussain, S. E., Rasheeduzzafar, Al-Musallam, A., and Al-Gahtani, A. S. (1995). "Factors affecting threshold chloride for reinforcement corrosion in concrete." Cement and Concrete Research, 25(7), 1543.

Ishikawa, T., Bresler, B., and Cornet, I. (1968). "Mechanism of Steel Corrosion in Concrete Structures." Materials Protection, 7(3), 45.

Izquierdo, D., Alonso, C., Andrade, C., and Castellote, M. (2004). "Potentiostatic determination of chloride threshold values for rebar depassivation - Experimental and statistical study." Electrochimica Acta, 49(17-18), 2731.

Janoo, V., Korhonen, C., and Hovan, M. (1999). "Measurement of water content in portland cement concrete." Journal of Transportation Engineering, 125(3), 245.

Jing, J. (2006). "Corrosion Resistance of Micro-Composite and Duplex Stainless Steels for Reinforced Concrete Bridge Decks." PhD thesis, University of Kansas, USA.

Joiret, S., Keddam, M., Nóvoa, X. R., Pérez, M. C., Rangel, C., and Takenouti, H. (2002). "Use of EIS, ring-disk electrode, EQCM and Raman spectroscopy to study the film of oxides formed on iron in 1 M NaOH." Cement Concrete Composites, 24(1), 7.

Jones, D. A. (1996.). Principles and prevention of corrosion. Prentice Hall, Englewood Cliffs, NJ.

Kahl, S. (2007). "Corrosion Resistant Alloy Steel (MMFX) Reinforcing Bar in Bridge Decks." Rep. No. R-1499, Michigan Department of Transportation, USA.

Kitowski, C. J., and wheat, H. G. (1997). "Effect of chlorides on reinforcing steel exposed to emulated concrete solutions." Corrosion, 53(3), 216.

Koch, G.H.; Brongers, M.P.H.; Thompson, N.G.; Virmani, Y. P.; and Payer, J. H. (2001). "Corrosion Costs and Preventive Strategies in the United States" Federal Highway Administration Report FHWA-RD-01-156, 30 Sep 2001.

Korhonen, C. J., Janoo, V., and Berini, C. (1997). "Time-domain reflectometry of water content in Portland cement concrete." US Army Corps of Engineers Journal,.

Li, L., and Sagues, A. A. (2001). "Chloride corrosion threshold of reinforcing steel in alkaline solutions - Open-circuit immersion tests." Corrosion, 57(1), 19.

Lihua, s., Qiwei, X., Bin, C., and Cheng, G. (2003). "Measurement of the frequency-dependent dielectric constant of concrete materials by TDR and wavelet modeling method." 626.

Liu, Y. (1996). "Modeling the Time-to-Corrosion Cracking of the Cover Concrete in Chloride Contaminated Reinforced Concrete Structures." PhD thesis, Virginia Polytechnic Institute and State University, Blacksburg, Virginia.

Lopez, W. (1992). “Influencia de la temperatura y el grado de humectación de los poros en la durabilidad de las estructuras de hormigón armado." PhD thesis, Complutense University of Madrid, Madrid, Spain (Cited in Alonso et al. 2002).

López, W., and Gonzalez, J. A. (1993). "Influence of the degree of pore saturation on the resistivity of concrete and the corrosion rate of steel reinforcement." Cement and Concrete Research, 23(2), 368.

Mammoliti, L. T., Brown, L. C., Hansson, C. M., and Hope, B. B. (1996). "Influence of surface finish of reinforcing steel and pH of the test solution on the chloride threshold concentration for corrosion initiation in synthetic pore solutions." Cement and Concrete Research, 26(4), 545.

Marchand, J., Bentz, D. P., Samson, E., and Maltais, Y. (2001). "Influence of calcium hydroxide dissolution on the transport properties of hydrated cement systems." Materials science of concrete special volume: Calcium hydroxide in concrete, J. Skalny, J. Gebauer, and I. and Odler, eds.,113.

Matsushima, I. (2002). "Effect of chloride concentration and pH on corrosion of carbon steel and stainless steel reinforcements." Zairyo-to-Kankyo, 51(10), 463.

Millard, S. G., Law, D., Bungey, J. H., and Cairns, J. (2001). "Environmental influences on linear polarization corrosion rate measurement in reinforced concrete." NDT E International, 34(6), 409.

MMFX Technologies corp. of North America (2007). "MMFX-2 Product Guide"

MMFX Technologies corp. of North America web page http://www.mmfx.com/prod_steel.shtml accessed on May 15, 2009

Mohammed, T. U., and Hamada, H. (2006). "Corrosion of steel bars in concrete with various steel surface conditions." ACI Materials Journal, 103(4), 233.

Moreno, M., Morris, W., Alvarez, M. G., and Duffó, G. S. (2004). "Corrosion of reinforcing steel in emulated concrete pore solutions effect of carbonation and chloride content." Corrosion Science, 46(11), 2681.

Nachiappan, V., and Cho, E. H. (2005). "Corrosion of high chromium and conventional steels embedded in concrete." Journal of Performance of Constructed Facilities, 19(1), 56.

Nadler, A., Gamliel, A., and Peretz, I. (1999). "Practical aspects of salinity effect on TDR-measured water content: A field study." Soil Science Society of America Journal, 63(5), 1070.

Parakala, S. R. (2005). "Galvanic Corrosion Aspects of Stainless Steel and Black Steel Reinforcement in Concrete." M.Sc. thesis, University of Ohio, Athens, Ohio, USA.

Page, C. L., and Vennesland, Q. (1983). "Pore solution composition and chloride binding capacity of silica-fume cement pastes." Materiaux Et Constructions, 16(91), 19.

Pernice, P., Aronne, A., and Muscetta, S. (1994). "Behaviour of stainless steel in $Ca(OH)_2$ saturated solution containing chlorides." Journal of Materials Science Letters, 13(4), 289.

Pfeifer, D. (2000). "High performance concrete and reinforcing steel with a 100-year service life." PCI J., 45(3), 46.

Pillai, R. G., and Trejo, D. (2005). "Surface condition effects on critical chloride threshold of steel reinforcement." ACI Materials Journal, 102(2), 103.

Pourbaix, M. (1972). "Theoretical and experimental considerations in corrosion testing." Corrosion Science, 12(2), 161.

Poursaee, A., and Hansson, C. M. (2007). "Reinforcing steel passivation in mortar and pore solution." Cement and Concrete Research, 37(7), 1127.

Pruckner, F. (2001). ""Corrosion and Protection of Reinforcement in Concrete Measurements and Interpretation"." PhD thesis, University of Vienna, .

Qian, S., Cusson, D., Chagnon, N., and Baldock, B. (2008). "Corrosion-Inhibiting systems for durable concrete bridges. II: Accelerated laboratory investigation." Journal of Materials in Civil Engineering, 20(1), 29.

Reval Stainless Steel web page http://www.reval-stainless-steel.com/composition.html accessed on June 30, 2009

Sahoo, G., and Balasubramaniam, R. (2008). "On the corrosion behaviour of phosphoric irons in emulated concrete pore solution." Corrosion Science, 50(1), 131.

Sánchez, M., Gregori, J., Alonso, C., García-Jareño, J. J., Takenouti, H., and Vicente, F. (2007). "Electrochemical impedance spectroscopy for studying passive layers on steel rebars immersed in alkaline solutions emulating concrete pores." Electrochimica Acta, 52.

Saremi, M., and Mahallati, E. (2002). "A study on chloride-induced depassivation of mild steel in emulated concrete pore solution." Cement and Concrete Research, 2138 1.

Sedriks, A. J. (1979). Corrosion of stainless steels. Wiley, New York.

Seibert, P. (1998). "Galvanic Corrosion Aspects of Stainless Steel and Black Steel Reinforcement in Concrete." PhD thesis, Queen's University, Canada.

Spellman, D.L., and Stratfull R.F. “Chlorides and Bridge Deck Deterioration,” State of California Department of Public Works, Division of Highways, Materials References 114 and Research Department, Paper Sponsored by Committee on Effect of Ice Control and Presented at 49th Annul Meeting (cited in Liu, 1996).

Stern, M., and Geary, A. L. (1957). "Electrochemical polarization." Journal of the Electrochemical Society, 104(1), 56.

Sun, Z. J. (2008). "Estimating volume fraction of bound water in Portland cement concrete during hydration based on dielectric constant measurement." Magazine of Concrete Research, 60(3), 205.

Tae, S. H., and Ujiro, T. (2007). "Corrosion resistance of Cr-bearing rebar in emulated concrete pore solutions." ISIJ International, 47(9), 1324.

Thompson, N. G., and Yunovich, M. (2003). "Tri-service corrosion conference." Life-cycle costing for bridges, .

Topp, G., and Reynolds, W. D. (1998). "Time domain reflectometry: A seminal technique for measuring mass and energy in soil." Soil Tillage Research, 47(1-2), 125.

Topp,G.C., and Davis, J.L. (1982). "MEASUREMENT OF SOIL WATER CONTENT USING TIME DOMAIN REFLECTOMETRY." Proceedings of the Canadian Hydrology Symposium, 269.

Trejo,D. and Pillai, R. G. (2003). "Accelerated Chloride Threshold Testing: Part I - ASTM A 615 and A 706 Reinforcement." ACI Materials Journal, 100(6), 519.

Trejo, D., and Pillai, R. (2004). "Accelerated chloride threshold testing - Part II: Corrosion-resistant reinforcement." ACI Materials Journal, 101(1), 57.

Tuutti, K. (1982). Corrosion of Steel in Concrete, Swedish Cement and Concrete Research Institute, Stochkolm. (Cited in Liu 1996)

Van Der Aa, J. P. C. M., and Boer, G. (1997). "Automatic moisture content measuring and monitoring system based on time domain reflectometry used in road structures." NDT E International, 30(4), 239.

Veleva, L., Alpuche-Aviles, M. A., Graves-Brook, M. K., and Wipf, D. O. (2005). "Voltammetry and surface analysis of AISI 316 stainless steel in chloride-containing emulated concrete pore environment." Journal of Electroanalytical Chemistry and Interfacial Electrochemistry, 578(1), 45.

Veleva, L., Alpuche-Aviles, M. A., Graves-Brook, M. K., and Wipf, D. O. (2002). "Comparative cyclic voltammetry and surface analysis of passive films grown on stainless steel 316 in concrete pore model solutions." Journal of Electroanalytical Chemistry and Interfacial Electrochemistry, 537(1), 85.

Vrable,J.B. and Wilde, B. E. (1980). "Electrical Potential Requirements for Cathodic Protection of Steel in Emulated Concrete Environments." Corrosion, 36(1), 18.

Xu, J., Jiang, L., and Wang, J. (2009). "Influence of detection methods on chloride threshold value for the corrosion of steel reinforcement." Construction Building Materials, 23(5), 1902.

Yonezawa, T., Ashworth, V., and Procter, R. (1988). "Pore solution composition and chloride effects on the corrosion of steel in concrete." *Corrosion,* 44(7), 489.

APPENDIX A

Summation of Test Results

This appendix presents the following data:

- Results of direct current DC corrosion measurements (Tables A.1 to A.6)
- Results of EIS corrosion measurements (Tables A.7 to A.11)
- Results of the study of the repeatability of the DC corrosion measurements (TableA.12)
- Results of the study of the repeatability of the EIS corrosion measurements (Table A.13)
- Results of the measured corrosion currents of carbon steel samples embedded in mortar at different ages (Table A.14)
- Results of TDR measurements of chloride free and chloride contaminated samples at different ages (Tables A.15 to A.28)

Table A.1 Results of DC corrosion measurements of Carbon Steel in fresh concrete pore solution

Cl^- (M)	After 1 hour		After 24 hours			After 7 days		
	E_{OC} (V) vs. SCE	i_{corr} ($\mu A/cm^2$)	E_{OC} (V) vs. SCE	R_P ($ohm.cm^2$)	i_{corr} ($\mu A/cm^2$)	E_{OC} (V) vs. SCE	R_P ($ohm.cm^2$)	i_{corr} ($\mu A/cm^2$)
0.001	-314	0.25	-271.4	1.41E+05	0.024	-243.6	2.67E+05	0.022
0.01	-312.2	0.44	-268.9	1.42E+05	0.046	-234.1	2.39E+05	0.007
0.05	-314	0.14	-274.8	1.22E+05	0.049	-299	8.15E+04	0.088
0.1	-305.3	0.22	-318.4	5.49E+04	0.23	-354.2	1.81E+04	0.54
0.5	-362.6	0.99	-445	1.11E+04	2.69	-527.1	3.03E+03	2.53
1	-373.5	1.01	-502	1.60E+04	4.59	-531.6	3.75E+03	7.50
2	-419.2	7.3	-524	3.67E+03	9.54	-543	4.39E+03	8.81

Table A.2 Results of DC corrosion measurement of Carbon Steel in carbonated concrete pore solution

Cl^- (M)	After 1 hour			After 24 hours		
	E_{OC} (V) vs. SCE	R_P (ohm.cm^2)	i_{corr} (μA/cm^2)	E_{OC} (V) vs. SCE	R_P (ohm.cm^2)	i_{corr} (μA/cm^2)
0.001	-738.2	1.41E+03	30.8	-728	1.53E+03	29.3
0.005	-735	1.25E+03	24.4	-732.9	1.82E+03	11.1
0.01	-736.5	1.22E+03	30.1	-733.4	1.72E+03	24.9
0.05	-740.3	1.27E+03	24.9	-740.5	1.76E+03	19.8
0.1	-738.9	1.16E+03	24.6	-738.2	1.60E+03	21.1
0.5	-738.9	1.23E+03	25.8	-739.2	1.30E+03	24.3
1	-741.1	1.14E+03	28.8	-737	1.26E+03	26.9
2	-733.7	1.44E+03	22.6	-733.5	1.70E+03	18.3

Table A.3 Results of DC corrosion measurements of Micro-Composite Steel in fresh concrete pore solution

Cl^- (M)	After 1 hour			After 24 hours			After 7 days		
	E_{OC} (V) vs. SCE	R_P (ohm.cm^2)	i_{corr} (μA/cm^2)	E_{OC} (V) vs. SCE	R_P (ohm.cm^2)	i_{corr} (μA/cm^2)	E_{OC} (V) vs. SCE	R_P (ohm.cm^2)	i_{corr} (μA/cm^2)
0.001	-310.5	1.33E+05	0.17	-284.6	2.92E+05	0.03	-256.9	6.90E+05	0.02
0.01	-332.2	1.00E+05	0.44	-288.7	2.34E+05	0.04	-252.8	5.87E+05	0.02
0.05	-324.6	8.69E+04	0.2	-299.4	1.53E+05	0.05	-257.4	5.13E+05	0.06
0.1	-321.1	1.19E+05	0.23	-303.4	1.54E+05	0.03	-240	5.89E+05	0.07
0.5	-315.4	1.02E+05	0.28	-365.8	4.04E+04	0.20	-422	6.09E+04	0.41
0.75	-330.6	7.90E+04	0.27	-390	8.30E+04	0.81	-414.2	3.44E+04	0.95
1	-362.2	6.70E+04	0.62	-436	9.42E+04	0.80	-447.2	1.43E+04	1.65
2	-373.7	2.69E+04	1	-442	2.66E+04	0.95	-471	1.63E+04	2

Table A.4 Results of DC corrosion measurements of Micro-Composite Steel in carbonated concrete pore solution

Cl^- (M)	After 1 hour			After 24 hours			After 7 days		
	E_{OC} (V) vs. SCE	R_P (ohm.cm^2)	i_{corr} (μA/cm^2)	E_{OC} (V) vs. SCE	R_P (ohm.cm^2)	i_{corr} (μA/cm^2)	E_{OC} (V) vs. SCE	R_P (ohm.cm^2)	i_{corr} (μA/cm^2)
0.001	-156.7	3.56E+06	0.01	-105.3	7.04E+06	0.01	-82.79	7.61E+06	0.01
0.005	-175.7	4.00E+06	0.01	-121.3	6.49E+06	0.01	-87	7.58E+06	0.01
0.01	-160.9	4.90E+06	0.01	-123.1	7.27E+06	0.01	-108	7.79E+06	0.01
0.05	-178.7	1.15E+06	0.01	-229	7.58E+05	0.01	-210	1.65E+06	0.01
0.1	-212	2.19E+06	0.01	-200	1.66E+06	0.01	-245.8	1.37E+06	0.04
0.5	-238	5.52E+04	0.02	-272	1.29E+05	0.41	-340	9.69E+04	1.91
1	-200	5.93E+05	0.47	-294.8	2.46E+04	0.95	-391.5	4.94E+03	11.2
2	-360	8.00E+03	4.25	-434	4.70E+03	7.34	-470	3.52E+03	25.2

Table A.5 Results of DC corrosion measurements of 316LN Stainless Steel in fresh concrete pore solution

Cl^- (M)	After 1 hour			After 24 hours			After 7 days		
	E_{OC} (V) vs. SCE	R_P (ohm.cm^2)	i_{corr} (μA/cm^2)	E_{OC} (V) vs. SCE	R_P (ohm.cm^2)	i_{corr} (μA/cm^2)	E_{OC} (V) vs. SCE	R_P (ohm.cm^2)	i_{corr} (μA/cm^2)
0.001	-325.6	2.39E+05	0.46	-268.2	6.25E+05	0.03	-231	1.44E+06	0.02
0.01	-324.3	2.86E+05	0.13	-280.1	5.51E+05	0.02	-234.8	1.45E+06	0.01
0.05	-320	2.24E+05	0.15	-285.8	5.19E+05	0.02	-255.8	1.07E+06	0.01
0.5	-319.8	2.81E+05	0.18	-270.4	6.22E+05	0.03	-261	9.83E+05	0.03
1	-319.7	2.56E+05	0.13	-284	7.08E+05	0.02	-296.3	8.41E+05	0.02
2	-328.8	6.73E+04	0.28	-266.9	6.72E+05	0.02	-295.8	7.93E+05	0.04

Table A.6 Results of DC corrosion measurements of 316LN Stainless Steel in carbonated concrete pore solution

Cl^- (M)	After 1 hour			After 24 hours			After 7 days		
	E_{OC} (V) vs. SCE	R_P (ohm.cm^2)	i_{corr} (μA/cm^2)	E_{OC} (V) vs. SCE	R_P (ohm.cm^2)	i_{corr} (μA/cm^2)	E_{OC} (V) vs. SCE	R_P (ohm.cm^2)	i_{corr} (μA/cm^2)
0.001	-165.3	6.12E+05	0.05	-125.1	1.41E+06	0.03	-122.4	2.01E+06	0.02
0.005	-152	9.34E+05	0.06	-130.8	1.29E+06	0.04	-122.9	2.09E+06	0.03
0.01	-139.2	1.10E+06	0.05	-171	6.61E+05	0.07	-227.4	1.33E+06	0.18
0.05	-182	1.45E+05	0.15	-218.7	2.69E+05	0.06	-111.1	1.99E+06	0.03
0.1	-177.3	4.30E+05	0.09	-111.6	9.41E+05	0.03	-107.6	1.96E+06	0.03
0.5	-120.6	8.70E+05	0.06	-99.7	1.06E+06	0.03	-117.2	1.47E+06	0.03
1	-115.2	8.88E+05	0.05	-110.7	1.11E+06	0.04	-158.3	5.90E+05	0.05
2	-103.2	1.25E+06	0.04	-100.4	1.68E+06	0.03	-77.82	7.94E+05	0.02

Table A.7 Results of EIS measurements of carbon steel in the non-carbonated concrete pore solution

Time (day)	Cl^- (M)	R_{el} (ohm.cm2)	C_{dl} (F/cm2)	R_{ct} (ohm.cm2)	C_f (F/cm2)	R_f (ohm.cm2)
1	0	20.25	2.33E-04	6.91E+04	2.83E-06	6.68E-02
2	0.01	20.25	2.40E-04	9.41E+04	3.97E-06	4.61E-02
3	0.05	20.17	2.48E-04	6.36E+04	5.52E-06	3.59E-02
4	0.1	19.71	2.62E-04	1.61E+04	7.70E-06	5.99E-02
5	0.5	15.79	2.75E-04	1.55E+04	1.14E-05	5.97E-02
6	1	10.24	3.35E-04	5.68E+03	1.83E-05	8.15E-02
7	2	10.31	3.84E-04	6.87E+03	6.05E-04	413.6

Table A.8 Results of EIS measurements of micro-composite steel in the non-carbonated concrete pore solution

Time (day)	Cl^- (M)	R_{el} (ohm.cm2)	C_{dl} (F/cm2)	R_{ct} (ohm.cm2)	C_f (F/cm2)	R_f (ohm.cm2)
1	0	12.14	1.62E-04	1.24E+05	3.04E-04	162.9
2	0.01	11.99	1.71E-04	6.62E+04	3.20E-04	100.4
3	0.05	11.79	1.55E-04	6.21E+04	3.33E-04	208.4
4	0.1	11.3	2.36E-04	4.21E+04	3.37E-04	624.2
5	0.5	9.154	2.46E-04	3.64E+04	3.59E-04	518.6
6	1	7.398	2.57E-04	3.11E+04	3.73E-04	438.9
7	2	6.353	2.72E-04	1.45E+04	4.37E-04	235.1

Table A.9 Results of EIS measurements of micro-composite steel in the carbonated concrete pore solution

Time (day)	Cl^- (M)	R_{el} (ohm.cm2)	C_{dl} (F/cm2)	R_{ct} (ohm.cm2)	C_f (F/cm2)	R_f (ohm.cm2)
1	0	5.98E+04	6.40E-15	5.95E+04	8.55E-06	1.66E+06
2	0.01	5.99E+04	4.49E-15	5.96E+04	8.95E-06	1.77E+06
3	0.05	5.98E+04	2.61E-15	5.96E+04	1.16E-05	1.23E+06
4	0.1	5.98E+04	1.98E-15	5.98E+04	1.56E-05	3.29E+05
5	0.5	6.00E+04	8.35E-16	6.00E+04	2.29E-05	8.73E+04
6	1	5.85E+04	1.06E-16	5.85E+04	8.00E-05	4.64E+03
7	2	5.83E+04	-1.27E-17	5.82E+04	2.36E-04	1.88E+03

Table A.10 Results of EIS measurements of 316LN stainless steel in the non-carbonated concrete pore solution

Time (day)	Cl^- (M)	R_{el} (ohm.cm2)	C_{dl} (F/cm2)	R_{ct} (ohm.cm2)	C_f (F/cm2)	R_f (ohm.cm2)
1	0	15.65	1.13E-04	2.65E+05	2.52E-04	121.2
2	0.01	15.83	1.18E-04	3.62E+05	2.64E-04	116.8
3	0.05	15.35	1.20E-04	4.22E+05	2.41E-04	78.37
4	0.1	17.03	1.20E-04	1.83E+05	2.36E-04	137.1
5	0.5	12.95	1.28E-04	3.90E+05	2.91E-04	106.4
6	1	11.24	1.29E-04	2.68E+05	2.91E-04	68.5
7	2	8.706	1.78E-04	1.05E+05	3.66E-04	485.7

Table A.11 Results of EIS measurements of 316LN stainless steel in the carbonated concrete pore solution

Time (day)	Cl^- (M)	R_{el} (ohm.cm2)	C_{dl} (F/cm2)	R_{ct} (ohm.cm2)	C_f (F/cm2)	R_f (ohm.cm2)
1	0	38.78	5.95E-05	2.47E+05	1.09E-10	428.3
2	0.01	33.6	6.16E-05	2.53E+05	1.78E-10	353.4
3	0.05	46.56	6.45E-05	2.40E+05	4.21E-10	187.6
4	0.1	45.21	7.48E-05	1.96E+05	8.48E-10	99.52
5	0.5	18.22	5.92E-05	2.30E+05	5.50E-09	21.73
6	1	22.55	7.11E-05	1.62E+05	8.76E-09	3.748
7	2	9.181	1.32E-04	1.16E+04	1.14E-08	4.459

Table A.12 Results of the study of the repeatability of DC corrosion measurements conducted on six Micro-Composite steel samples immersed in fresh concrete pore solution contaminated with 0.1M of NaCl

Sample #	After 1 hour			After 24 hours			After 7 days		
	E_{OC} mV	I_{corr} A/cm^2	R_P ohm.cm^2	E_{OC} mV	I_{corr} A/cm^2	R_P ohm.cm^2	E_{OC} mV	I_{corr} A/cm^2	R_P ohm.cm^2
1	-298.5	9.60E-08	2.19E+05	-205.3	5.39E-08	6.78E+05	-211.7	4.34E-08	9.75E+05
2	-302.9	9.67E-08	2.19E+05	-229.5	5.29E-08	7.54E+05	-203.7	3.63E-08	1.19E+06
3	-294.5	9.71E-08	2.34E+05	-216.4	5.10E-08	6.87E+05	-195	4.11E-08	1.23E+06
4	-305.7	9.23E-08	2.08E+05	-219.4	4.90E-08	7.26E+05	-200.3	3.64E-08	1.21E+06
5	-303.3	9.62E-08	2.52E+05	-213.5	5.32E-08	7.94E+05	-196.9	3.46E-08	9.70E+05
6	-282.6	8.98E-08	2.32E+05	-208.2	5.48E-08	7.39E+05	-224.3	3.66E-08	9.18E+05
Mean	-297.92	9.47E-08	2.27E+05	-215.38	5.25E-08	7.30E+05	-205.32	3.81E-08	1.08E+06
Standard Deviation	8.50	2.95E-09	1.54E+04	8.64	2.12E-09	4.31E+04	11.0	3.40E-09	1.42E+05
Standard error S_m	3.47	1.20E-09	6.27E+03	3.53	8.64E-10	1.76E+04	4.49	1.39E-09	5.78E+04
t* S_m	8.92	3.08E-09	16113.9	9.07	2.22E-09	45232	11.54	3.57E-09	148546

Table A.13 Results of the study of the repeatability of EIS corrosion measurements conducted on six Micro-Composite steel samples immersed in fresh concrete pore solution contaminated with 0.05 M of NaCl increased to 0.1 M after 24 hours and 48 hours, respectively.

Sample #	Cl^- = 0.05M/ after 1 hours					Cl^- = 0.1M/ after 48 hours				
	R_{el} ohm	R_{ct} K.ohm	R_f ohm	C_{dl} µF	C_f µF	R_{el} ohm	R_{ct} K.ohm	R_f ohm	C_{dl} µF	C_f µF
1	4.405	8.27E+02	1.10E+02	3.06E+01	6.33E+01	4.0	9.97E+02	1.37E+02	3.12E+01	6.45E+01
2	4.22	8.34E+02	1.20E+02	3.24E+01	6.87E+01	4.17	1.02E+03	1.70E+02	3.31E+01	6.94E+01
3	4.28	6.12E+02	1.60E+02	3.40E+01	6.20E+01	4.3	7.43E+02	2.20E+02	3.47E+01	6.35E+01
4	4.079	7.04E+02	1.17E+02	3.35E+01	4.93E+01	3.96	8.41E+02	1.58E+02	3.39E+01	5.03E+01
5	4.346	8.40E+02	1.12E+02	3.07E+01	6.43E+01	4.07	7.09E+02	2.32E+02	3.40E+01	3.98E+01
6	4.127	7.38E+02	1.61E+02	3.51E+01	9.62E+01	4.13	1.01E+03	1.46E+02	3.31E+01	7.04E+01
Mean	4.24	7.59E+02	3.27E+01	6.73E+01	1.11E+02	4.10	8.86E+02	3.33E+01	5.96E+01	1.77E+02
Standard Deviation S	0.13	9.16E+01	1.82E+00	15.57	23.95	0.12	1.40E+02	1.19E+00	12.1	39.62
Standard Error S_m	0.05	3.74E+01	0.744569	6.36	9.77	0.05	5.73E+01	0.49	4.94	16.17
t* S_m	0.13	9.61E+01	1.91E+00	16.34	25.12	0.13	1.47E+02	1.25E+00	12.68	41.56

Table A.14 Corrosion current density i_{corr} of six Carbon Steel samples embedded in mortar contaminated with NaCl of 5% of cement weight at different ages

Sample #	1 day	3 days	7 days	14 days	28 days	60 days
1	2.64	1.80	0.887	7.02E-01	1.86E-01	8.76E-02
2	2.35	2.60	2.48	5.04E-01	3.53E-01	5.11E-02
3	6.94	1.39	2.47	6.65E-01	3.64E-01	7.50E-02
4	5.35	2.05	2.42	7.27E-01	2.05E-01	9.74E-02
5	2.27	2.35	2.58	7.93E-01	1.63E-01	2.04E-02
6	3.18	2.59	2.54	5.83E-01	2.93E-01	2.65E-02

Table A.15 TDR results for Cl^- free mortar samples after 1 day

Sample #	L_1 (ft)	L_2 (ft)	ΔL (ft)	$\Delta L/L_0$	ε	WC (m^3/m^3)
1	7.66	9.84	2.18	5.11	26.13	0.26
2	7.664	9.368	1.72	4.04	16.34	0.14
3	7.648	9.624	1.98	4.63	21.47	0.20
4	7.648	9.392	1.74	4.09	16.72	0.15
5	7.644	9.884	2.24	5.25	27.58	0.27

Table A.16 TDR results for Cl^- contaminated mortar samples after 1 day

Sample #	L_1 (ft)	L_2 (ft)	ΔL (ft)	$\Delta L/L_0$	ε	WC (m^3/m^3)
1	7.632	11.992	4.36	10.22	104.50	1.17
2	7.648	11.448	3.80	8.91	79.38	0.88
3	7.66	11.96	4.30	10.08	101.65	1.14
4	7.648	11.736	4.09	9.58	91.87	1.02
5	7.64	11.120	3.48	8.16	66.58	0.73

Table A.17 TDR results for Cl^- free mortar samples after 3 days

Sample #	L_1 (ft)	L_2 (ft)	ΔL (ft)	$\Delta L/L_0$	ε	WC (m^3/m^3)
1	7.656	9.408	1.75	4.11	16.87	0.15
2	7.66	9.288	1.63	3.82	14.57	0.12
3	7.64	9.52	1.88	4.41	19.43	0.18
4	7.644	9.292	1.65	3.86	14.93	0.13
5	7.68	9.36	1.68	3.94	15.52	0.13

Table A.18 TDR results for Cl^- contaminated mortar samples after 3 days

Sample #	L_1 (ft)	L_2 (ft)	ΔL (ft)	$\Delta L/L_0$	ε	WC (m^3/m^3)
1	7.632	9.52	1.89	4.43	19.60	0.18
2	7.636	9.42	1.78	4.18	17.50	0.16
3	7.64	9.608	1.97	4.61	21.29	0.20
4	7.64	9.568	1.93	4.52	20.44	0.19
5	7.66	9.62	1.96	4.60	21.12	0.20

Table A.19 TDR results for Cl^- free mortar samples after 7 days

Sample #	L_1 (ft)	L_2 (ft)	ΔL (ft)	$\Delta L/L_0$	ε	WC (m^3/m^3)
1	7.64	9.116	1.48	3.46	11.98	0.09
2	7.64	9.136	1.50	3.51	12.30	0.10
3	7.64	9.128	1.49	3.49	12.17	0.10
4	7.648	9.08	1.43	3.36	11.27	0.09
5	7.648	9.176	1.53	3.58	12.84	0.10

Table A.20 TDR results for Cl^- contaminated mortar samples after 7 days

Sample #	L_1 (ft)	L_2 (ft)	ΔL (ft)	$\Delta L/L_0$	ε	WC (m^3/m^3)
1	7.648	9.272	1.62	3.81	14.50	0.12
2	7.64	9.224	1.58	3.71	13.79	0.11
3	7.64	9.204	1.56	3.67	13.45	0.11
4	7.64	9.172	1.53	3.59	12.90	0.10
5	7.64	9.168	1.53	3.58	12.84	0.10

Table A.21 TDR results for Cl^- free mortar samples after 14 days

Sample #	L_1 (ft)	L_2 (ft)	ΔL (ft)	$\Delta L/L_0$	ε	WC (m^3/m^3)
1	7.640	8.984	1.34	3.15	9.93	0.07
2	7.640	9.004	1.36	3.20	10.23	0.07
3	7.640	9	1.36	3.19	10.17	0.07
4	7.640	8.972	1.33	3.12	9.75	0.07
5	7.640	9.10	1.46	3.42	11.72	0.09

Table A.22 TDR results for Cl^- contaminated mortar samples after 14 days

Sample #	L_1 (ft)	L_2 (ft)	ΔL (ft)	$\Delta L/L_0$	ε	WC (m^3/m^3)
1	7.640	9.160	1.52	3.56	12.70	0.10
2	7.640	9.160	1.52	3.56	12.70	0.10
3	7.648	9.144	1.50	3.51	12.30	0.10
4	7.640	8.996	1.36	3.18	10.11	0.07
5	7.640	9.148	1.51	3.54	12.50	0.10

Table A.23 TDR results for Cl^- free mortar samples after 21 days

Sample #	L_1 (ft)	L_2 (ft)	ΔL (ft)	$\Delta L/L_0$	ε	WC (m^3/m^3)
1	7.648	8.958	1.31	3.07	9.43	0.06
2	7.644	8.924	1.28	3.01	9.06	0.06
3	7.644	8.864	1.22	2.87	8.22	0.05
4	7.640	8.8	1.16	2.73	7.45	0.04
5	7.640	8.85	1.21	2.84	8.05	0.05

Table A.24 TDR results for Cl^- contaminated mortar samples after 21 days

Sample #	L_1 (ft)	L_2 (ft)	ΔL (ft)	$\Delta L/L_0$	ε	WC (m^3/m^3)
1	7.644	9.014	1.37	3.22	10.38	0.07
2	7.644	8.964	1.32	3.10	9.62	0.07
3	7.640	8.93	1.29	3.02	9.09	0.06
4	7.648	8.888	1.24	2.91	8.45	0.05
5	7.644	8.924	1.28	3.01	9.04	0.06

Table A.25 TDR results for Cl^- free mortar samples after 28 days

Sample #	L_1 (ft)	L_2 (ft)	ΔL (ft)	$\Delta L/L_0$	ε	WC (m^3/m^3)
1	7.664	8.93	1.27	2.97	8.81	0.06
2	7.64	8.992	1.35	3.17	10.05	0.07
3	7.644	8.932	1.29	3.02	9.12	0.06
4	7.64	8.688	1.04	2.45	5.99	0.02
5	7.64	8.75	1.11	2.60	6.77	0.03

Table A.26 TDR results for Cl^- contaminated mortar samples after 28 days

Sample #	L_1 (ft)	L_2 (ft)	ΔL (ft)	$\Delta L/L_0$	ε	WC (m^3/m^3)
1	7.648	8.978	1.33	3.12	9.72	0.07
2	7.648	8.948	1.30	3.04	9.25	0.06
3	7.656	8.926	1.27	2.97	8.84	0.06
4	7.64	8.86	1.22	2.86	8.20	0.05
5	7.64	8.89	1.25	2.93	8.59	0.05

Table A.27 TDR results for Cl^- free mortar samples after 60 days

Sample #	L_1 (ft)	L_2 (ft)	ΔL (ft)	$\Delta L/L_0$	ε	WC (m^3/m^3)
1	7.664	8.884	1.22	2.86	8.18	0.05
2	7.664	8.908	1.24	2.92	8.51	0.05
3	7.636	8.780	1.14	2.68	7.19	0.04
4	7.664	8.708	1.04	2.45	5.99	0.02
5	7.636	8.884	1.25	2.93	8.56	0.05

Table A.28 TDR results for Cl^- contaminated mortar samples after 60 days

Sample #	L_1 (ft)	L_2 (ft)	ΔL (ft)	$\Delta L/L_0$	ε	WC (m^3/m^3)
1	7.660	8.84	1.18	2.76	7.60	0.04
2	7.648	8.858	1.21	2.84	8.08	0.05
3	7.648	8.988	1.34	3.14	9.87	0.07
4	7.644	8.724	1.08	2.52	6.36	0.03
5	7.64	8.9	1.26	2.94	8.66	0.06

APPENDIX B

Estimation of Cl^-/OH^- ratio

The following are the steps to calculate Cl^-/OH^- ratio

Step (1) Mass of NaCl (g) * $\frac{m.mCl}{m.mCl + m.mNa}$ = mass of Cl^- (g)

Step (2) $\frac{\text{mass of Cl (gm)}}{m.mCl(gm/L)}$ = mol. of Cl^-

Step (3) Concentration of Cl^- = $\frac{\text{mol. of Cl}}{\text{volume of total solution (L)}}$

Step (4) $[OH]^- = 10^{(pH-14)}$

Then divide (3)/ (4)